EVALUATION OF INITIAL SUBGRADE VARIABILITY ON THE OHIO SHRP TEST ROAD

INTERIM REPORT

for

(CONTINUED MONITORING OF INSTRUMENTED PAVEMENT IN OHIO - State Job No. 14652(0))

for

OHIO DEPARTMENT OF TRANSPORTATION
and
FEDERAL HIGHWAY ADMINISTRATION

By
Shad M. Sargand
Russ Professor of Civil Engineering

Daniel L. Wasniak
Research Engineer
Ohio Research Institute for Transportation and the Environment

Teruhisa Masada
Assistant Professor of Civil Engineering

David Beegle
Research Assistant, Civil Engineering

Ohio University
Ohio Research Institute for Transportation and the Environment
Civil Engineering Department

January 2000

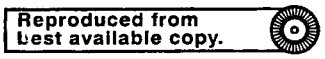

1. Report No.	2. Government Accession No.	3. Recipient's Catalog No.
FHWA/OH-2000/004		

4. Title and Subtitle	5. Report Date
EVALUATION OF INITIAL SUBGRADE VARIABILITY ON THE OHIO SHRP TEST ROAD INTERIM REPORT FOR THE PROJECT TITLED: CONTINUED MONITORING OF INSTRUMENTED PAVEMENT IN OHIO	January, 2000
	6. Performing Organization Code
	8. Performing Organization Report No.
7. Author(s) Shad Sargand	10. Work Unit No. (TRAIS)
9. Performing Organization Name and Address Ohio University Department of Civil Engineering Athens, OH 45701	11. Contract or Grant No. State Job No. 14652(0)
	13. Type of Report and Period Covered Interim Report
12. Sponsoring Agency Name and Address Ohio Department of Transportation 1600 West Broad Street Columbus, OH 43223	14. Sponsoring Agency Code

15. Supplementary Notes

Prepared in cooperation with the U.S. Department of Transportation, Federal Highway Administration

16. Abstract

The Ohio Department of Transportation (ODOT) currently uses density and moisture measured with a nuclear density gauge as the principal criteria for approving subgrade construction in Ohio. This procedure is time consuming, thereby restricting the number of tests that can be performed, and the device is limited to measuring density in the top 12 inches of material.

When the subgrade on mainline sections of the Ohio SHRP Test Road was completed and accepted by ODOT in 1995, nondestructive tests (NDT) performed with the Falling Weight Deflectometer (FWD) indicated considerable variation in stiffness within and between the 36 test sections in the SPS-1, SPS-2 and SPS-9 experiments. While this variation could be attributed to several factors, laboratory tests on subgrade samples demonstrated a definite sensitivity of stiffness to moisture.

After being opened to traffic, four sections in the SPS-1 experiment experienced severe rutting in the subgrade. The most distressed areas in two of these sections studied in detail coincided with locations of low stiffness under the FWD load plate, either on the subgrade or on the completed pavement system. Had these areas been addressed during construction, it is likely the service life of these sections would have been extended significantly. Because of the speed of NDT and because it assesses the in-situ stiffness of the entire pavement structure, density-based specifications for subgrade construction should be replaced with NDT-based specifications.

17. Key Words	18. Distribution Statement
subgrade variability; stiffness; nondestructive testing	No Restrictions. This document is available to the public through the National Technical Information Service, Springfield, Virginia 22161

19. Security Classif. (of this report)	20. Security Classif. (of this page)	21. No. of Pages	22. Price
Unclassified	Unclassified		

Form DOT F 1700.7 (8-72) Reproduction of completed page authorized

EVALUATION OF INITIAL SUBGRADE VARIABILITY ON THE OHIO TEST ROAD

Table of Contents

Table of Contents(continued)

List of Tables

List of Figures

List of Figures(continued)

List of Figures(continued)

Chapter 1

Introduction

1.1 General Statement

The construction and maintenance of highway pavements cost state and federal agencies billions of dollars each year. Premature deterioration of highways is a major component of this expenditure. This early decline in pavement performance demonstrates the need for improvement in existing pavement design and construction methods. Finding economical ways to prevent premature deterioration is a main concern of all agencies responsible for the transportation infrastructure.

While pavements typically perform up to design standards, localized areas of premature distress may require early attention. This distress may be in the form of rutting, cracking or other types of failure. Under repeated traffic loading and environmental cycling, these areas tend to expand to the point where the pavement loses serviceability and rehabilitation is required. Non-uniformity or variability within the pavement structure causes these early failures. More effective methods for monitoring and testing the various lifts of subgrade, base, and pavement as they are constructed may significantly reduce non-uniformity in the pavement system.

Non-destructive testing with the Falling Weight Deflectometer (FWD), Dynamic Cone Penetrometer (DCP), and Dynaflect is becoming more widely accepted for evaluating pavement conditions. These methods can be used to identify potential problem areas in the subgrade, base, and pavement that will create premature distress. By preventing this premature distress, overall service life of the pavement will be extended and transportation agencies will save a substantial amount of money that would otherwise be used for rehabilitation or replacement of the pavement. Performing these tests during various stages of construction, especially at completion of the subgrade, will be very cost effective.

1.2 Objectives

The objective of this investigation is to determine the extent of initial subgrade variability on the Ohio SHRP Test Road and to recommend methods of improving

uniformity in future construction projects. The report is structured in the following format to effectively meet this objective.

- Present project background and subgrade information including soil classification and water tables.
- Describe procedures used in field testing on subgrade and present soil density and moisture data.
- Determine subgrade modulus using the Boussinesq equation and Falling Weight Deflectometer (FWD) data.
- Examine the linearity of subgrade soil with a comprehensive statistical analysis.
- Investigate correlations between moisture/density nuclear gauge readings and moduli of the subgrade.
- Present procedures and results of laboratory subgrade modulus testing.
- Present a case study performed on Section 390101 of Ohio-SHRP Test Road.
- Present nondestructive testing options for improving subgrade uniformity.
- Discuss conclusions that can be drawn from the data and make recommendations for future construction procedures.

Chapter 2

Project Background and Subgrade Information

2.1 Site Description

The Ohio Department of Transportation constructed an experimental pavement for SHRP on U.S.23 in Delaware County, just north of the city of Delaware, Ohio. This three mile long pavement is located in a 51.8-meter (170 feet) wide median of an existing four lane highway. This site was chosen so the performance of several pavement sections could be compared at one site with uniform topography, soil, and climate.

The Ohio SHRP Test Road (DEL-23-17.48) includes a total of 40 test sections of experimental pavement, 21 constructed of portland cement concrete and 19 constructed of asphalt concrete. Thirty-six test sections lie within the mainline test road, incorporating three of the nine Specific Pavements Studies (SPS) formulated by the Strategic Highway Research Program (SHRP). The northbound test sections were constructed of PCC and contain the SPS-2 experiment. The southbound test sections were constructed of asphalt concrete (AC) and contain the SPS-1 and SPS-9 experiments. Two sections each of AC and PCC in SPS-8 were located on a ramp to southbound US23.

The focus of SPS1, 2, and 8 experiments was to study the effect of various structural factors on pavement performance and to verify pavement models and designs. Some prominent factors included in the experiments were the use of different paving materials and layer thicknesses in the subgrade, base, and pavement. To study the effects of these parameters on pavement performance, a consistent subgrade was to be constructed throughout the project. This would theoretically eliminate the subgrade as a variable in the analysis of pavement performance. SPS-9 sections were built to test the new Superpave specifications.

2.2 Soil Classification

Eliminating the subgrade as a variable in comparing pavement performance simplifies the evaluation of various materials and layer thicknesses in the base and pavement. Although undesirable material was removed and replaced with borrow from

an adjacent pit, considerable variability remained in the U.S. 23 subgrade. Final soil classifications were determined by ODOT and are presented in Table 2.1.

Table 2.1: Soil Classification.

PCC Section	Soil Classification	AC Section	Soil Classification
390201		390101	
390202	A-6	390102	
390203		390103	
390204		390104	
390205	A-6	390105	
390206		390106	
390207	A-6	390107	A-7-6
390208		390108	
390209		390109	
390210		390110	A-4/A-4a
390211	A-6	390111	A-6
390212		390112	
390259		390159	
390260		390160	A-4/A-4a
390261		390901	
390262	A-6	390902	A-4/A-4a
390263		390903	
390264			
390265			

2.3 Water Table

Piezometer wells were placed in various locations along the test road to monitor water table elevation throughout the project. There are four wells along the PCC sections at project Stations 279+85, 298+01, 346+00 and 401+00 (Sections 390204, 390212, 390201, and 390208). Another five wells are located along the AC sections at project Stations 417+02, 397+00, 372+00, 337+00, and 279+50 (Sections 390103, 390108, 390102, 390104, and 390901). The water tables were measured from the top of the well with a Geokon Piezometer. Measurements were taken every month to observe seasonal fluctuations. Sections 390108 and 390212 are drained. All other sections with piezomter wells are undrained. The presence of pavement drainage does not affect the depth of the

water table at the piezometers. The water table remained rather stable throughout the year and relatively close to the subgrade surface in some sections. Figures 2.1 through 2.9 show the elevation of the water table compared to the pavement surface elevation for each well.

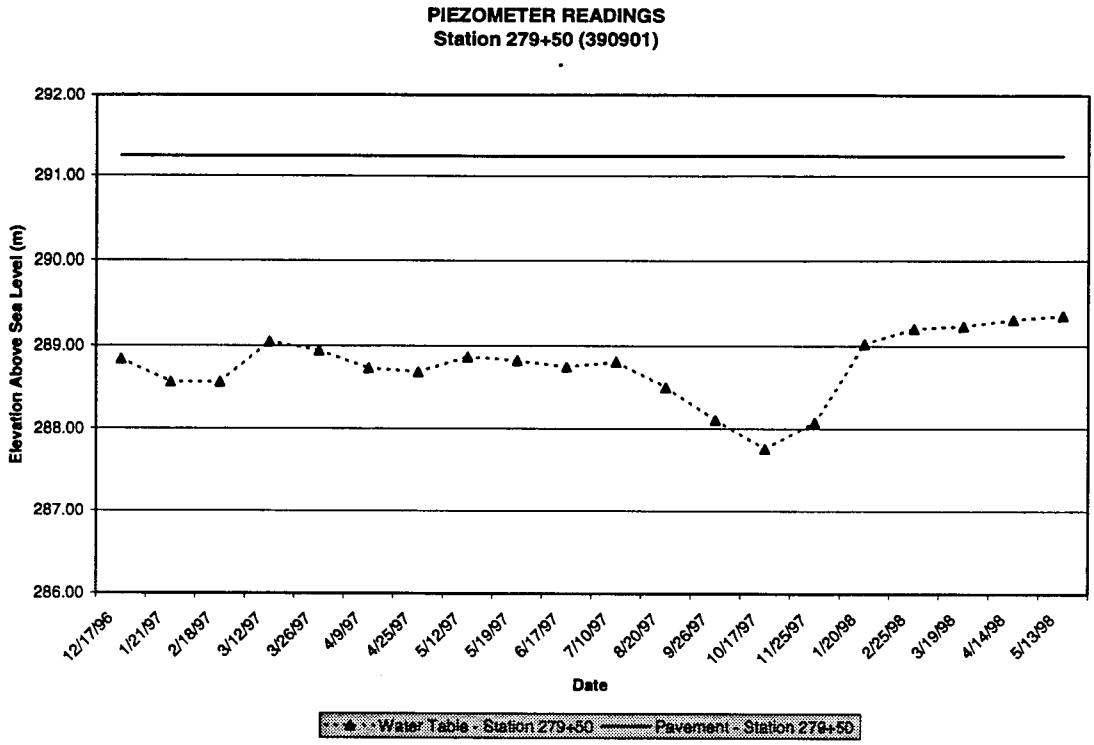

Figure 2.1: Piezometer Readings Station 279+50

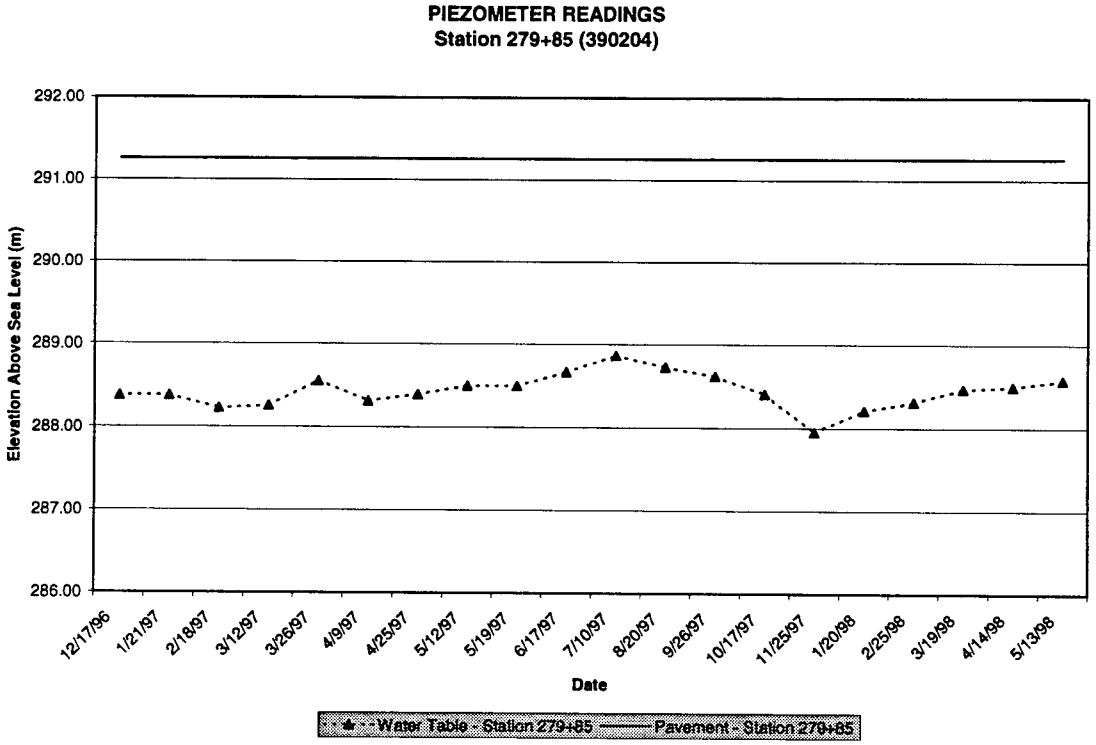

Figure 2.2: Piezometer Readings Station 279+85

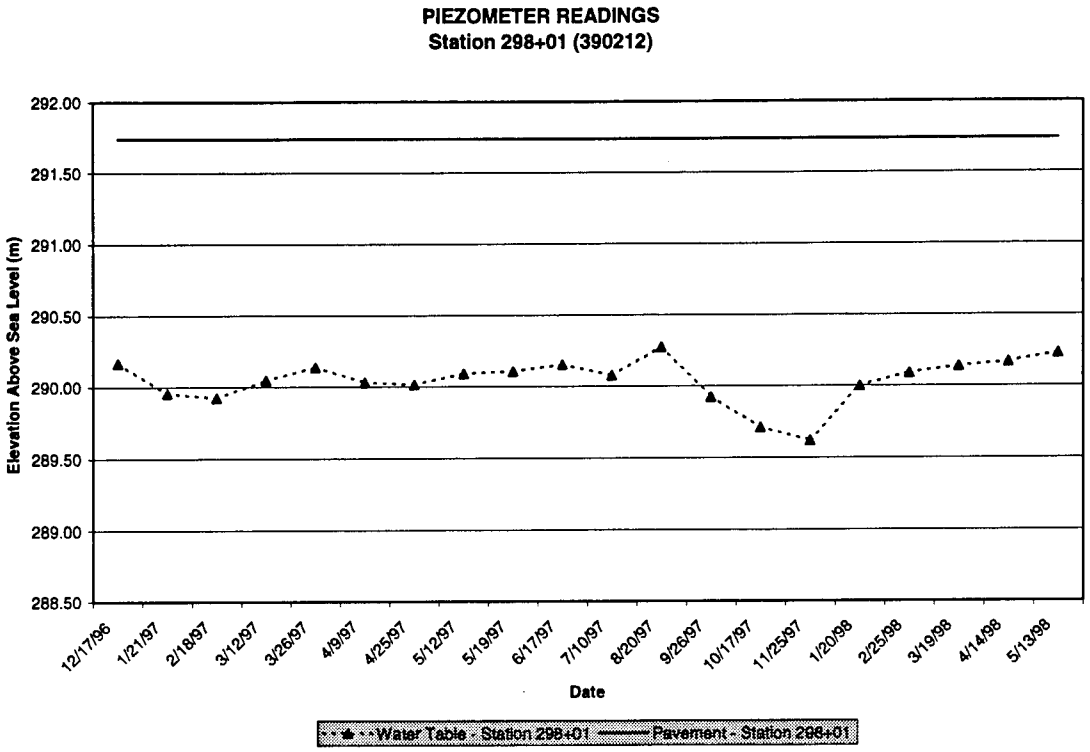

Figure 2.3: Piezometer Readings Station 298+01

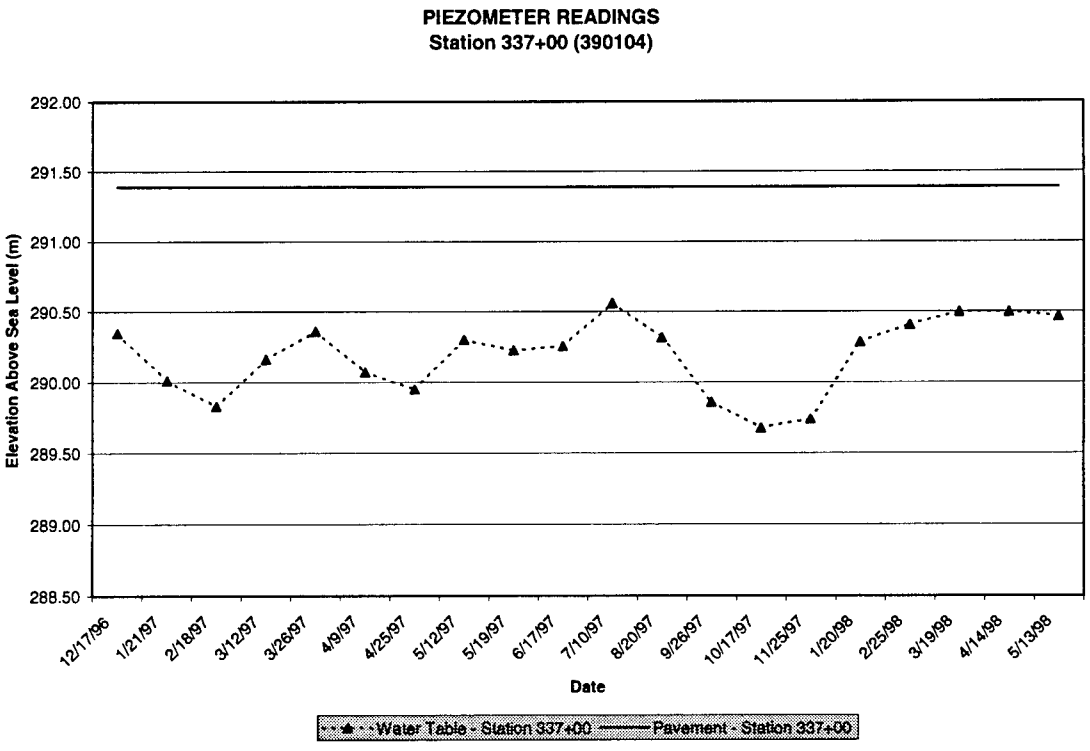

Figure 2.4: Piezometer Readings Station 337+00

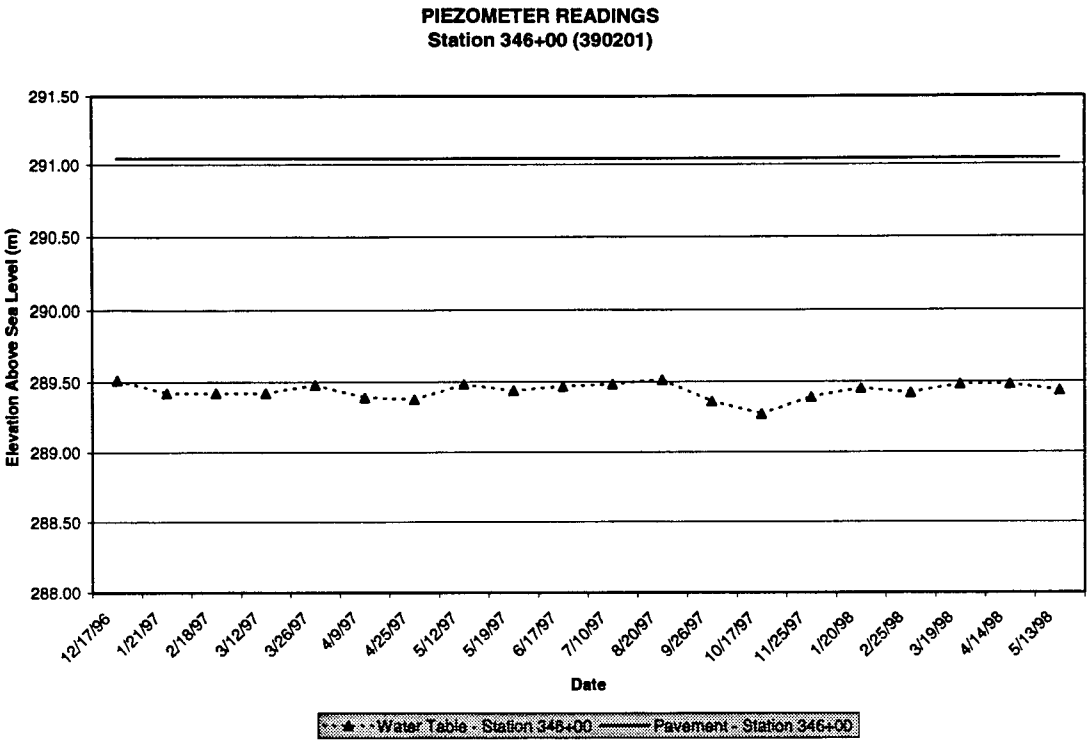

Figure 2.5: Piezometer Readings Station 346+00

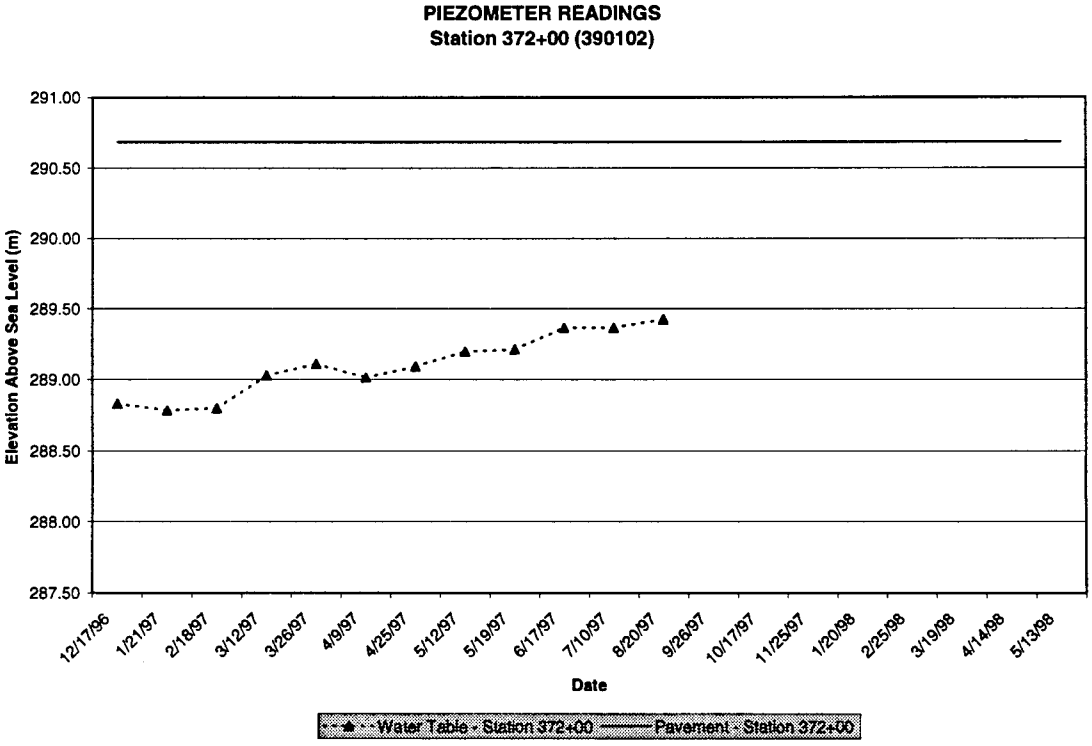

Figure 2.6: Piezometer Readings Station 372+00

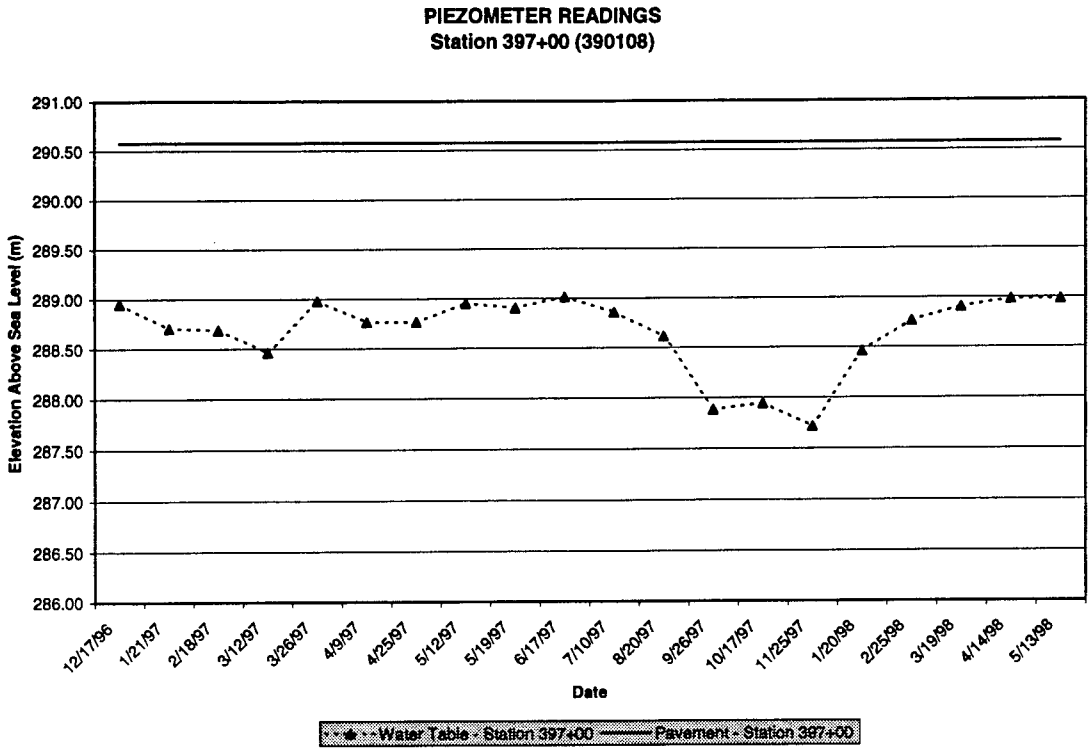

Figure 2.7: Piezometer Readings Station 397+00

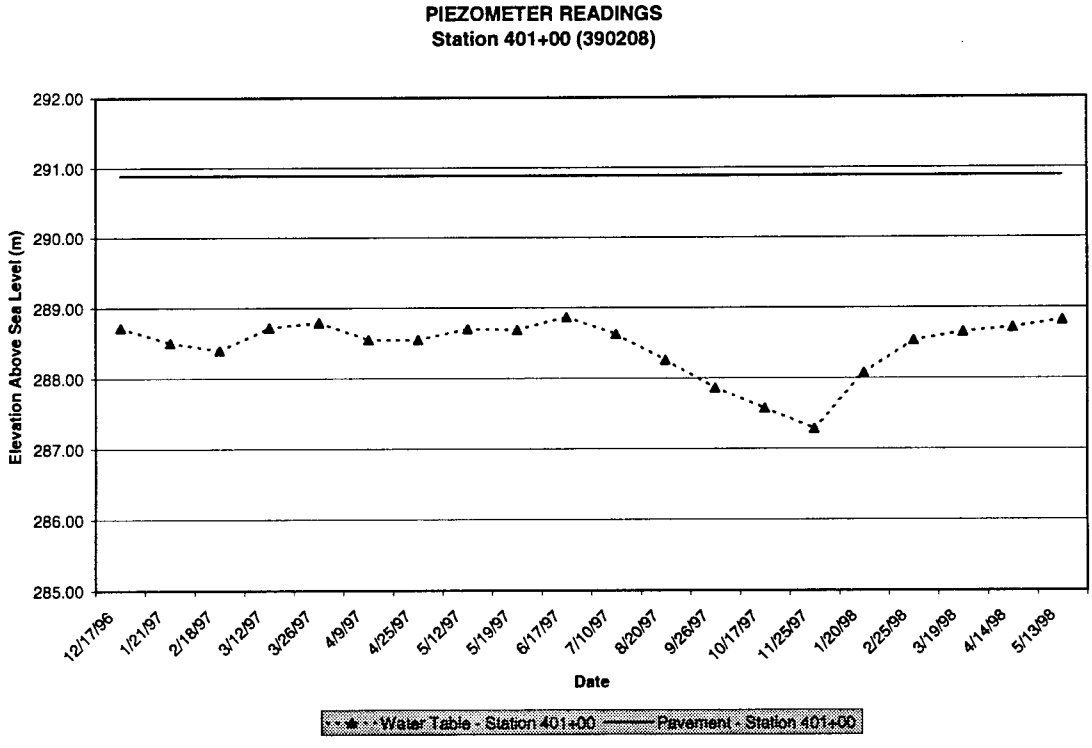

Figure 2.8: Piezometer Readings Station 401+00

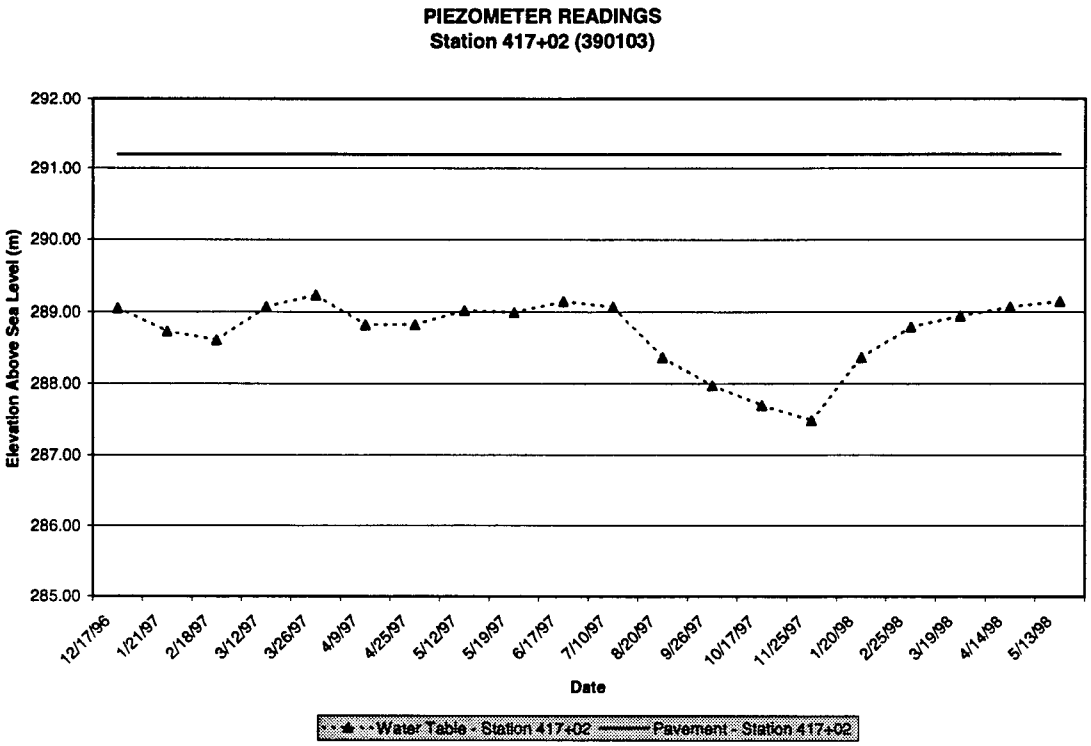

Figure 2.9: Piezometer Readings Station 417+02

Chapter 3

Field Testing of Subgrade

3.1 Introduction

As part of the requirements of the Strategic Highway Research Program (SHRP) Specific Pavement Studies, extensive field-testing was performed on the subgrade in each test section. Experiments included Falling Weight Deflectometer and nuclear density testing. Four universities participating in this research project monitored the volumetric moisture content on a monthly basis to obtain variations in soil moisture.

3.2 Falling Weight Deflectometer (FWD)

Falling Weight Deflectometer tests were performed on each test section in the centerline and right wheel path of the driving lane, in accordance with SHRP procedures. Centerline tests started at SHRP Station 0+25 and went every 15.24 meters (50-feet) up to SHRP Station 4+75. Wheel path tests started at SHRP Station 0+00 and went every 15.24 meters (50-feet) up to SHRP station 5+00. Subgrade FWD tests included four different weights with two drops at each weight, for a total of eight drops at each station. The tests were performed soon after the subgrade soil had been completed and approved by ODOT and SHRP specifications.

3.3 Initial Density and Moisture

Subgrade density and moisture measurements were taken with a nuclear density gauge along the centerline of the driving lane in each section at a depth of 304-mm (12 inches) below the finished surface. A minimum of three measurements were made in each test section, usually at SHRP Stations 1+00, 2+50, and 4+00. The nuclear density and moisture results are presented in Tables 3.1 and 3.2. Each measurement is the average of four readings taken 90 degrees apart. Nuclear density and moisture testing were conducted approximately at the same time as the FWD testing.

Table 3.1: Subgrade Density and Moisture in Northbound Lanes.

SHRP Section	SHRP Station	Project Station	Dry Unit Weight (pcf)	Dry Unit Weight (kg/m^3)	Moisture Content (%)
390259	1+00	266+50	113.5	1818.1	7.6
	2+50	268+00	115.5	1850.1	10.0
	4+00	269+50	116.0	1858.1	8.6
390204	1+00	276+50	120.9	1936.6	10.7
	2+50	278+00	124.1	1987.9	9.5
	4+00	279+50	128.5	2058.4	9.1
	5+50	281+00	129.9	2080.8	7.4
390212	1+00	295+00	121.6	1947.8	8.8
	2+50	296+50	129.2	2069.6	9.4
	4+00	298+00	127.1	2035.9	9.5
390210	1+00	304+50	118.1	1891.8	7.7
	2+50	306+00	114.8	1838.9	9.3
	4+00	307+50	115.2	1845.3	9.4
	5+50	309+00	116.3	1862.9	11.8
390260	1+00	312+50	123.9	1984.7	11.1
	2+15	313+65	117.4	1880.6	13.2
	4+00	315+50	123.0	1970.3	10.5
390202	1+00	320+00	128.6	2060.0	8.8
	2+50	321+50	123.8	1983.1	10.4
	4+00	323+00	121.3	1943.0	12.0
	5+50	324+50	123.0	1970.3	10.7
390206	1+00	328+50	119.9	1920.6	10.3
	2+50	330+00	122.6	1963.9	9.9
	4+00	331+50	117.4	1880.6	10.2
390205	1+00	336+75	116.4	1864.5	11.7
	2+50	338+25	122.1	1955.9	10.7
	4+00	339+75	117.2	1877.4	10.5
	5+25	341+00	117.0	1874.2	9.9
390201	1+00	344+00	117.4	1880.6	11.7
	2+50	345+50	121.5	1946.2	11.3
	3+25	346+25	120.0	1922.2	10.2
390209	1+00	351+25	113.7	1821.3	15.2
	2+50	352+75	121.0	1938.2	12.0
	4+00	354+25	119.6	1915.8	8.0
	5+50	355+75	120.9	1936.6	6.9
390261	1+00	358+75	120.7	1933.4	7.5
	2+50	360+25	121.0	1938.2	9.3
	4+00	361+75	120.5	1930.2	10.2
390211	1+00	370+00	121.0	1938.2	10.4
	2+50	371+50	121.8	1951.0	10.2
	4+00	373+00	116.3	1862.9	7.7
	5+25	374+50	115.8	1854.9	8.3
390265	1+00	377+10	124.2	1989.5	8.2
	2+90	379+00	121.6	1947.8	9.6
	4+00	380+10	120.0	1922.2	7.9
390203	1+00	385+00	120.7	1933.4	8.7
	2+50	386+50	121.1	1939.8	8.0
	4+00	388+00	119.4	1912.6	8.4
390207	0+50	390+75	120.2	1925.4	7.6
	1+00	392+75	119.8	1919.0	8.0
	2+50	393+75	121.4	1944.6	8.1
	4+00	395+25	121.4	1944.6	8.4
390208	1+00	398+75	115.5	1850.1	8.9
	2+50	400+25	114.7	1837.3	9.6
	4+00	401+75	115.4	1848.5	9.5
390262	1+00	406+25	121.6	1947.8	8.5
	2+50	407+75	123.6	1979.9	8.8
	4+00	409+25	116.2	1861.3	9.3
	5+50	410+75	118.7	1901.4	8.4

SHRP Section	SHRP Station	Project Station	Dry Unit Weight (pcf)	Dry Unit Weight (kg/m^3)	Moisture Content (%)
390263	1+00	415+50	117.3	1879.0	12.8
	2+50	417+00	121.6	1947.8	10.5
	4+00	418+50	119.3	1911.0	10.5
390264	1+00	423+50	124.7	1997.5	9.1
	2+50	425+00	120.2	1925.4	11.9
	4+00	426+50	110.0	1762.0	11.7
	5+50	428+00	106.9	1712.4	16.7

Table 3.2: Subgrade Density and Moisture in Southbound Lanes.

SHRP Section	SHRP Station	Project Station	Dry Unit Weight(pcf)	Dry Unit Weight(kg/m^3)	Moisture Content(%)
390901	5+50	278+00	117.7	1885.4	14.0
	4+00	279+50	122.6	1963.9	11.5
	2+50	281+00	130.4	2088.8	9.4
	1+00	282+50	125.6	2011.9	8.2
390903	4+00	295+50	121.7	1949.4	8.6
	2+50	297+00	130.3	2087.2	8.6
	1+00	298+50	126.4	2024.7	9.2
390902	5+50	304+50	122.3	1959.1	10.9
	4+00	306+00	124.3	1991.1	10.6
	2+50	307+50	125.6	2011.9	10.0
	1+00	309+00	116.8	1871.0	11.5
390112	4+00	321+00	124.5	1994.3	8.8
	2+50	322+50	124.3	1991.1	8.8
	1+00	324+00	117.0	1874.2	8.5
390111	4+00	329+00	126.3	2023.1	7.9
	2+50	330+50	113.4	1816.5	11.6
	1+00	332+00	124.3	1991.1	9.6
	0-50	333+50	125.8	2015.1	8.5
390104	4+00	337+00	123.2	1973.5	8.9
	2+50	338+50	119.4	1912.6	9.0
	1+00	340+00	116.6	1867.8	9.8
390106	5+50	342+50	127.3	2039.2	9.0
	4+00	344+00	123.3	1975.1	9.4
	2+50	345+50	124.9	2000.7	9.5
	1+75	346+25	121.9	1952.7	11.2
390101	4+00	351+00	120.2	1925.4	12.4
	2+50	352+50	114.1	1827.7	7.9
	1+00	354+00	116.0	1858.1	6.4
390107	4+00	359+00	117.3	1879.0	6.2
	2+50	360+50	123.0	1970.3	6.7
	1+00	362+00	123.5	1978.3	7.6
	0-50	363+50	118.4	1896.6	8.8
390102	4+00	371+00	128.1	2052.0	7.4
	2+50	372+50	117.3	1879.0	9.8
	1+00	374+00	128.4	2056.8	7.7
390160	3+25	378+75	125.1	2003.9	8.1
	2+50	379+50	122.2	1957.5	9.2
	1+00	381+00	121.9	1952.7	7.6
	0-50	382+50	124.4	1992.7	8.5
390105	4+00	388+50	117.5	1882.2	9.9
	2+50	390+00	116.8	1871.0	9.9
	1+00	391+50	118.5	1898.2	9.4

SHRP Section	SHRP Station	Project Station	Dry Unit Weight(pcf)	Dry Unit Weight(kg/m^3)	Moisture Content(%)
390108	4+50	395+25	123.2	1973.5	7.8
	2+10	397+65	113.0	1810.1	8.8
	1+00	398+75	116.1	1859.7	8.8
	0-50	400+25	118.0	1890.2	7.1
390109	4+00	402+50	115.6	1851.7	10.8
	2+50	404+00	121.0	1938.2	9.7
	1+00	405+50	122.6	1963.9	8.6
390110	4+00	409+50	119.7	1917.4	9.6
	2+50	411+00	116.7	1869.4	9.2
	1+00	412+50	117.5	1882.2	10.3
	0-50	414+00	120.6	1931.8	9.0
390103	4+00	416+75	121.7	1949.4	7.8
	2+50	418+25	118.6	1899.8	8.0
	1+00	419+75	119.1	1907.8	7.3
390159	4+00	429+00	118.6	1899.8	11.6
	2+50	430+50	123.1	1971.9	10.4
	1+00	432+00	115.1	1843.7	11.8

3.4 Variation of Moisture Content

Time-domain reflectometry (TDR) probes are used to collect volumetric moisture content. This probe works by sending an electromagnetic wave through a medium and any obstruction returns a portion of the wave back to the source. The dielectric constant of a material (ratio of capacitance of that material to the capacitance of air) is a function of moisture content. A change in the dielectric creates a wave reflection and makes it possible to monitor the moisture content of materials.

Ten TDR probes, numbered from top to bottom, were installed (according to LTPP protocol) in each of the 17 mainline sections containing seasonal instrumentation at the following depths:

a. If the top granular base/subbase layer was greater than 300-mm (12-in.), the first TDR probe was placed 6 inches below the bottom of the lowest stabilized layer.

b. Otherwise, the probe was placed at mid-depth of the top granular base/subbase layer.

c. The next seven TDR probes were placed at 150-mm (6-in.) intervals. The bottom two TDR probes were placed at 300-mm (12-in.) intervals.

The volumetric moisture content is collected on a monthly basis using a mobile system consisting of a CR10, Tektronix cable tester, and a portable PC. The gravimetric moisture content (ω) is more suitable for design purposes since most samples are measured by weight. Therefore, volumetric content was converted to gravimetric content using the density of the soil. The gravimetric moisture content from the top three TDR probes for each environmental section is plotted in Figures 3.1 through 3.15.

These figures do not indicate trends in moisture content that suggests any significant seasonal effects. This may be due to the pavement surfaces being relatively new and impervious to moisture penetration. Another factor is that the environmental instrumentation was placed away from the edge of pavement and joints. Surface moisture may not affect the readings until the pavement begins to crack.

The moisture content of the third gauge was around 20% for all sections regardless of base type and drainage. This reading is generally higher than the first and second gauge, which indicates that the moisture is coming from the below the pavement system. Sections with an undrained dense graded aggregate base (DGAB) had a moisture content around 15% at the top sensor, while the drained DGAB section had a moisture content around 12% at the top sensor. The top sensor in sections with DGAB is located within the base layer and the top sensor in sections with other base types lies in the subgrade. In sections with a free draining base (PATB or PCTB), the moisture content at the top sensor tended to be around 10%, with some variations from section to section probably due to the difference in the water tables. These readings indicate the free draining bases seem to be functioning as designed by removing excess moisture. Stabilized bases (LCB or ATB) generally showed higher moisture contents then any other base type, from 20% to 40 %. These base types may produce false readings by trapping excess moisture. Cracks forming in the base, especially LCB, allow moisture to collect in localized areas.

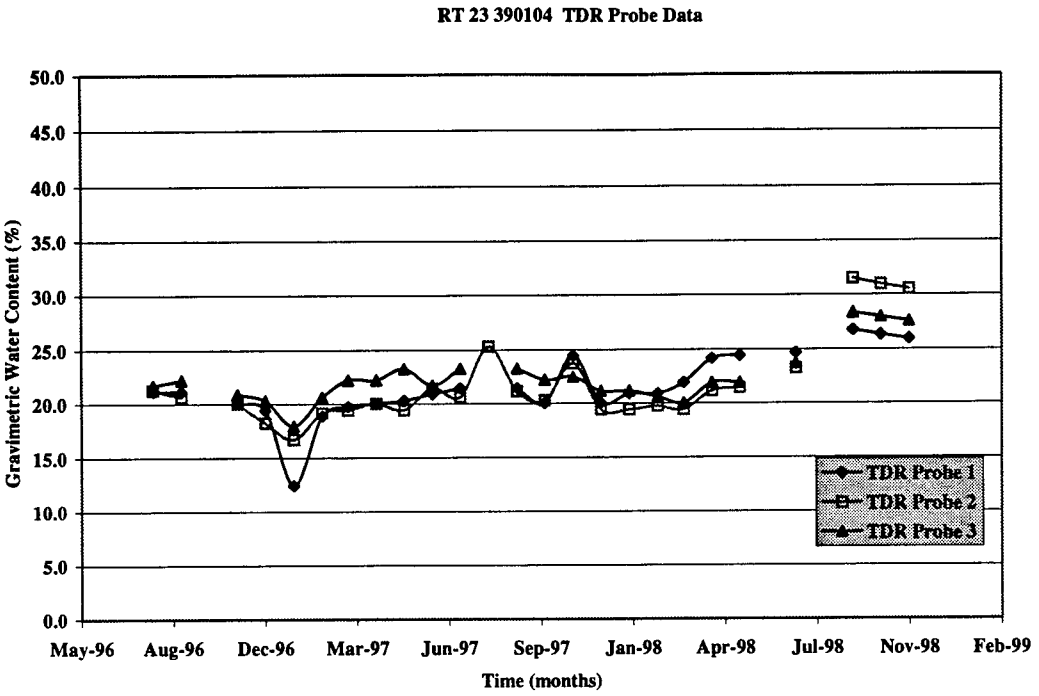

Figure 3.1: TDR Data 390104

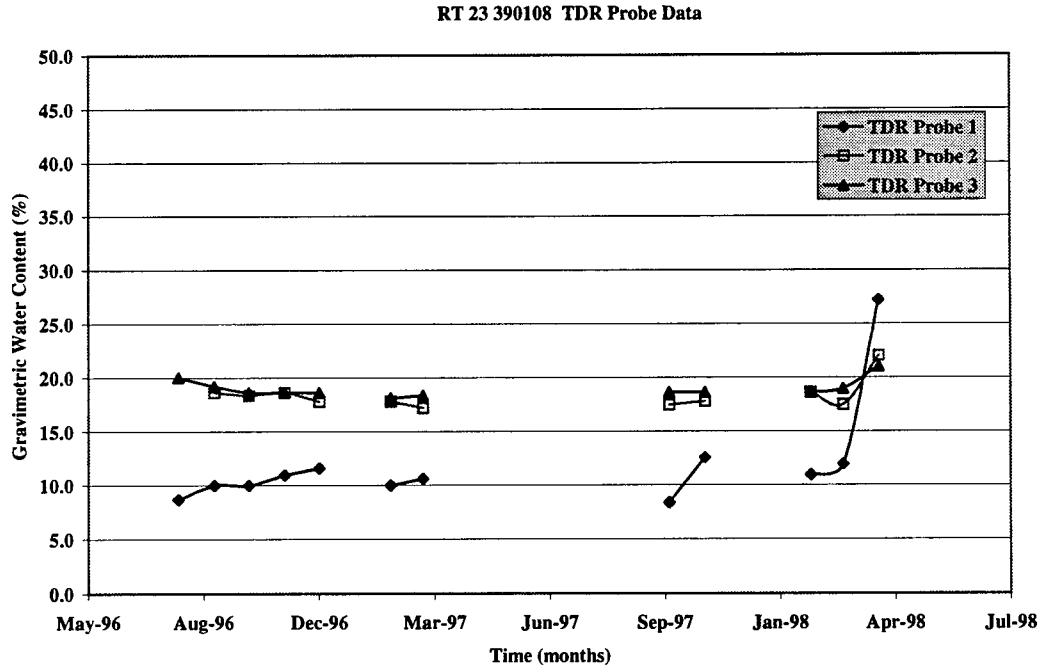

Figure 3.2: TDR Data 390108

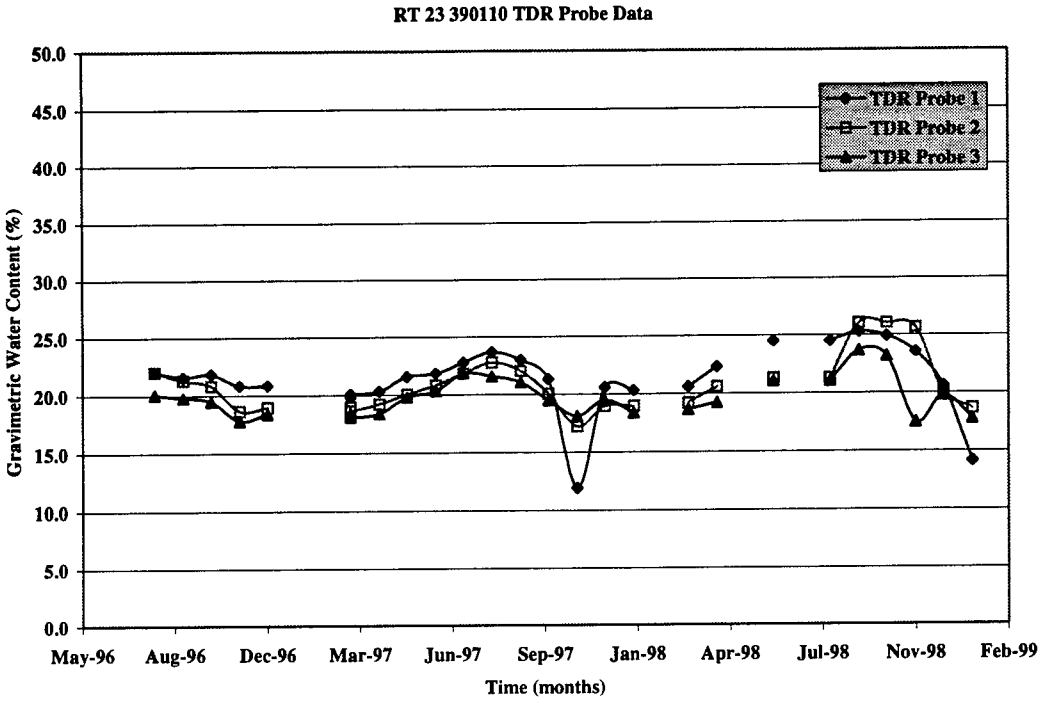

Figure 3.3: TDR Data 390110

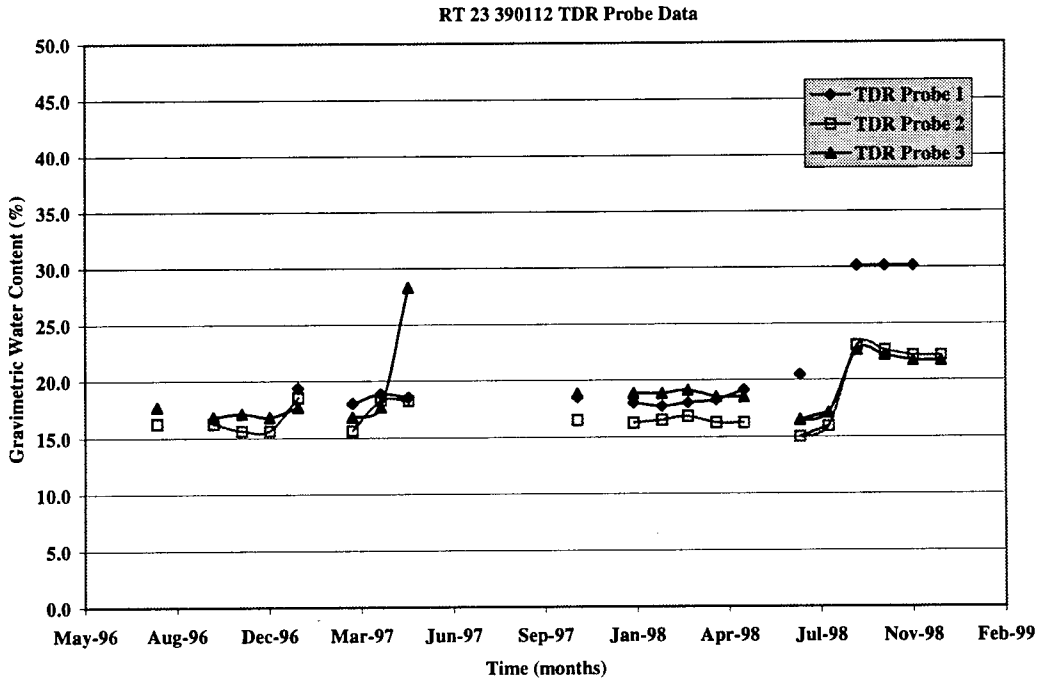

Figure 3.4: TDR Data 390112

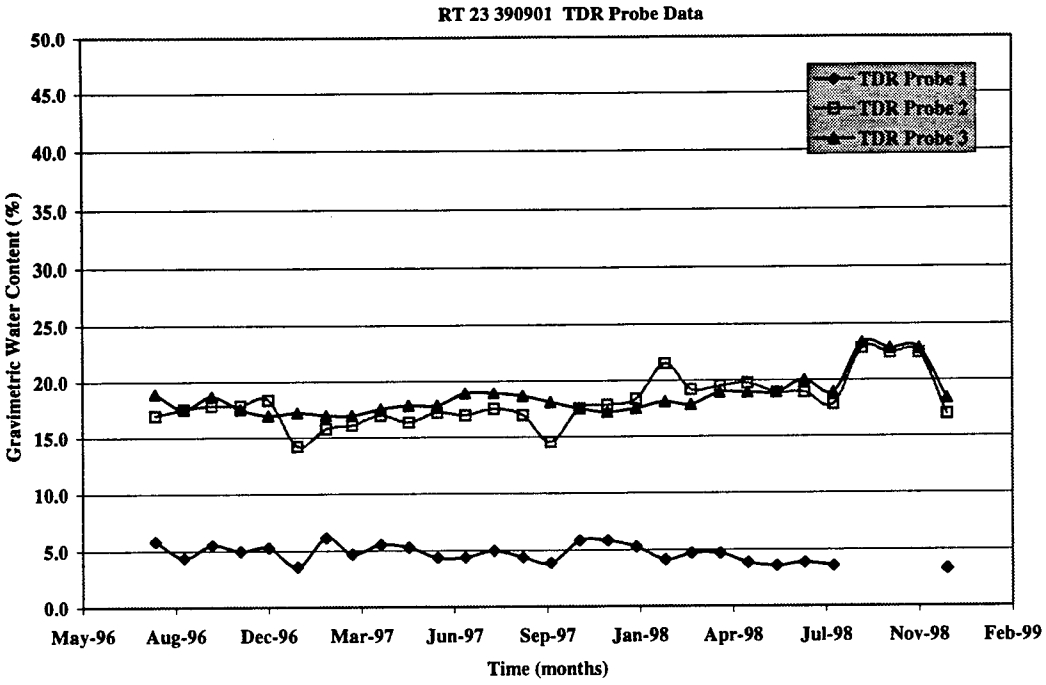

Figure 3.5: TDR Data 390901

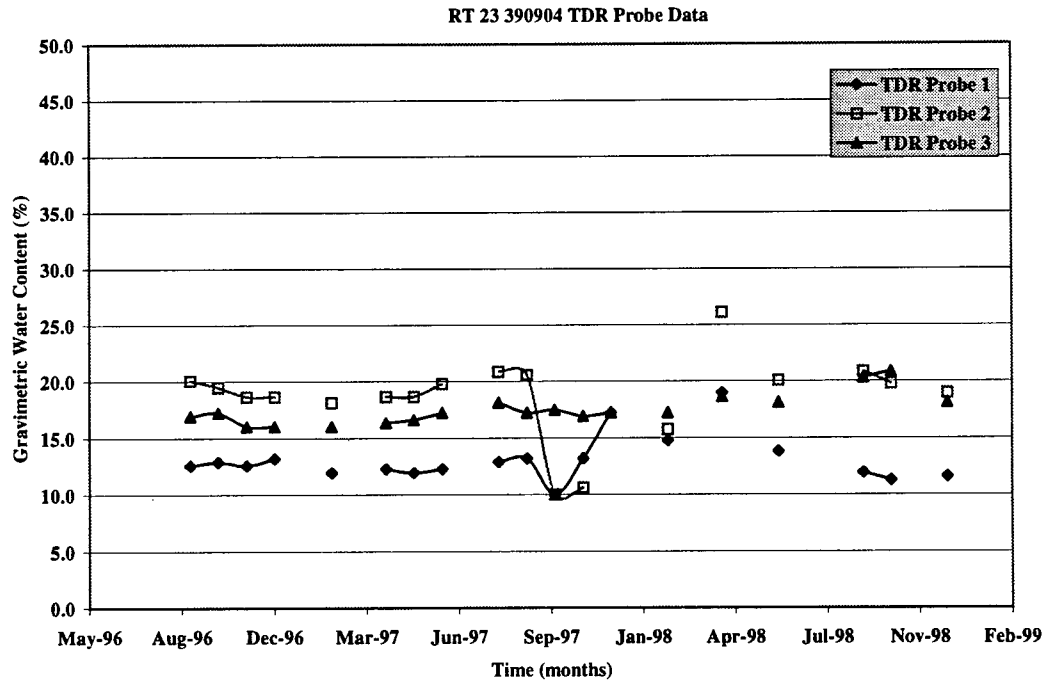

Figure 3.6: TDR Data 390904

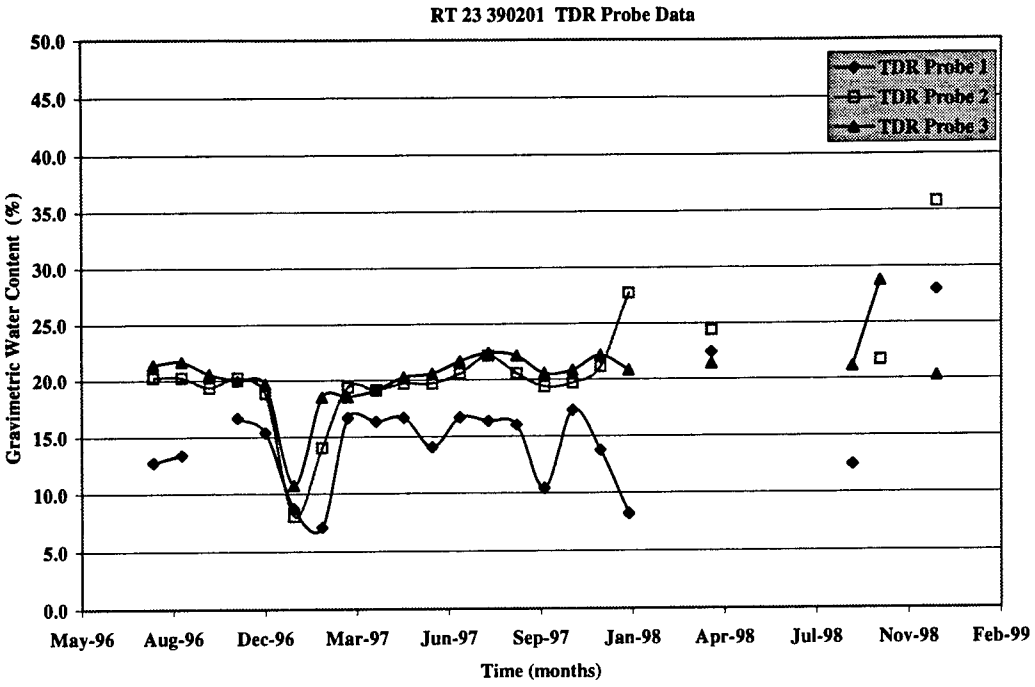

Figure 3.7: TDR Data 390201

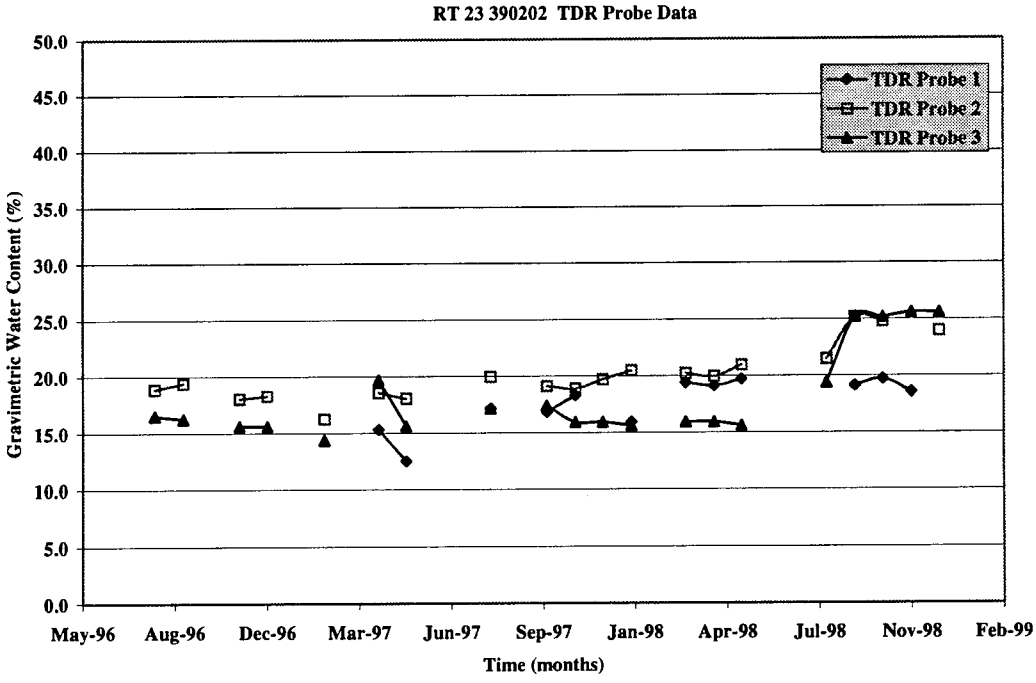

Figure 3.8: TDR Data 390202

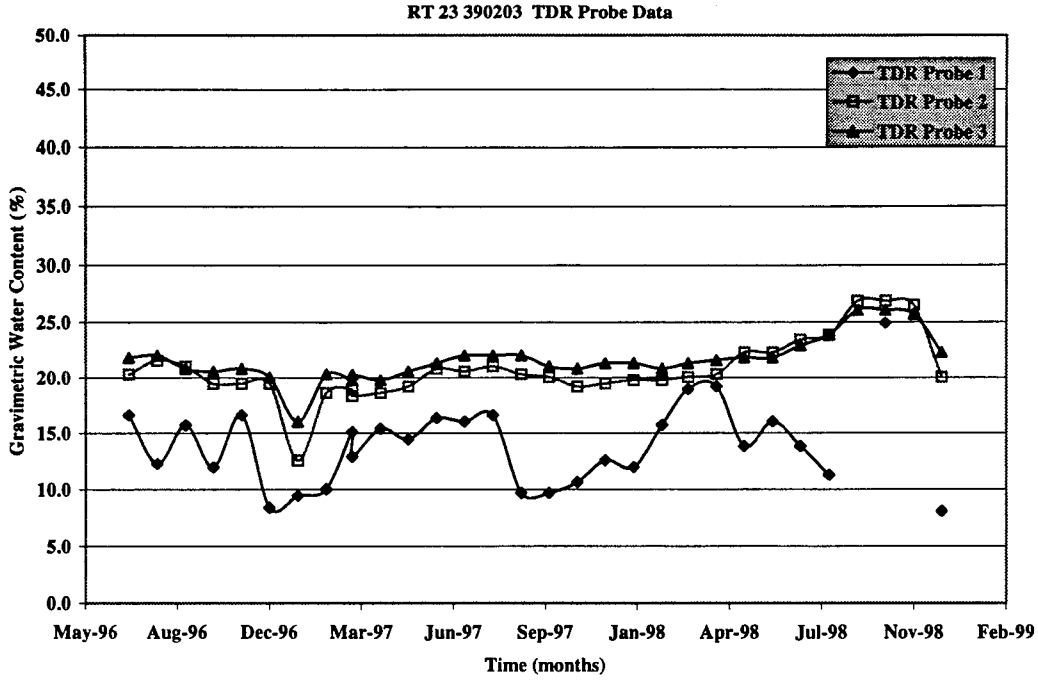

Figure 3.9: TDR Data 390203

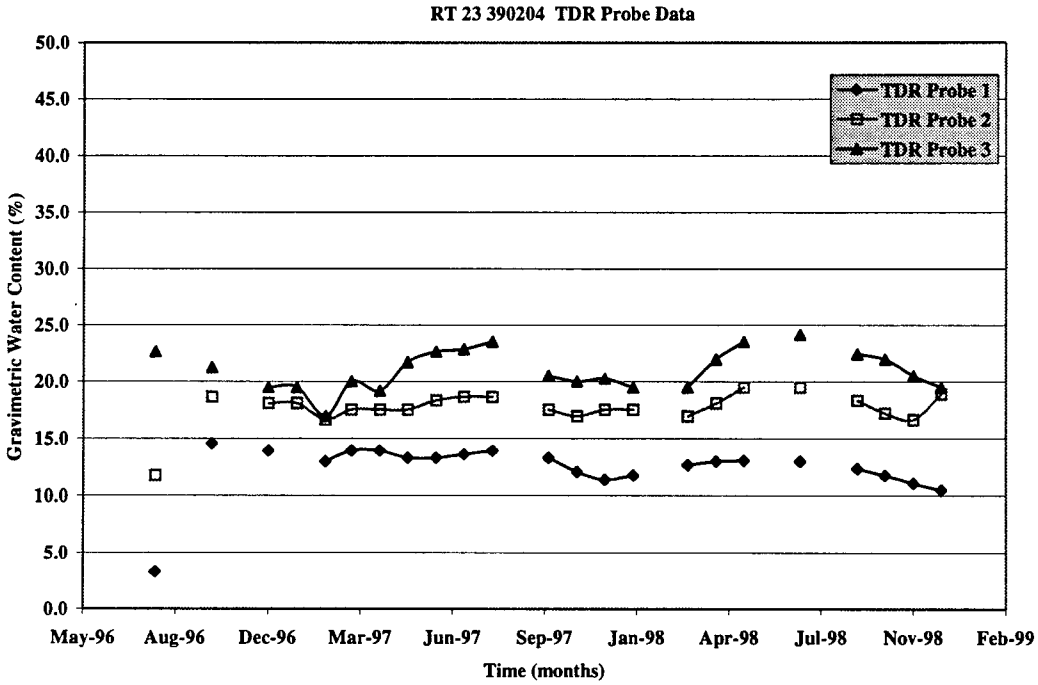

Figure 3.10: TDR Data 390204

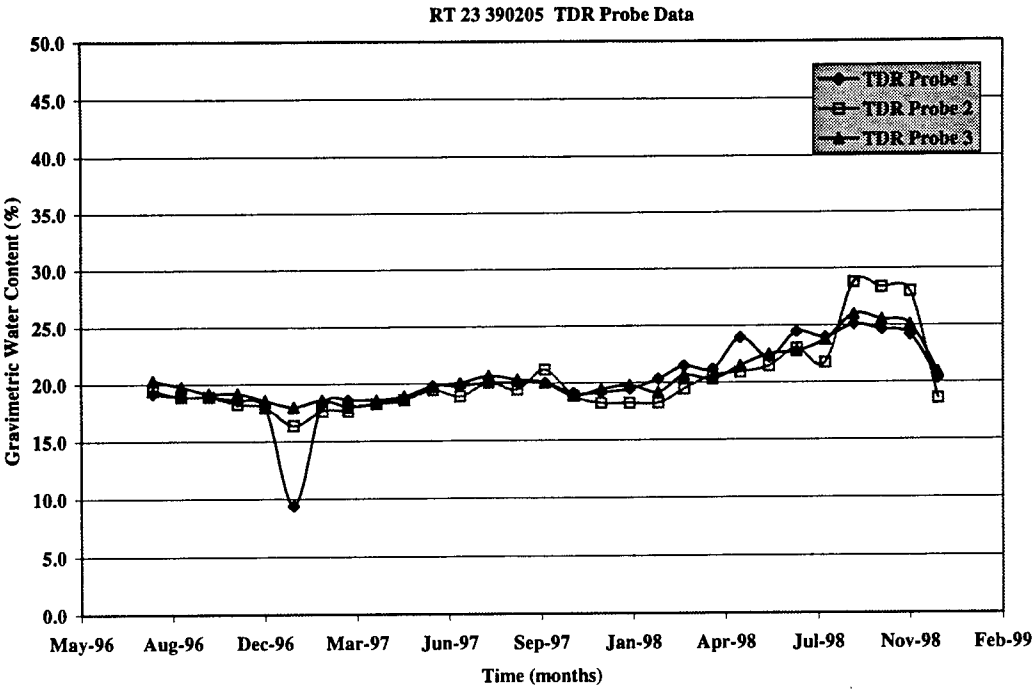

Figure 3.11: TDR Data 390205

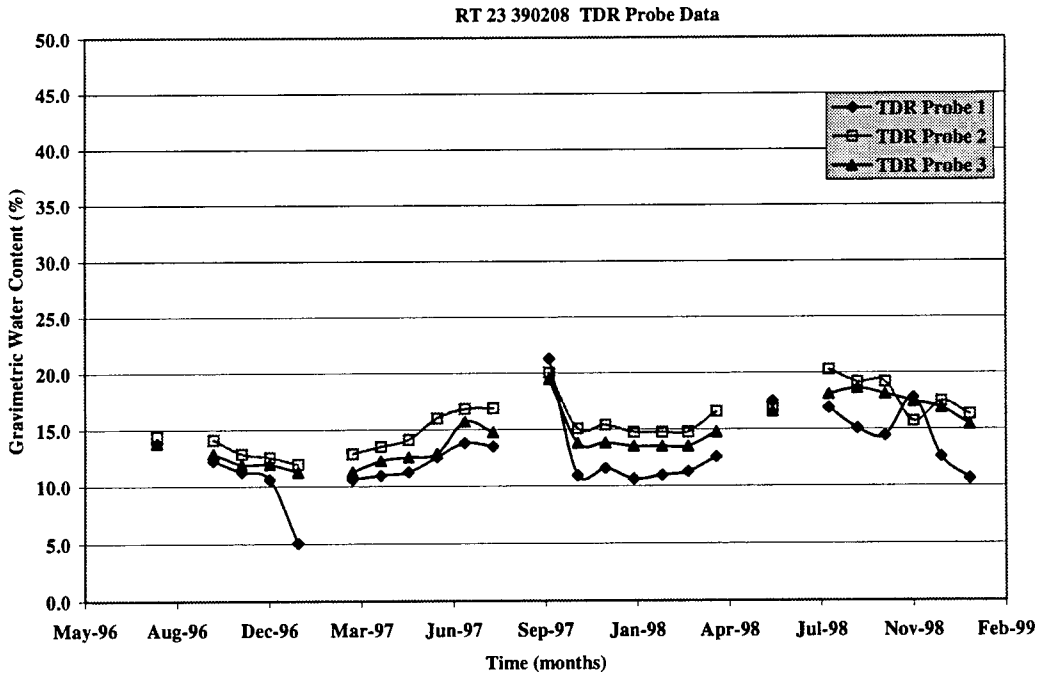

Figure 3.12: TDR Data 390208

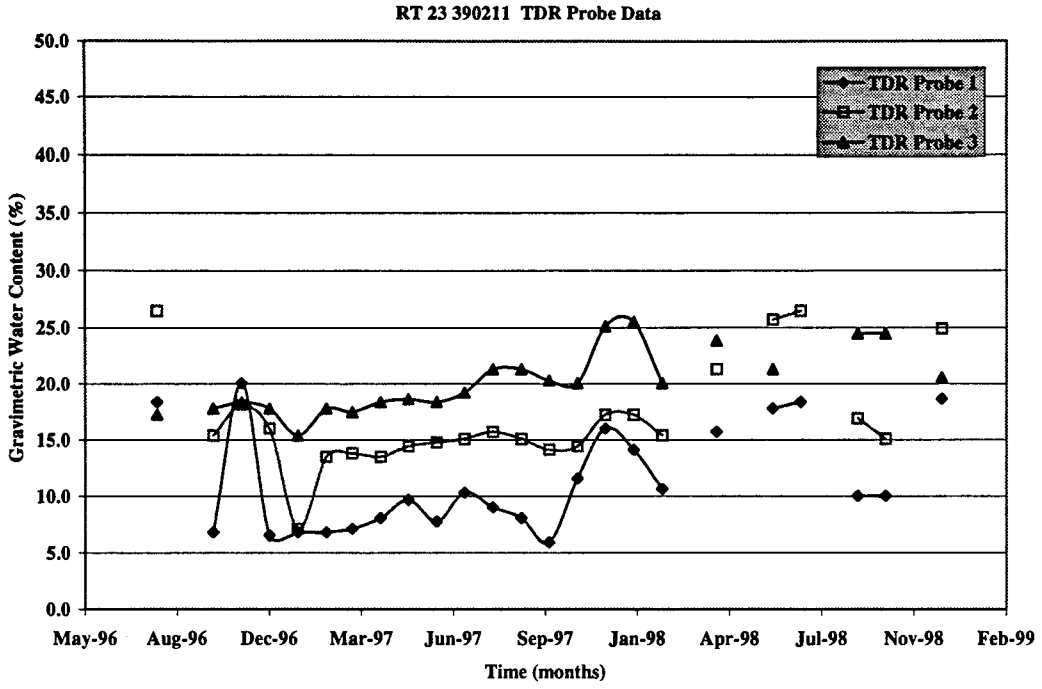

Figure 3.13: TDR Data 390211

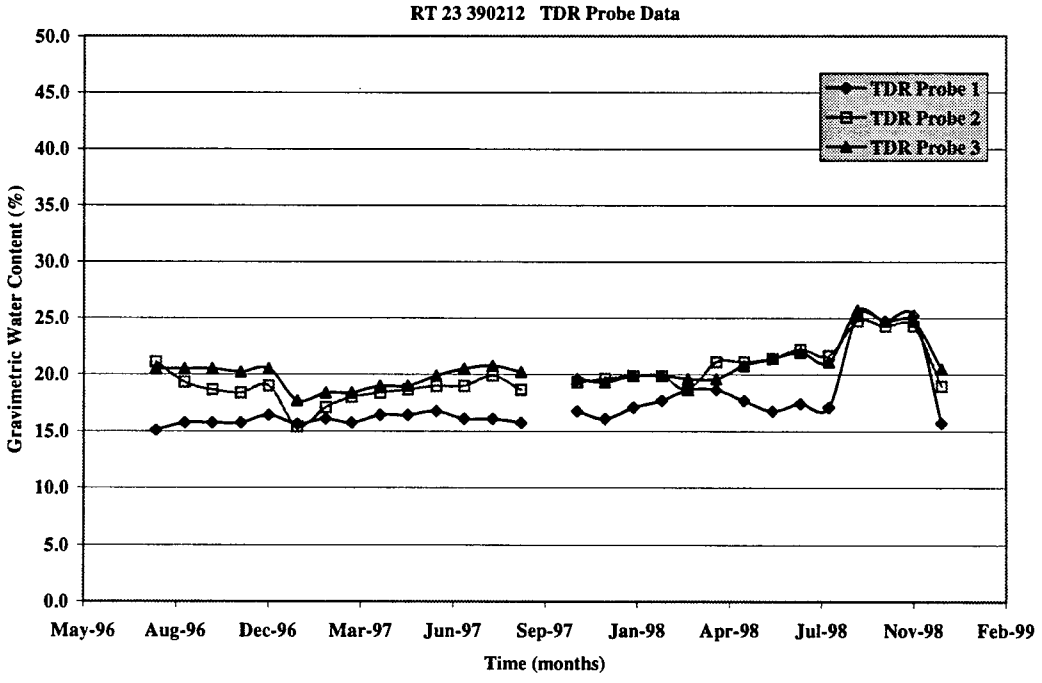

Figure 3.14: TDR Data 390212

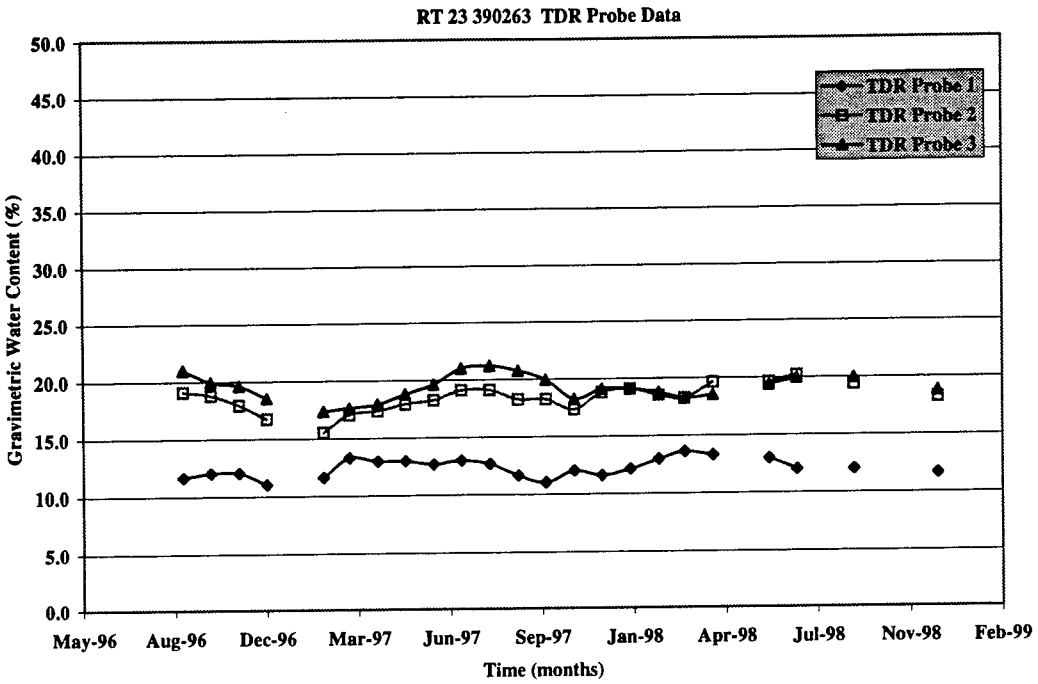

Figure 3.15: TDR Data 390263

Chapter 4

Analysis of Field Data

4.1 Falling Weight Deflectometer (FWD) Data

FWD data for the subgrade include deflection measurements for sets of drops at several hundred locations. At each location, four loads were applied twice each, for a total of eight drops with a circular plate having a radius of 150-mm (5.9-in.). The deflection measurements indicate the peak deflections measured at seven points on the surface at various distances from the center of the loaded area. The first of those points is directly under the load and is the only one considered here.

The Boussinesq equation is a theoretical relationship between the force applied at a point on the surface of an elastic half-space and the deflection at any point in the half-space. Some of the assumptions implicit in the Boussinesq equation are not entirely realistic for any real subgrade. It is assumed to be a linear, elastic, homogeneous, isotropic half-space; and the load is supposed to be applied uniformly over the circular area. That the subgrade is a half-space seems a reasonable approximation, but its linearity, elasticity, homogeneity, and isotropy are doubtful. Linearity may be tested through analysis of the FWD data but the other properties must be simply presumed.

For use with FWD data the Boussinesq equation may be integrated over a circular loaded area. If the pressure P is assumed to be uniform over a circle of radius r, the resulting deflection of the surface of the half-space at the center of the circle is

$$D = \frac{2r\left(1-\nu^2\right)P}{E} \qquad \text{(Equation 4.1)}$$

in terms of the elastic modulus E and the Poisson ratio ν. Assumption of uniform deflection under the load gives a different result:

$$D = \frac{\pi r\left(1-\nu^2\right)P}{2E} \qquad \text{(Equation 4.2)}$$

In this case, the pressure is not uniform; P is the average pressure on the loaded surface. The case of Equation 4.1 is approximated by a load applied through a flexible tire, while

Equation 4.2 is correct for a rigid loaded plate. The FWD load is between the two extremes but is probably closer to the case of Equation 4.2. Therefore, the equation used herein to compute the elastic modulus is from Equation 4.2,

$$E = \frac{\pi r\left(1-\nu^2\right)P}{2D} \qquad \text{(Equation 4.3)}$$

It will be noted that use of Equation 4.1 would result in modulus values 27 percent higher than those obtained from Equation 4.3. Additional information on this analysis is provided in Section 7.4.

To investigate the linearity of the subgrade, the best-fit modulus $\underline{E}$ and the deviation of the FWD data from a straight line were computed for each location. A Poisson ratio of 0.4 was assumed for calculations. Referring to Figure 4.1, observe that if the *i*th data point is plotted with $D_i\underline{E}$ on the horizontal axis and $\frac{1}{2}\pi r(1-\nu^2)P$ on the vertical axis, it should ideally fall on the line of unit slope. As in Figure 4.1, define d_i to be the deviation (distance) of point *i* from that line. Then it can be shown that

$$d_i = \frac{\frac{1}{2}\pi r\left(1-\nu^2\right)P - \underline{E}D_i}{\sqrt{2}}. \qquad \text{(Equation 4.4)}$$

The best-fit modulus is found by minimizing the sum of the deviations for all eight drops,

$$\frac{\partial}{\partial \underline{E}}\left(\sum_{i=1}^{8} d_i^2\right) = 0, \qquad \text{(Equation 4.5)}$$

which yields

$$\underline{E} = \frac{\frac{1}{2}\pi r\left(1-\nu^2\right)\sum_{i=1}^{8} P_i D_i}{\sum_{i=1}^{8} D_i^2}. \qquad \text{(Equation 4.6)}$$

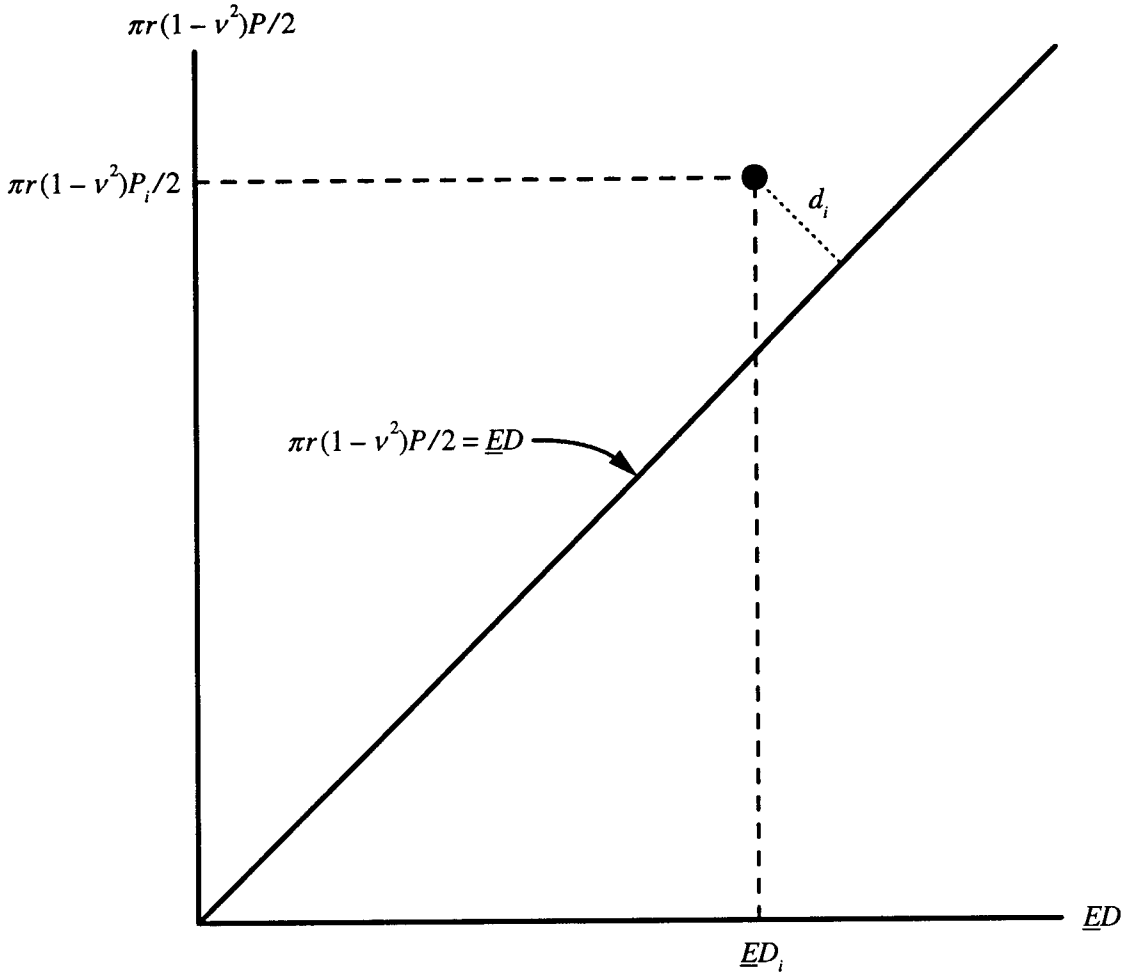

Figure 4.1: Illustration of deviation d_i for pressure P_i and deflection D_i for use in finding best-fit modulus $\underline{E}$.

The RMS (root-mean-squared) deviation provides a useful measure of the linearity of the data. At each location, the RMS deviation was calculated as

$$\Delta = \sqrt{\frac{1}{8}\sum_{i=1}^{8} d_i^2}\,, \qquad \text{(Equation 4.7)}$$

which is in units of force per unit length, or N/m. The corresponding dimensionless quantity,

$$\delta = \frac{\Delta}{\sqrt{\left[\tfrac{1}{2}\pi r\left(1-\nu^2\right)P_8\right]^2 + \left(\underline{E}D_8\right)^2}}\,, \qquad \text{(Equation 4.8)}$$

indicates the RMS deviation relative to the last drop; that is, the RMS deviation is equivalent to a deviation in pressure of $\pm P_8\delta$ and a deviation in deflection of $\pm D_8\delta$. Of course, the quantity δ could just as well have been calculated relative to the first drop. In that case δ would have been about twice as large since P_1 and D_1 are approximately half the size of P_8 and D_8.

Figure 4.2 plots the value of δ at each test location along the northbound and southbound lanes. It can be seen that for most locations δ is less than five percent, and it is less than fourteen percent for every location. The best fit for the worst location, Station 345+00 northbound, can be observed in Figure 4.3. The FWD results for that location are obviously erratic, particularly for the highest load. Figure 4.4 shows the fit for a typical location, Station 295+75 northbound, with $\delta = 0.023$. The linear fit here is excellent. Another location, Station 337+75 northbound, having a moderately high RMS deviation of $\delta = 0.051$ is shown in Figure 4.5. As that figure demonstrates, a five-percent deviation does not represent a significant degree of nonlinearity. Only 8.5 percent of the locations are worse than the one in Figure 4.5. Therefore, the assumption of linearity appears to be reasonable for the great majority of locations.

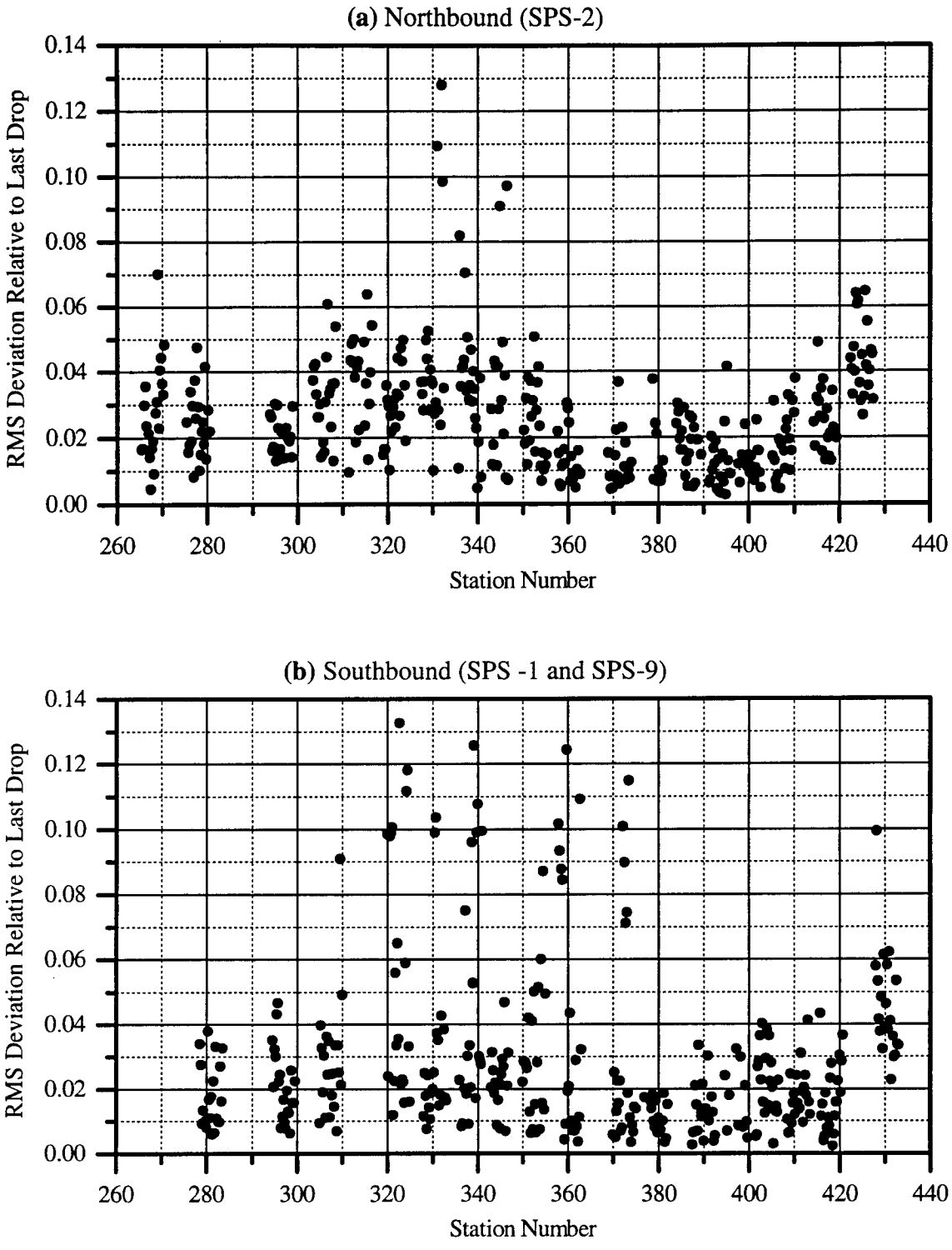

Figure 4.2: RMS deviation of pressure and deflection data from a straight line at each FWD test location, as a fraction of the measured pressure and deflection for the last drop.

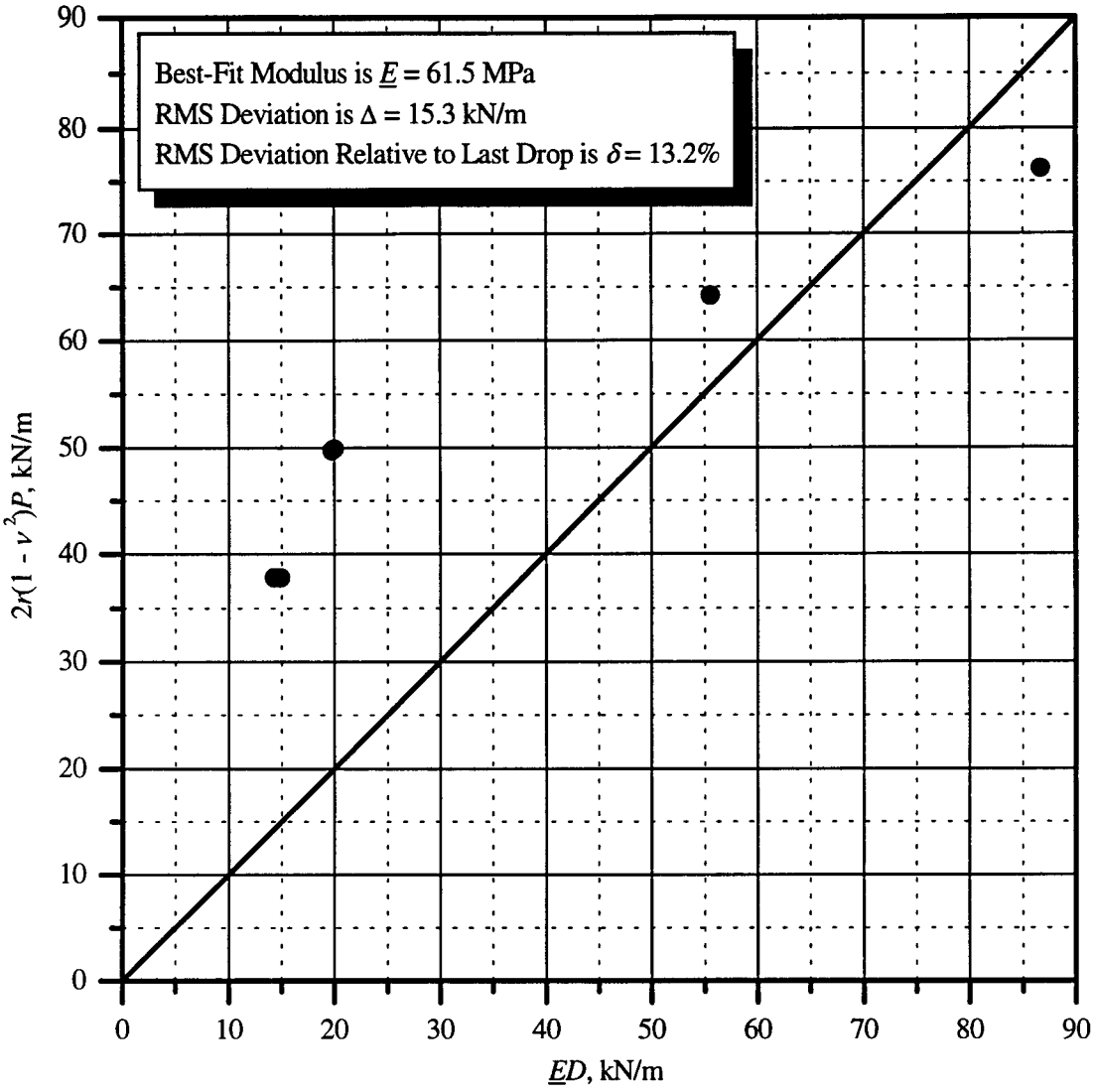

Figure 4.3: Pressure and deflection data and best-fit line for the location having the worst RMS deviation, Station 345+00 northbound.

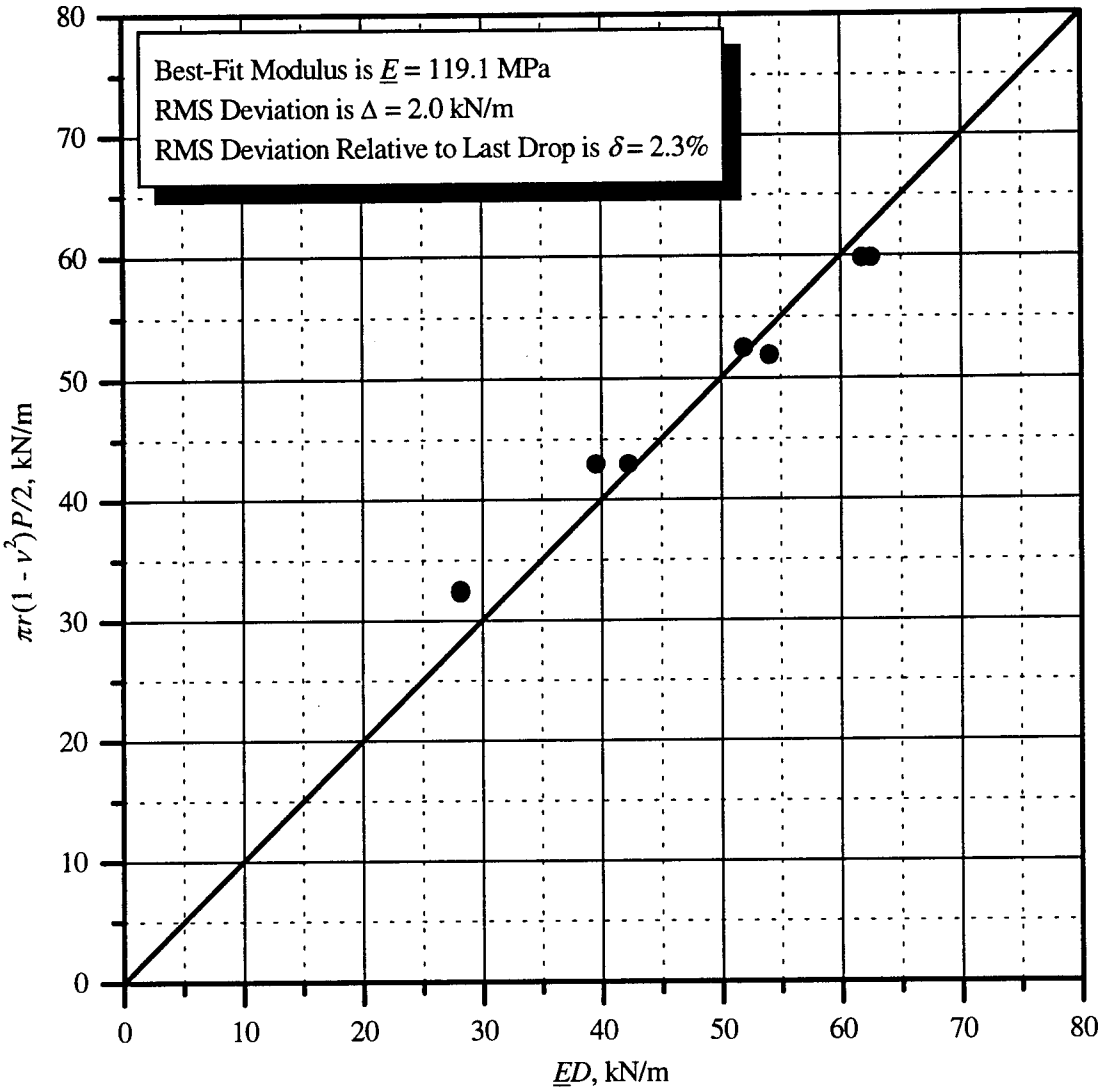

Figure 4.4: Pressure and deflection data and best-fit line for a location having a typical RMS deviation, Station 295+75 northbound.

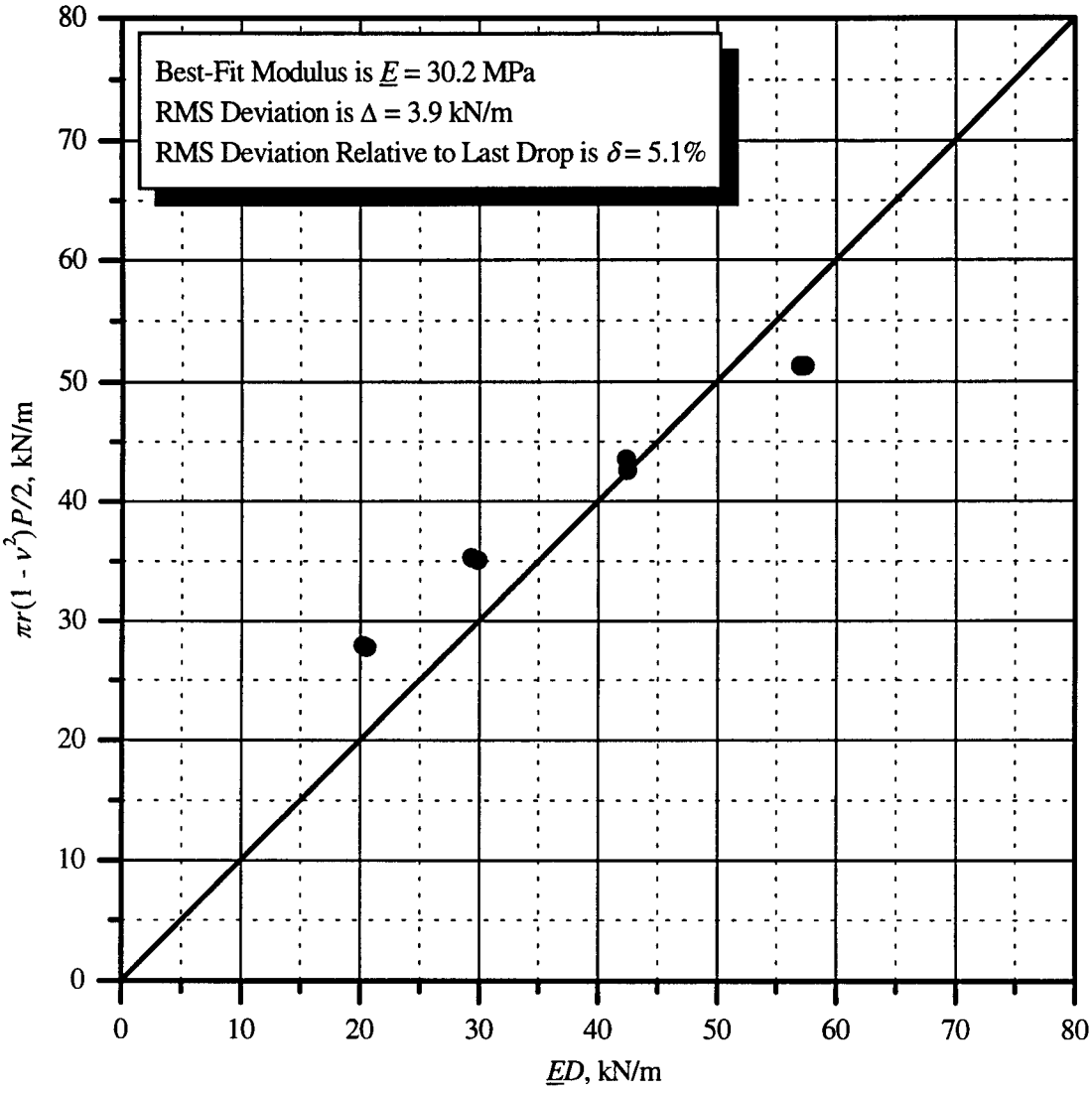

Figure 4.5: Pressure and deflection data and best-fit line for a location having a moderately high RMS deviation, Station 337+75 northbound.

With linearity established, the variability of the modulus was evaluated in several ways. First, Figure 4.6 shows $\underline{E}$ at each location along the northbound and southbound lanes, computed as in Equation 4.6. Next, Figure 4.7 presents the same data as histograms, and Figure 4.8 is a single histogram encompassing all the data. The modulus ranges from 14.3 to 423.2 MPa (2.1 to 61.4 ksi). The mean moduli,

$$\overline{E} = \frac{1}{n}\sum_{i=1}^{n} \underline{E}_i \,, \qquad \text{(Equation 4.9)}$$

in which $\underline{E}_i$ is the best-fit modulus for location i, are 100.8 MPa (14.6 ksi) for the northbound lane, 108.9 MPa (15.8 ksi) for the southbound lane, and 104.6 MPa (15.1 ksi) for both lanes combined. The standard deviation of the $\underline{E}$ values was calculated for each lane individually and for the entire project by

$$\sigma_{\underline{E}} = \sqrt{\frac{1}{n-1}\sum_{i=1}^{n}\left(\underline{E}_i - \overline{E}\right)^2} \qquad \text{(Equation 4.10)}$$

and the coefficient of variation was likewise calculated by

$$V_{\underline{E}} = \frac{\sigma_{\underline{E}}}{\overline{E}} \,. \qquad \text{(Equation 4.11)}$$

Table 4.1 lists the mean, standard deviation, and coefficient of variation for each lane and for the entire project. It must be noted that the standard deviations are very large, indicating—as do Figures 4.6-4.8—a high degree of variability in the subgrade modulus.

Table 4.1: Mean, standard deviation, and coefficient of variation of the modulus as computed from the FWD data.

Locations	Mean Modulus (MPa)	Standard Deviation (MPa)	Coefficient of Variation
Northbound (SPS-1)	100.8	57.2	0.567
Southbound (SPS-1 and SPS-9)	108.9	56.1	0.515
Entire Project	104.6	56.8	0.543
Note: 1 MPa = 145 psi			

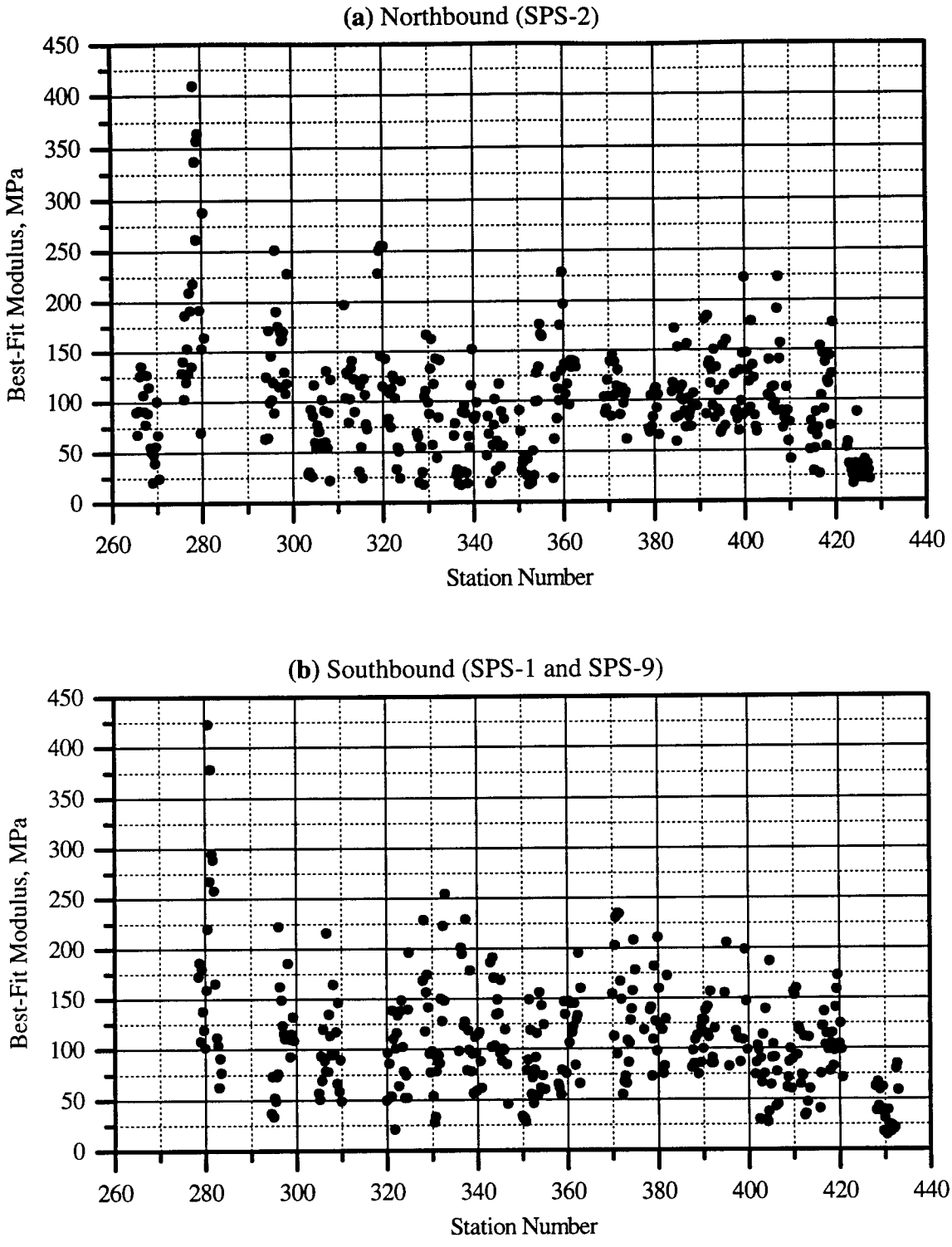

Figure 4.6: Best-fit modulus at each FWD test location.

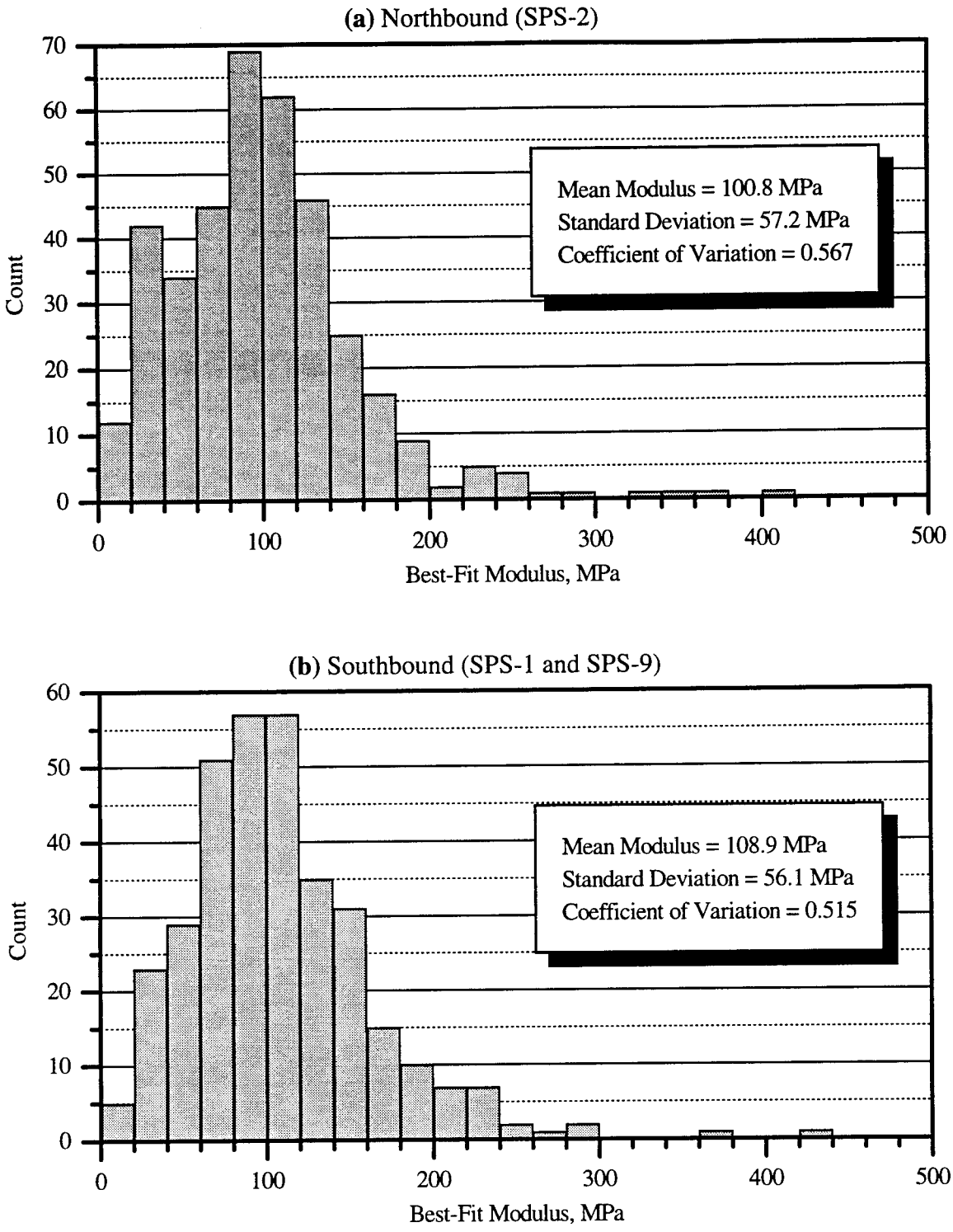

Figure 4.7: Histograms of the best-fit moduli from Figure 4.6.

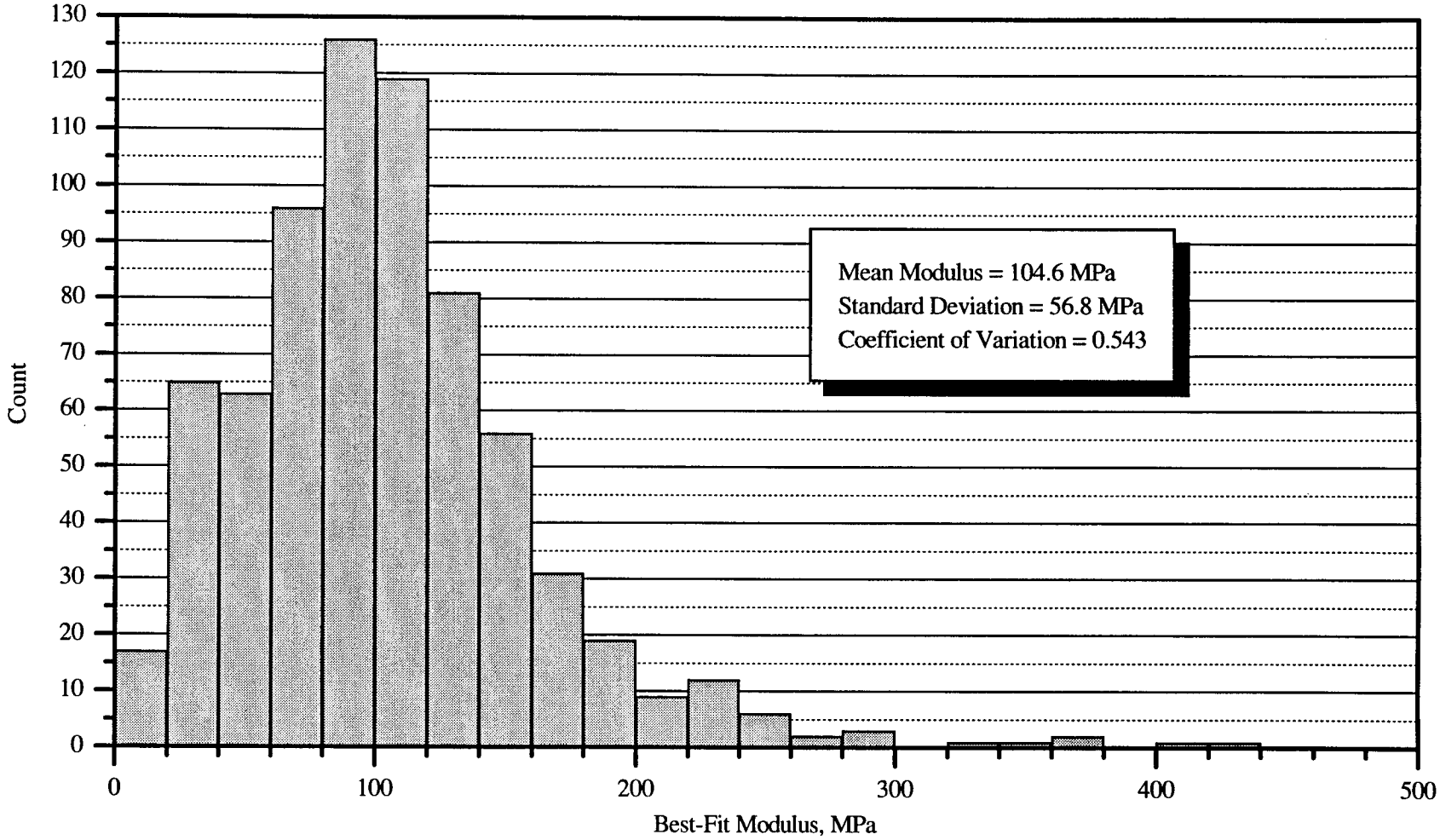

Figure 4.8: Histogram of best-fit moduli for all mainline sections.

Next, the variability within each section was examined. Tables 4.2 and 4.3 list for each section the maximum and minimum moduli, the mean modulus, the standard deviation, and the coefficient of variation. These quantities were calculated from the best-fit moduli at each location by Equations 4.9–4.11. It is apparent that the subgrade modulus fluctuates widely even within a single section.

4.2 Moisture and Density Data

The moisture and density data were acquired at only two or three locations within each test section. Because those locations never coincided with FWD test locations, it was not possible to develop a meaningful relationship between the moisture content and density readings, and the modulus results found in the previous section. Moreover, it should be emphasized that moisture and density were sampled at about 30 cm (12 in.) below the subgrade surface. Thus, while FWD testing measures the composite response of several layers of subgrade, the moisture and density data represent only a single layer of soil.

The moisture-content measurements at various locations can be seen in Figure 4.9. Similarly, Figure 4.10 illustrates the density measurements. Figure 4.11 presents a plot of moisture against density. It evinces no clear correlation between the two quantities.

Figure 4.12 shows the best-fit moduli from Equation 4.6 plotted as a function of moisture content. Only those FWD locations within 10 m of a moisture/density sampling point were included. Figure 4.13 is the comparable plot for density. These figures would appear to deter further attempts to relate the single-layer moisture or density to the modulus found by Boussinesq's equation.

Table 4.2: Minimum, maximum, and mean modului, standard deviation, and coefficient of variation for each Northbound section (SPS-2).

Section Number	Minimum Modulus (MPa)	Maximum Modulus (MPa)	Mean Modulus (MPa)	Standard Deviation (MPa)	Coefficient of Variation
390201	18.6	117.0	62.4	28.6	0.459
390202	23.7	255.0	123.4	70.0	0.567
390203	58.8	171.9	103.0	28.2	0.274
390204	69.3	409.2	205.3	95.4	0.465
390205	16.9	151.6	64.3	37.1	0.576
390206	17.5	166.3	87.8	46.1	0.524
390207	67.3	183.9	117.8	36.2	0.307
390208	68.6	222.2	112.7	39.0	0.346
390209	17.3	176.4	71.6	54.1	0.756
390210	21.7	130.5	71.1	31.4	0.441
390211	61.6	145.2	109.3	21.2	0.194
390212	63.1	251.2	140.9	49.0	0.348
390259	20.5	135.5	79.0	33.9	0.429
390260	24.3	196.6	101.5	41.6	0.409
390261	23.1	228.6	124.1	43.9	0.353
390262	41.4	222.4	107.8	42.6	0.396
390263	26.4	176.8	93.7	42.7	0.455
390264	17.2	87.2	34.3	15.8	0.459
390265	65.9	112.2	88.7	18.3	0.207
Note: 1 MPa = 145 psi					

Table 4.3: Minimum, maximum, and mean modului, standard deviation, and coefficient of variation for each southbound section (SPS-1 and SPS-9).

Section Number	Minimum Modulus (MPa)	Maximum Modulus (MPa)	Mean Modulus (MPa)	Standard Deviation (MPa)	Coefficient of Variation
390101	28.2	155.6	80.6	40.1	0.498
390102	54.5	234.8	140.5	58.3	0.415
390103	40.5	172.1	108.2	30.2	0.279
390104	56.1	228.8	116.2	48.7	0.419
390105	74.5	156.5	107.2	22.8	0.213
390106	45.7	190.6	123.3	40.9	0.332
390107	54.8	195.3	115.6	39.4	0.341
390108	81.9	205.3	130.7	44.0	0.336
390109	27.0	186.4	79.4	39.2	0.493
390110	33.6	159.3	89.3	37.5	0.420
390111	27.5	254.5	124.7	62.0	0.497
390112	20.6	196.0	95.3	43.4	0.455
390159	14.3	84.3	39.8	22.0	0.554
390160	72.5	210.4	128.5	38.6	0.300
390901	62.3	423.2	186.0	99.6	0.536
390902	33.4	222.2	106.9	47.8	0.447
390903	48.7	215.5	98.8	41.1	0.416
Note: 1 MPa = 145 psi					

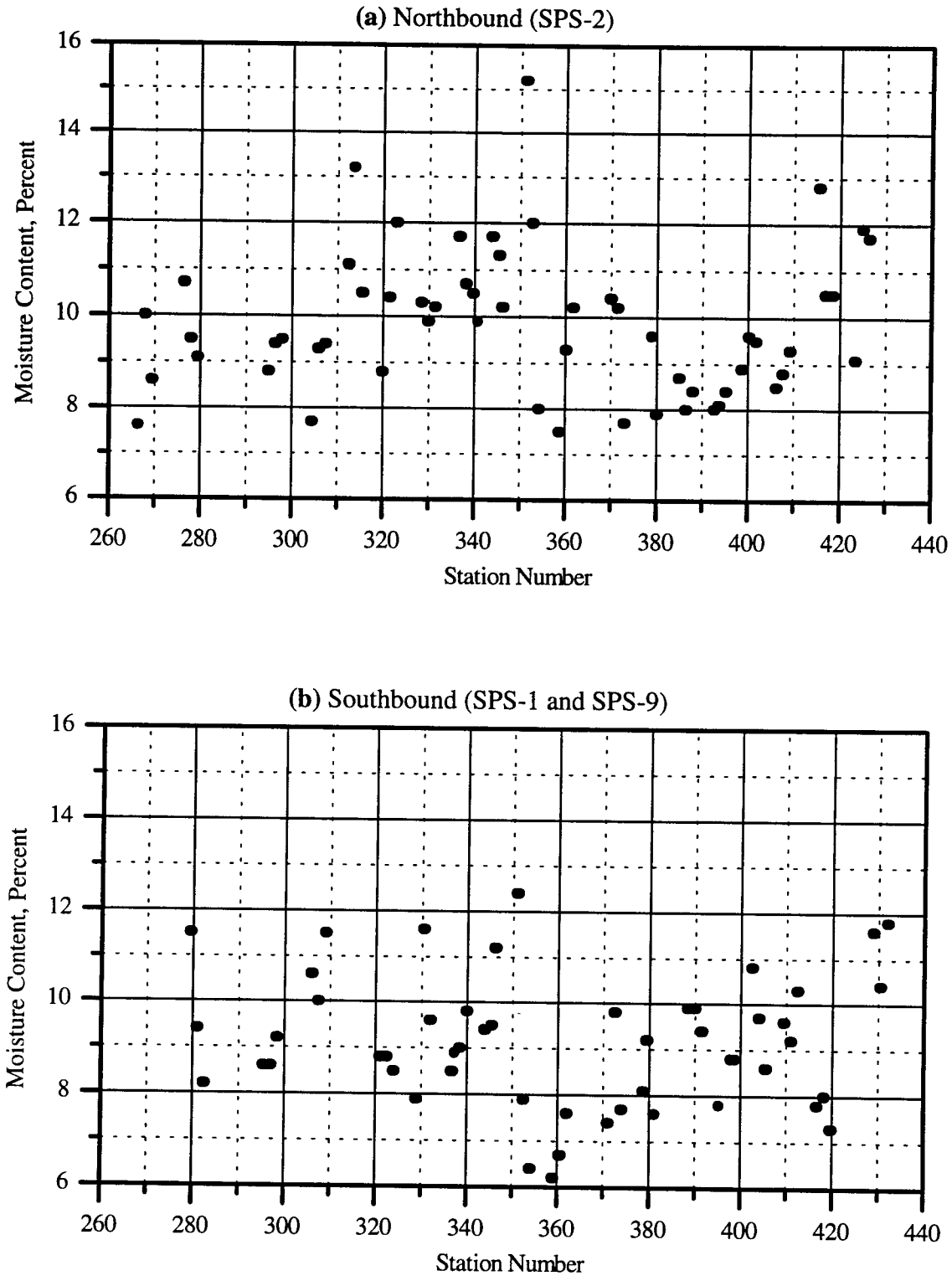

Figure 4.9: Moisture-content measurements at various locations.

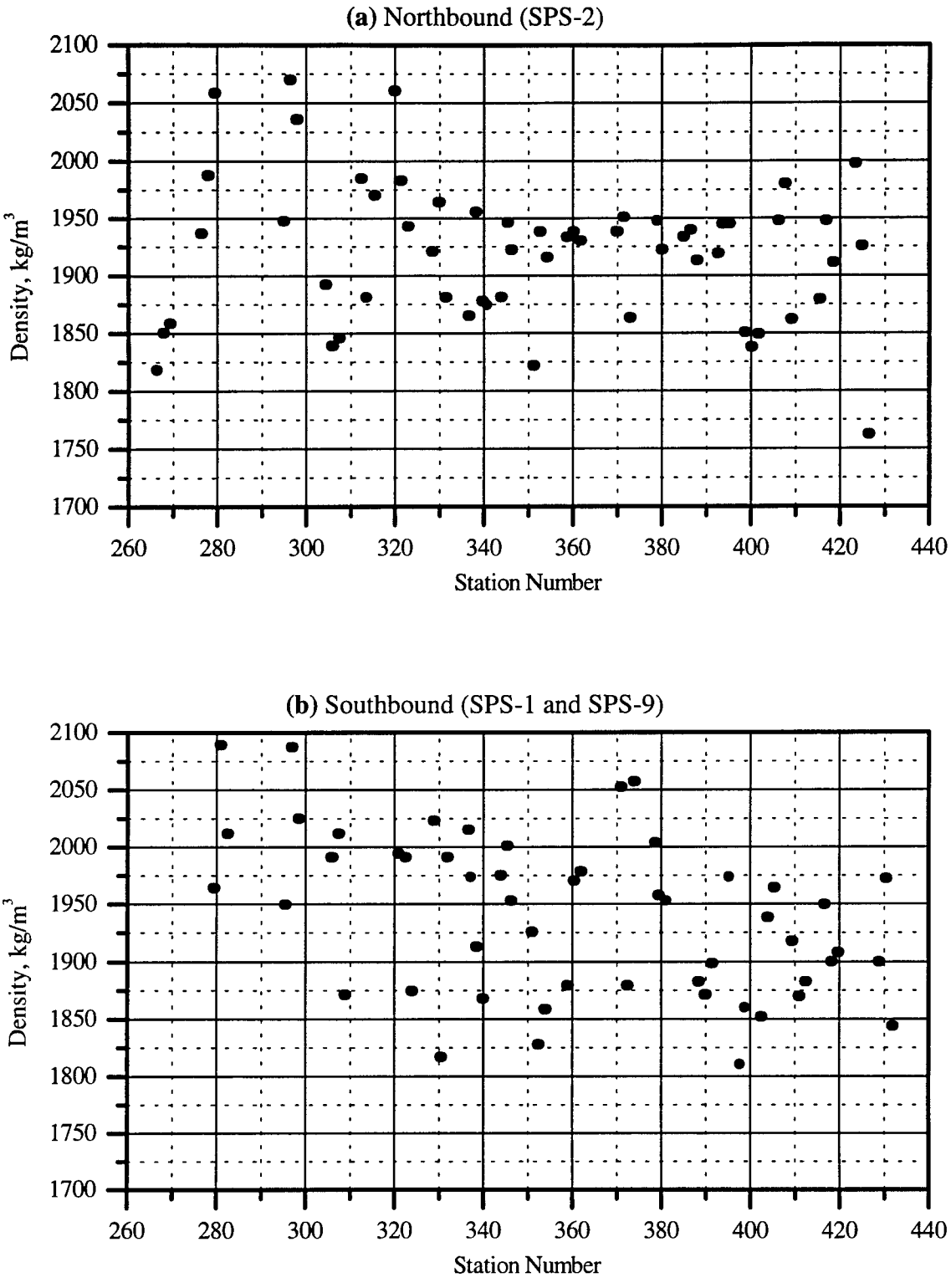

Figure 4.10: Density measurements at various locations.

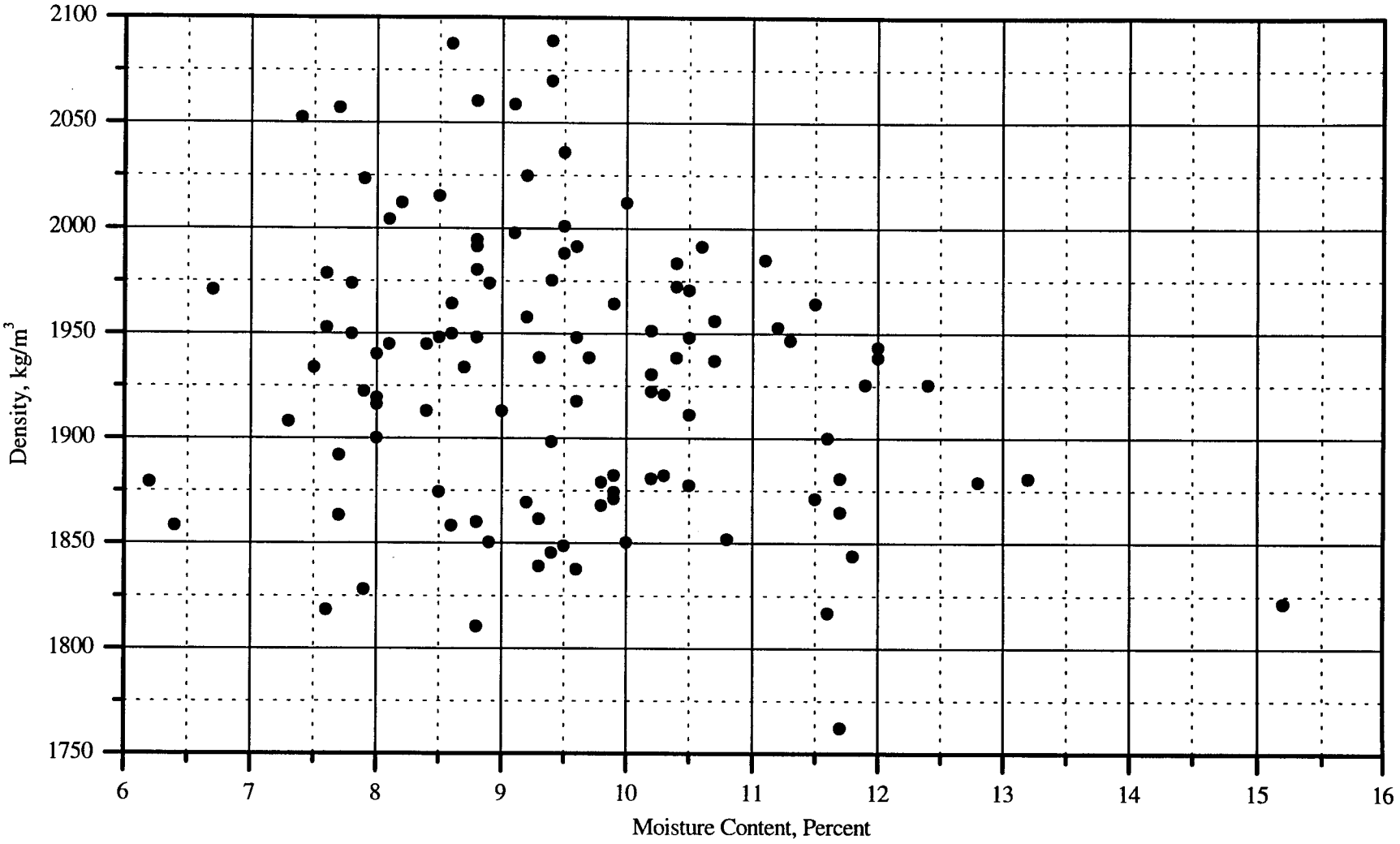

Figure 4.11: Observed relationship between density and moisture.

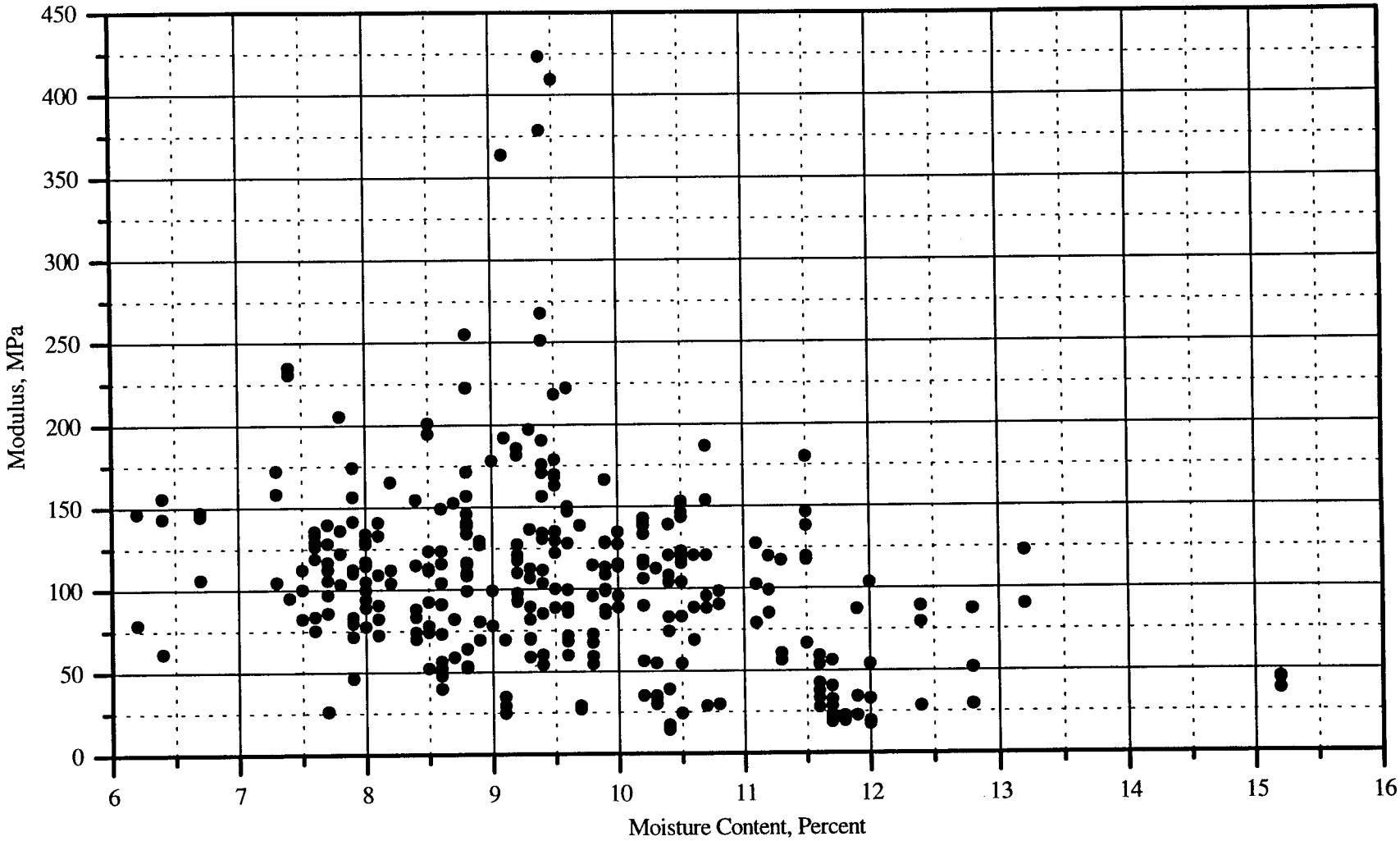

Figure 4.12: Modulus values from FWD tests within 30 m of a moisture sample.

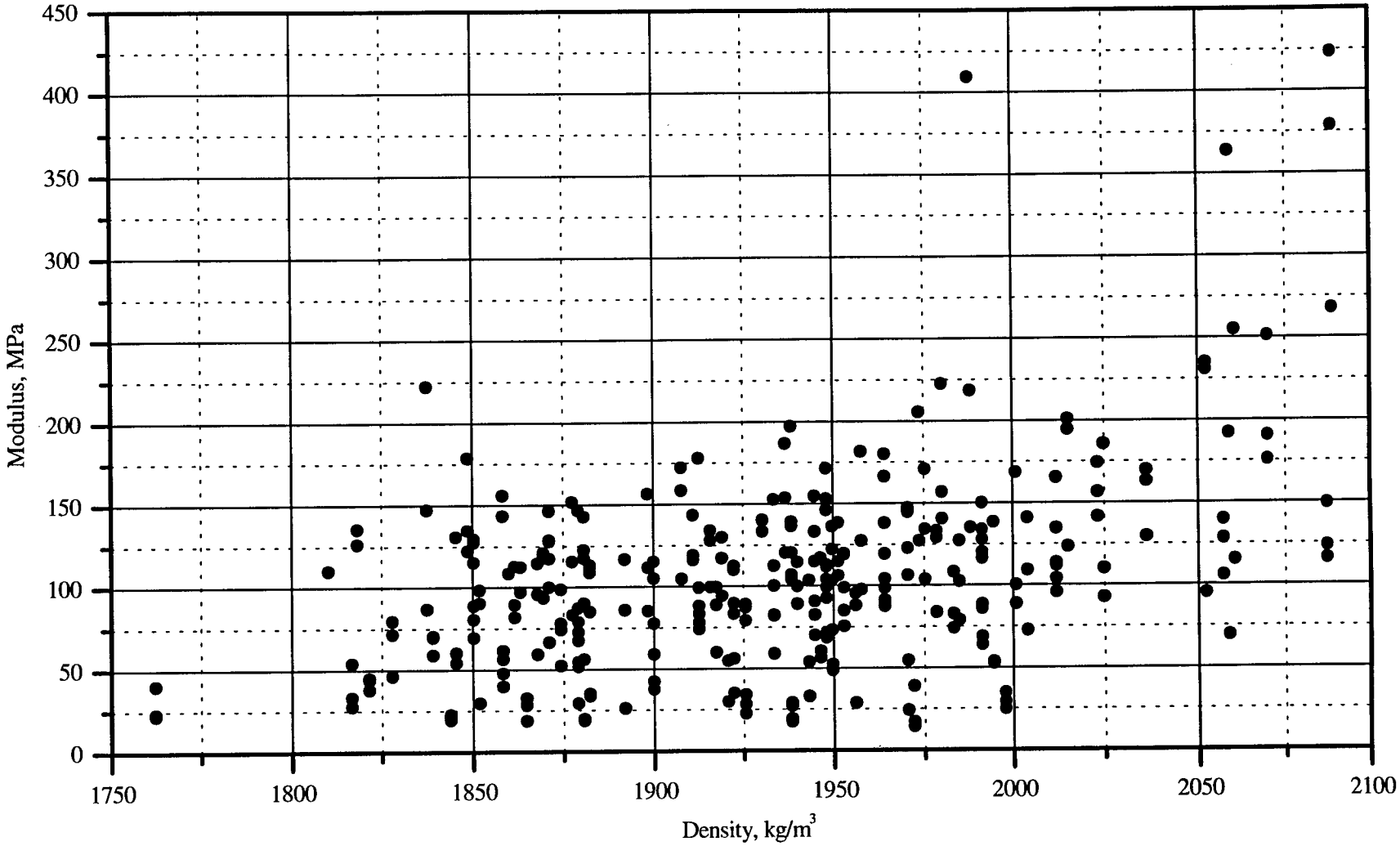

Figure 4.13: Modulus values from FWD tests within 30 m of a density sample.

Chapter 5

Laboratory Resilient Modulus Testing of Subgrade Soils

5.1 Introduction

Representative samples of the subgrade soil were subjected to resilient modulus testing (SHRP Protocol P-46) in the OU-ORITE laboratory. SHRP requires each sample be tested at or near the in-situ moisture and density conditions. However, laboratory work done in the current study exceeded the SHRP requirement in that each soil sample, compacted as close to its in-situ dry density as possible, was tested at a minimum of three different moisture contents. This was done to reflect the fact that the during the subgrade preparation, the control on the moisture content was not as good as that on the dry unit weight (or compaction rate). The moisture contents varied widely in the field during construction. In addition, during the span of the field study, the moisture conditions of the subgrade soils are expected to fluctuate due to seasonal and year-to-year variations in the climate. The following summarizes information on the test system, test procedure, soil samples tested, and test results.

5.2 System Description

The resilient modulus test system utilized in this study is state-of-the-art equipment, which features a large triaxial chamber, an electro-servo controlled actuator, and computerized signal conditioning, load command generation, and data acquisition. Figure 5.1 shows 17 components in the system. Seven Major components include the following:

1) Triaxial Pressure Chamber: The chamber is an acrylic cylinder, reinforced with stainless steel tapes. Its pressure rating is 1034.2 kPa (150 psi). It is large enough to accept up to a 15.24-centimeter (6-inch) diameter, 30.48-centimeter (12-inch) height specimen. It incorporates a top assembly, which includes the hydraulic actuator and linear variable differential transformers (LVDTs).

2) Loading Actuator: The closed-loop servo electro-hydraulic controlled actuator is compact enough to rest within the top assembly for the triaxial chamber. The actuator

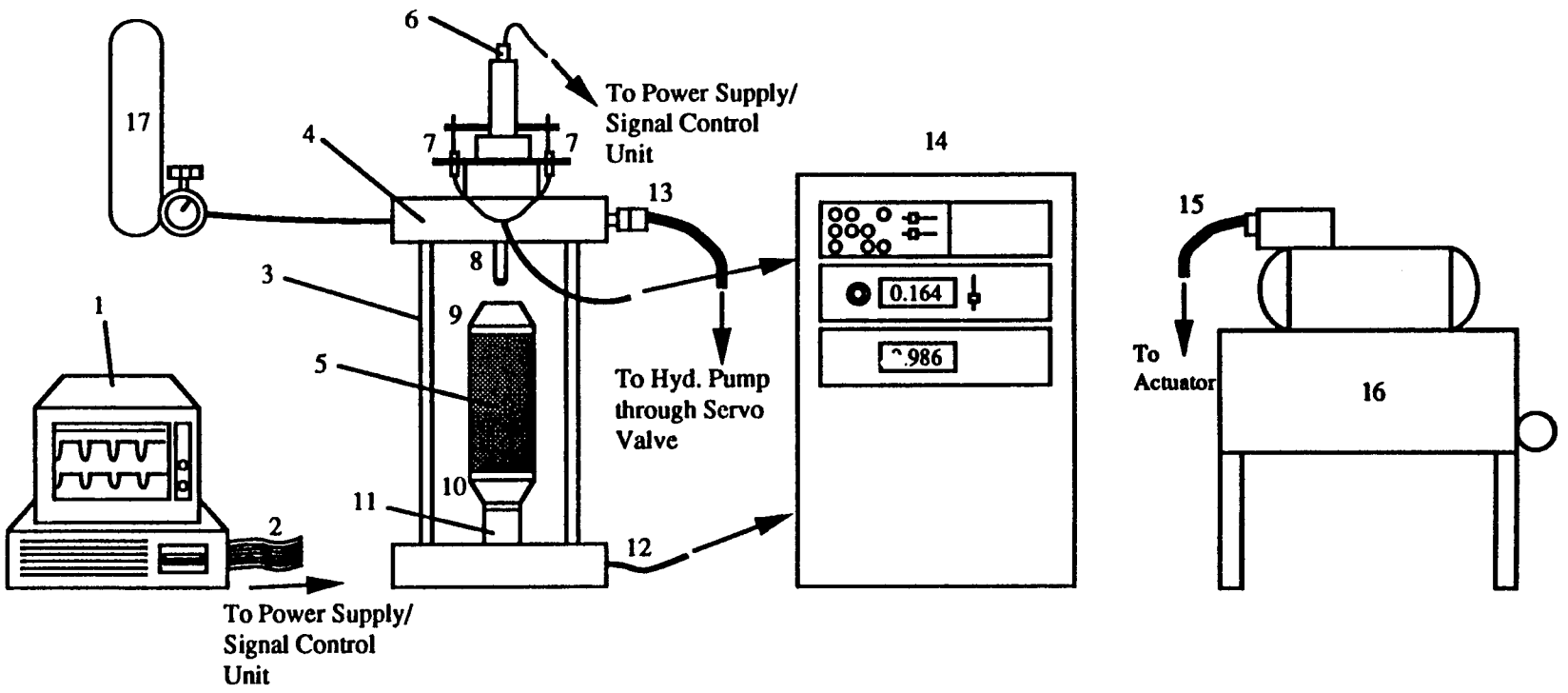

1 - IBM PC

2 - Interface Ribbon Cable

3 - Trixial Chamber

5 - Test Specimen in Rubber Membrane

6 - System LVDT

7 - Mineature LVDTs

8 - Actuator Piston

9 - Top End Platen

10 - Bottom End Platen

11 - Load Cell

12 - Cable for Load Cell

13 - Hydraulic Hose Attachment

14 - Power Supply/Signal Conditioning Unit for Servo Valve, Load Cell, and LVDTs

15 - Hydraulic Hose Attachment

16 - Hydraulic Pump

17 - Air Pressure Source

Figure 5.1. Overall Set-Up of Resilient Modulus Test System

piston has a total stroke ± 6.35 centimeters (± 2.5 inches) and is capable of applying cycles of user-specified wave form (ex. haversine) repeatedly by receiving signals from the computer unit.

3) Computerized Signal Generator/Data Acquisition System: The IBM computer, along with power supply and signal conditioning units for the sensors make up this system. Signal conditioning of each sensor can be done either manually or electronically. The software in the computer is specifically developed to perform the resilient modulus test. It features digital gain controls, real time display of the sensor readings and resilient modulus during each load sequence, basic data analysis, and report generation capabilities.

4) Hydraulic Pump: The manually operated hydraulic pump supplies approximately 6894.7 kPa (1,000-psi) working pressure to the actuator for loading.

5) Compressed Air Source: The confining pressure needed during the resilient modulus testing is supplied through a compressed air source and controlled manually by a pressure regulator.

6) Load Cell: This strain-gauge based load cell has a capacity of 635-kg (1,400-lbs.) and situated just below the lower platen, inside the triaxial chamber.

7) Linear Variable Differential Transformers (LVDTs): Three LVDTs are used to measure deformations in the test specimen during each test. A long-range (± 25 mm, ± 1.0-inch range) LVST, called the system LVDT, is mounted within the top assembly. The two miniature LVDTs, having a range of ± 6.35mm (± 0.25 inch), can be mounted coaxially either on the loading piston or on the test specimen directly through a pair of ring clamps.

5.3 Typical Test Procedure

Laboratory test procedures employed in this study complied with standard SHRP protocol P-46. The following is a systematic account of the test procedure, which applies only to the cases in which a disturbed sample of cohesive soil material is utilized to prepare the test specimen.

Step 01: Obtain an air-dried, well-pulverized soil sample. Add a desired amount of water to the soil. Mix the soil and water thoroughly. Leave the soil/water mixture inside a sealed container at a normal room temperature for at least 12 hours.

Step 02: Compact the soil in five lifts inside a 7.112-cm (2.8-in.) diameter split mold by applying the static compaction method described in Attachment C to the SHRP Protocol P46.

Step 03: Extract the soil specimen from the split mold. Measure its diameter, height, and total mass.

Step 04: Place the soil specimen between the top and bottom platens. Cover the soil specimen with a rubber membrane. Install rubber O-rings to seal the membrane ends.

Step 05: Place the soil specimen plus the platens into the triaxial chamber. Connect the drainage line to the bottom platen.

Step 06: Complete the assembly of the triaxial chamber.

Step 07: Lower the loading piston so that it would apply a small seating load to the top platen. Apply a confining pressure of 41.4 kPa (6 psi).

Step 08: Adjust all the sensor (load cell, LVDTs) readings to zero.

Step 09: Begin initial conditioning load cycles (see Table 5.1). During this stage, adjust the gain on the loading to optimize the deformation response.

Step 10: At the end of the initial conditioning, start the load sequences. Go through the load sequences from top to bottom as they appear in Table 5.1. Occasionally change the confining pressure.

Step 11: At the completion of the test, measure the final specimen height. Break the specimen in two halves. Take two moisture content test samples. Determine the moisture content by placing these soil samples into a standard laboratory oven.

Step 12: Get a hard copy of the data as well as a disk copy. Analyze the data.

Table 5.1: Loading Sequence for Resilient Modulus Test

Load Sequence No.	Confining Pressure kPa (psi)	Deviator Stress kPa (psi)	Number of Load Applications
0	41.4 (6.0)	27.6 (4.0)	500
1	41.4 (6.0)	13.8 (2.0)	100
2	41.4 (6.0)	27.6 (4.0)	100
3	41.4 (6.0)	41.4 (6.0)	100
4	41.4 (6.0)	55.2 (8.0)	100
5	41.4 (6.0)	68.9 (10.0)	100
6	27.6 (4.0)	13.8 (2.0)	100
7	27.6 (4.0)	27.6 (4.0)	100
8	27.6 (4.0)	41.4 (6.0)	100
9	27.6 (4.0)	55.2 (8.0)	100
10	27.6 (4.0)	68.9 (10.0)	100
11	13.8 (2.0)	13.8 (2.0)	100
12	13.8 (2.0)	27.6 (4.0)	100
13	13.8 (2.0)	41.4 (6.0)	100
14	13.8 (2.0)	55.2 (8.0)	100
15	13.8 (2.0)	68.9 (10.0)	100

[Note]: Load Sequence No. 0 constituted the initial conditioning load cycles.

5.4 Description of Subgrade Soil Samples

A total of 15 bag samples of the subgrade soil were recovered in the field and transported to the OU-ORITE laboratory for further testing. These included six samples from SPS-1 (390106, 390107, 390108, 390110, 390111, and 390160), six samples from SPS-2 (390202, 390205, 390207, 390209, 390211, and 390262), two samples from SPS-8 (390809 and 390810), and one sample from SPS-9 (390902). For these soil samples, the in-situ moisture and dry unit weight data were recorded by a nuclear gauge at the time of subgrade preparation. Based on the soil classification data supplied by ODOT (see Section 2.2), the soil samples were divided into the following three groups:

* A-7-6 Group ------- 390107.
* A-6 Group ---------- 390111, 390202, 390205, 390207, 390211, 390262.
* A-4/A-4a Group --- 390110, 390160, 390809, 390810, 390902.

Three soil samples (390106, 390108, 390209) not mentioned above could not be placed into one of the soil groups due to insufficient data.

5.5 Test Results

During each test, the test specimen was subjected to a total of fifteen load sequences, as listed in Table 5.1. Each load sequence actually consisted of one hundred repetitions of a load cycle. The load applied in each load cycle had a pulse-type stress wave form, as shown in Figure 5.2, and the computerized data acquisition system stored sensor readings from the last five load cycles and computed the mean values.

Typical test data obtained during Test No. 5 (on Soil Sample 390810) are summarized in Table 5.2. The resilient modulus remained high at low levels of deviator stress. As the deviator stress increased, the resilient modulus sharply decreased. The resilient modulus stayed almost constant beyond the deviator stress of about 62.1 kPa (9-psi). Effect of confining stress was negligible on the resilient properties of the all three soil types. Figure 5.3 is a standard graphical presentation of the same data, using a log-log scale. Here, a strong correlation was found between the resilient modulus (M_r) and

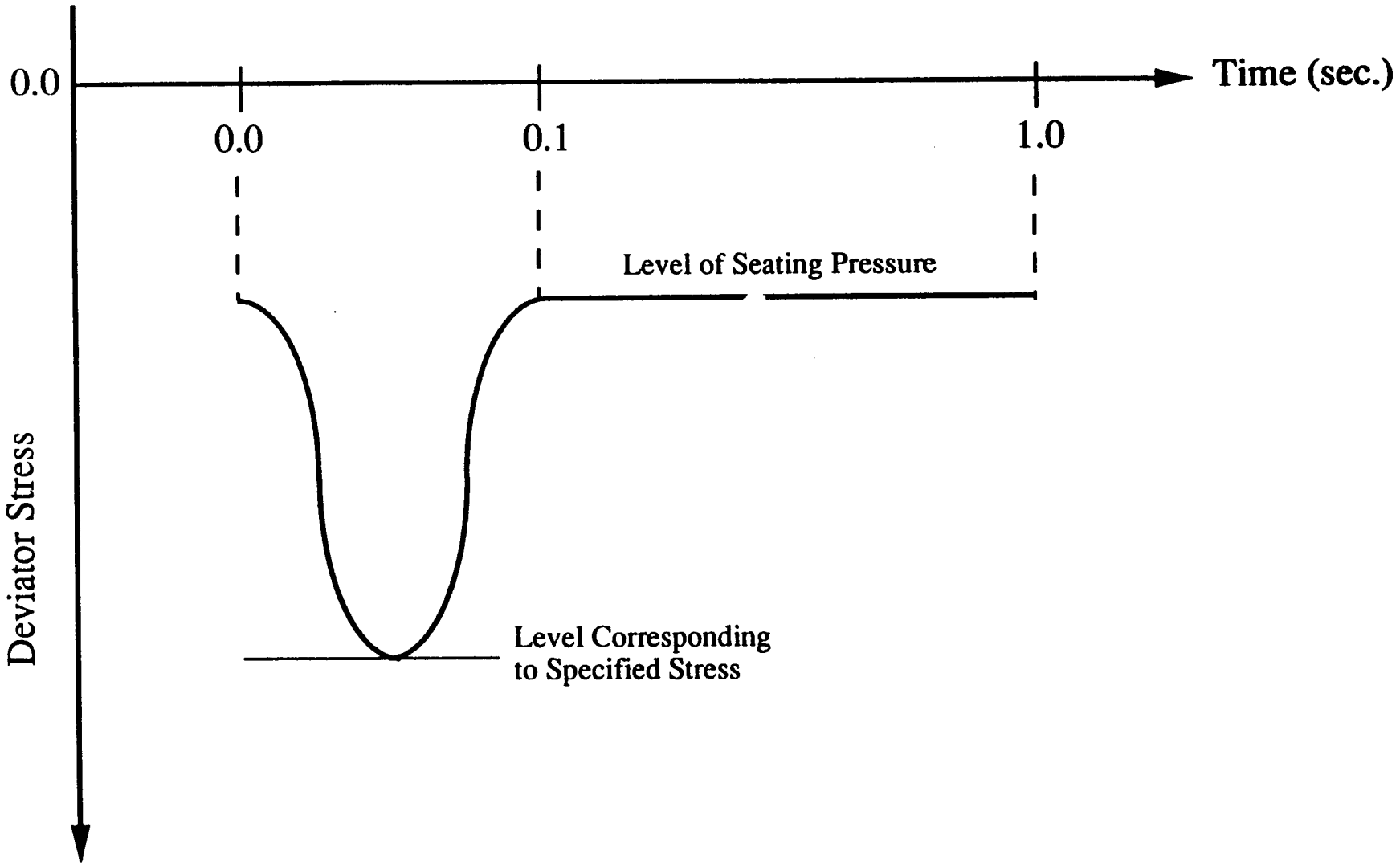

Figure 5.2: Stress Wave Form of a Typical Load Cycle

Table 5.2: Typical Resilient Modulus Test Data

Test No. :	5	
Soil Type :	A-4	
Section No. :	390810	
Specimen Size :	Diameter	= 70.6 mm (2.78 in.).
	Height	= 153.7 mm (6.05 in.).
Moisture Content :	18.1 % (Field),	17.3 % (Lab.)
Dry Unit Weight :	Field	= 17.08 kN/m3 (108.7 pcf).
	Laboratory	= 17.34 kN/m3 (110.4 pcf).

Confining Pressure kPa (psi)	Mean of Applied Deviator Stress kPa (psi)	Mean of Recovered (or Resilient) Strain mm/mm or in./in.	Mean of Resilient Modulus MPa (ksi)
---	---	---	---
41.4 (6.0)	09.58 (1.39)	0.000053	181.93 (26.39)
41.4 (6.0)	33.16 (4.81)	0.000325	102.03 (14.80)
41.4 (6.0)	49.64 (7.20)	0.000561	088.52 (12.84)
41.4 (6.0)	64.05 (9.29)	0.00078	082.18 (11.92)
41.4 (6.0)	77.21 (11.20)	0.00104	074.25 (10.77)
---	---	---	---
27.6 (4.0)	09.72 (1.41)	0.00005	192.96 (27.99)
27.6 (4.0)	33.09 (4.80)	0.000313	105.82 (15.35)
27.6 (4.0)	49.91 (7.24)	0.000554	090.04 (13.06)
27.6 (4.0)	65.01 (9.43)	0.000798	081.56 (11.83)
27.6 (4.0)	78.38 (11.37)	0.001058	074.04 (10.74)
---	---	---	---
13.8 (2.0)	09.79 (1.42)	0.000054	180.42 (26.17)
13.8 (2.0)	32.82 (4.76)	0.000312	105.20 (15.26)
13.8 (2.0)	50.05 (7.26)	0.000549	091.14 (13.22)
13.8 (2.0)	64.46 (9.35)	0.000783	082.38 (11.95)
13.8 (2.0)	78.66 (11.41)	0.00106	073.70 (10.69)

[Note]: The mean value is computed among the last 5 load cycles of each load sequence.

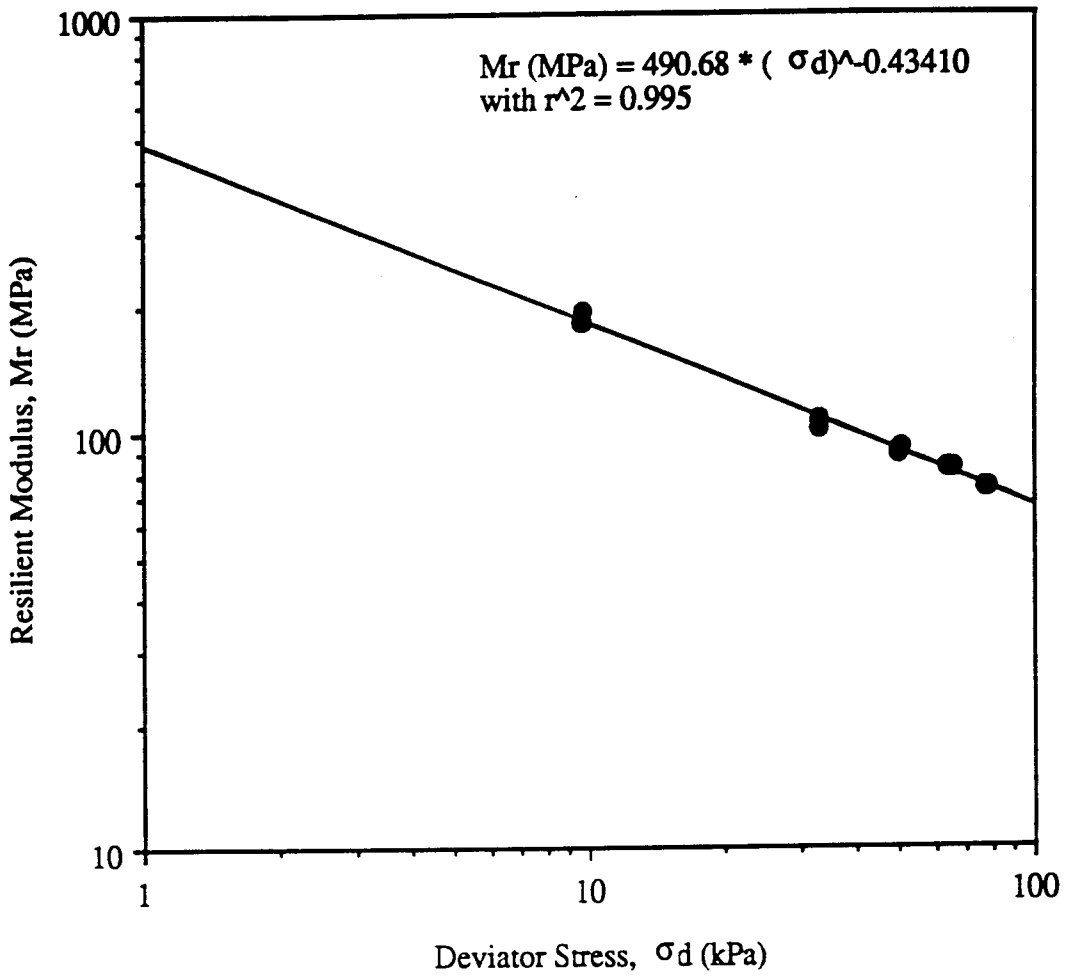

Figure 5.3: Plot of Typical Resilient Modulus Test Data
(See Table 5.3 for Details)

the deviator stress (σ_d). The relationship between them is expressed through two parameters K and n as:

$$M_r = K * (\sigma_d)^n \qquad \text{(Equation 5.1)}$$

In the above test, the values of the two parameters, K and n, were determined to be 490.6 MPa and -0.434, respectively. Once the values of the parameters are known, the resilient modulus at any deviator stress level can be computed from the above formula. Tables 5.3.(a) through (c) summarize per soil group the basic test data and results from each resilient modulus test performed.

5.6 Analysis of Test Results

An examination of the data presented in Tables 5.3.(a) through 5.3.(c) reveals a wide range of the resilient modulus exhibited by the subgrade soil samples as a direct result of largely varying moisture conditions. Here, it must be made clear that the back-calculated elastic modulus (E) discussed in the previous section is not equivalent to the resilient modulus (M_r) presented in this section. Each elastic modulus computed from the FWD test data represented an elastic property of the in-situ composite pavement section, which consisted of a few different layered materials. However, the resilient modulus measured in the laboratory represented a dynamic property of the subgrade soil alone.

A very limited amount of data was established for the A-7-6 soil group, since this soil type was found in a few isolated areas. When its moisture content was increased from 10.5 to 21.8% (while the dry unit weight remained almost unchanged), the resilient modulus declined by more than 80% under the deviator stress levels considered. Figures 5.4.(a) and (b) present the dry unit weight vs. the moisture content and the resilient modulus vs. the moisture content plots for this soil group. The relationship between the resilient modulus and the moisture content is nonlinear and shaped like one side of a bell. As the deviator stress level increases, the correlation curve becomes flatter and shifts into lower positions.

Table 5.3.(a): Resilient Modulus Test Summery for Subgrade Soil Samples (A-7-6 Soils)

Test No.	Sample I.D.	Moisture Content (%)	Dry Unit Weight (kN/m3)	Soil Type	Values of: K (MPa) n	Resilient Modulus (MPa) @ Deviator Stress (kPa) of : 13.79	27.58	41.36
15	390107	10.5	18.09	A-7-6	603.92: - 0.475	173.7	125	103.1
16	390107	13.5	18.01	A-7-6	484.24: - 0.424	159.2	118.6	99.9
18	390107	21.8	17.43	A-7-6	406.89: - 0.971	31.9	16.3	11
20	390107	16.1	18.24	A-7-6	618.46: - 0.843	67.8	37.8	26.8
	Minimum :	10.5	17.43					
	Average :	15.5	17.94					
	Maximum :	21.8	18.24					
	Std. Deviation :	4.15	0.355					

[Notes] 1. The two parameters, K and n, are used to express the resilient modulus (Mr) as a function of deviator stress (σ_d) : $Mr = K (\sigma_d)^n$

2. Conversion factors: 1 kN/m^3 = 6.369 pcf ; 1 kPa = 0.145 psi ; 1 MPa = 0.145 ksi.

Table 5.3.(b) : Resilient Modulus Test Summary for Subgrade Soil Samples (A-6 Soils)

Test No.	Sample I.D.	Moisture Content (%)	Dry Unit Weight (kN/m3)	Soil Type	Values of : K (MPa) n	Resilient Modulus (MPa) @ Deviator Stress (kPa) of : 13.79	27.58	41.36
01	390211	7.6	17.14	A-6	253.65: - 0.445	78.9	58	48.4
09	390211	11.5	17.69	A-6	295.14: - 0.301	134	108.8	96.2
17	390211	11.9	17.65	A-6	332.91: - 0.266	165.7	137.8	123.7
19	390211	18.4	17.63	A-6	256.60: - 0.827	29.3	16.5	11.9
21	390211	17.7	17.16	A-6	290.24: - 0.696	46.7	28.9	21.8
22	390211	10.4	17.47	A-6	250.06: - 0.333	104.7	83.07	72.6
23	390207	17.6	17.49	A-6	1,249.0:- 0.987	93.8	47.3	31.7
24	390207	16	17.8	A-6	226.65: - 0.630	43.4	28.1	21.7
25	390207	14.1	18.42	A-6	315.45: - 0.530	78.5	54.4	43.9
28	390207	12.5	18.92	A-6	911.39: - 0.653	164.4	104.5	80.2
33	390202	12.5	18.06	A-6	679.74: - 0.645	125.1	80	61.6
34	390202	18.3	18.16	A-6	251.45: - 0.714	38.6	23.6	17.6
36	390202	10	18.87	A-6	1,024.6:- 0.744	145.5	86.9	64.3
41	390262	15	17.91	A-6	815.83: - 0.658	145.2	92	70.5
42	390262	20.5	15.83	A-6	1,746.4:- 1.283	60.3	24.7	14.8
44	390262	18.9	17.65	A-6	085.82: - 0.501	23	16.3	13.3
51	390205	16.1	17.84	A-6	1,365.4:- 0.803	166.1	95.2	68.7
55	390205	15.5	17.32	A-6	282.28: - 0.503	75.4	53.2	43.4
56	390205	15.1	17.29	A-6	797.76: - 0.674	136.2	85.3	64.9
52	390111	12.7	18.32	A-6	159.06: - 0.382	58.6	44.8	38.4
53	390111	19.7	16.64	A-6	493.50: - 0.598	102.8	67.9	53.3
	Minimum :	7.6	15.83					
	Average :	14.9	17.68					
	Maximum :	20.5	18.92					
	Std. Deviation :	3.43	0.684					

[Notes] 1. The two parameters, K and n, are used to express the resilient modulus (Mr) as a function of deviator stress (σ_d) : $Mr = K (\sigma_d)^n$

2. Conversion factors: 1 kN/m^3 = 6.369 pcf ; 1 kPa = 0.145 psi ; 1 MPa = 0.145 ksi.

Table 5.3.(c): Resilient Modulus Test Summery for Subgrade Soil Samples (A-4 Soils)

Test No.	Sample I.D.	Moisture Content (%)	Dry Unit Weight (kN/m3)	Soil Type	Values of : K (MPa) n	Resilient Modulus (MPa) @ Deviator Stress (kPa) of : 13.79	27.58	41.36
03	390810	14.5	16.49	A-4	308.10: - 0.330	129.6	103.1	90.2
04	390810	14.8	16.47	A-4	315.03: - 0.345	127.4	100.3	87.2
05	390810	17.3	17.33	A-4	490.49: - 0.434	157.1	116.3	97.6
06	390810	21.3	16.77	A-4	708.90: - 0.696	114.2	70.5	53.2
07	390810	21.2	16.77	A-4	283.51: - 0.414	95.7	71.8	60.7
08	390810	21.5	16.74	A-4	112.51: - 0.196	67.3	58.7	54.3
---	---	---	---	---	---	---	---	---
26	390902	15	18.71	A-4	177.39: - 0.230	97	82.7	75.4
31	390902	14.4	19.77	A-4	204.30: - 0.221	114.4	98.2	89.8
10	390809	17.8	16.69	A-4	268.20: - 0.341	109.6	86.6	75.4
11	390809	17.5	16.74	A-4	321.73: - 0.306	144.2	116.6	103
12	390809	20	16.38	A-4	567.44: - 0.589	121.1	80.5	60.9
13	390809	20.7	16.63	A-4	401.28: - 0.468	117.5	85	70.3
---	---	---	---	---	---	---	---	---
37	390160	13.8	17.74	A-4	513.00: - 0.513	133.5	93.6	76
38	390160	18.1	18.04	A-4	216.05: - 0.721	32.6	19.8	14.8
39	390160	11	19.04	A-4	530.46: - 0.411	180.5	135.7	114.9
40	390160	13.9	18.62	A-4	227.28: - 0.392	81.3	62	52.8
---	---	---	---	---	---	---	---	---
54	390110	16.6	17.4	A-4	1,134.2:- 0.836	126.5	70.9	50.5
57	390110	15.7	17.91	A-4	223.18: - 0.421	74	55.2	46.6
58	390110	20.1	17.11	A-4	545.78: - 0.780	70.5	41.1	29.9
59	390110	14.8	17.77	A-4	725.66: - 0.752	100.9	59.9	44.2
	Minimum :	11	16.38					
	Average :	17	17.46					
	Maximum :	21.5	19.77					
	Std. Deviation :	2.96	0.947					

[Notes] 1. The two parameters, K and n, are used to express the resilient modulus (Mr) as a function of deviator stress (σ_d) : $Mr = K (\sigma_d)^n$

2. Conversion factors: 1 kN/m^3 = 6.369 pcf ; 1 kPa = 0.145 psi ; 1 MPa = 0.145 ksi.

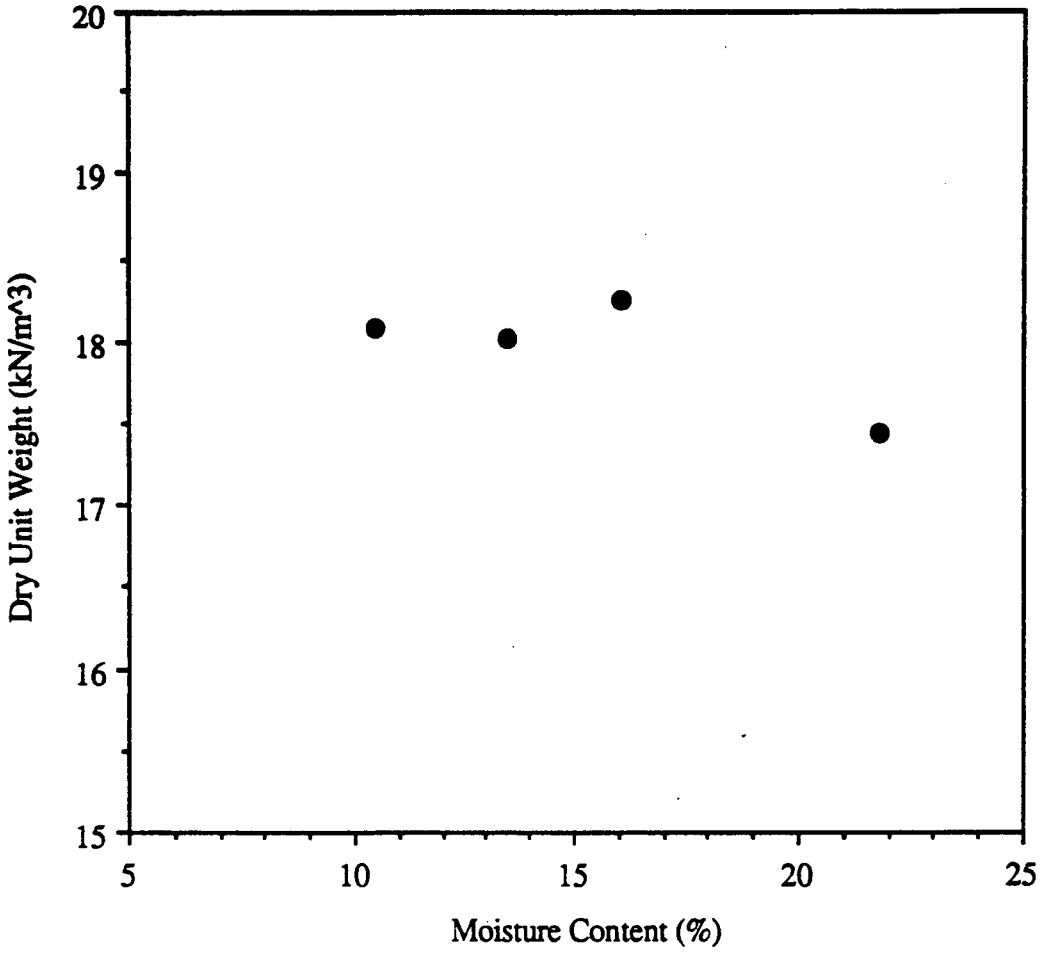

Figure 5.4.(a): Dry Unit Weight Vs. Moisture Content Plot for A-7-6 Soil Specimens

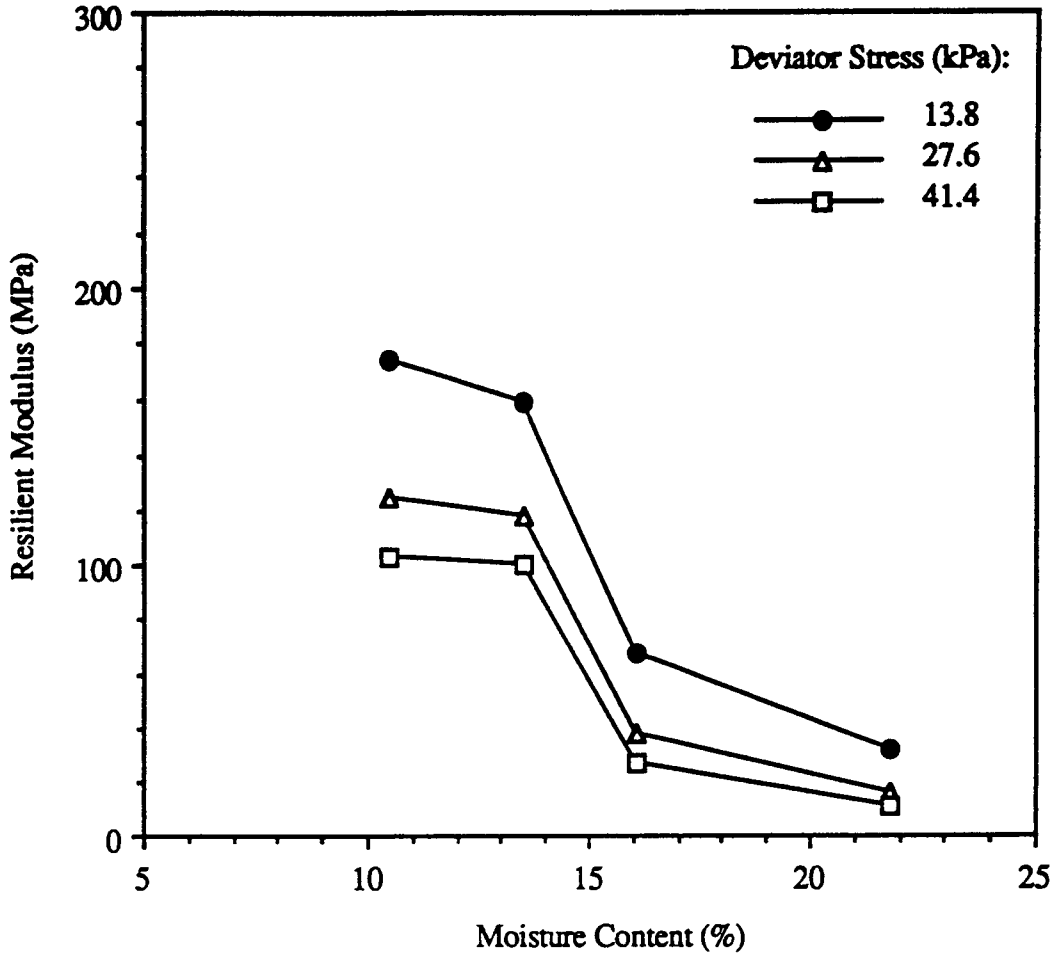

Figure 5.4.(b): Resilient Modulus Vs. Moisture Content Plot for A-7-6 Soil Specimens

Among the test specimens belonging to the A-6 soil group, the moisture content was varied widely between 7.6 and 20.5% in the laboratory, while their dry unit weights were maintained mostly within 17.7 ± 0.7 kN/m^3 (112.6 ± 4.4 pcf) (see Figure 5.5.a). The static compaction method described in Attachment C to the SHRP Protocol P46 is not a constant energy method. That is why the plot shown in Figure 5.5.(a) has considerable amount of scatter in the data. The resulting resilient modulus exhibited a wide range spanning from 13.1 to 206.8 MPa (1.9 to 30 ksi). Figures 5.5.(b) through 5.5.(d) present a general correlation between the resilient modulus and the moisture content under each deviator stress level. In spite of some scattering, it appears the correlation is characterized by a bell-shaped curve. The bell shape emerges since the resilient modulus generally decreases with the moisture content and lower resilient moduli are measured at very low moisture contents. As the deviator stress level increases, the bell-shape curve tends to become flatter and moves to a lower position.

Among the test specimens belonging to the A-4 soil group, the moisture content was varied widely from 11 to 21.5% in the laboratory, while their dry unit weights were maintained mostly within 17.5 ± 0.9 kN/m^3 (111.2 ± 6 pcf). The resulting resilient modulus exhibited a wide range covering from 14.5 to 180.6 MPa (2.1 to 26.2 ksi). Examination of the plots shown in Figures 5.6.(b) through (d) can yield a similar comment on the relationship between the resilient modulus and the moisture content. That is that a general correlation between the resilient modulus and the moisture content is characterized by a bell-shaped curve. Again, as the deviator stress level increases, the bell-shape curve tends to become flatter and moves to a lower position.

In comparing all three soil types, it appears that the higher the clay content in the soil, the more sensitive its resilient property is to changes in the moisture content. Additional insights into the resilient behavior of the subgrade soils may be obtained by examining the data presented in Tables 5.3.(a) through (c). In Table 5.3.(a), a comparison of the results between Test Nos. 15 and 16 points out that an increase in the moisture content leads to a decline in the resilient modulus when the dry unit weight stays about constant. This same trend is also detected in Table 5.3.(b) through comparisons between Test Nos. 1 and 21, 9 and 44, 17 and 44, and 22 and 23. In Table 5.3.(c), comparisons

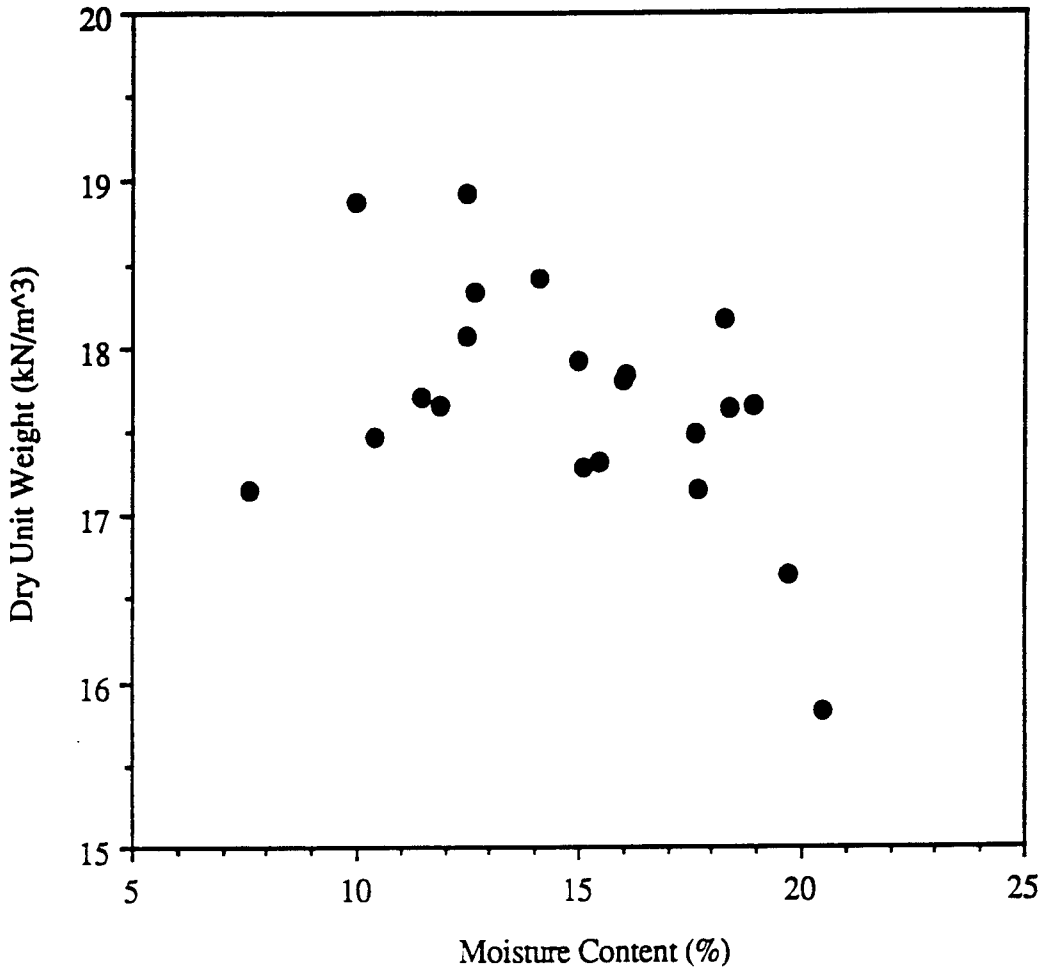

Figure 5.5.(a): Dry Unit Weight Vs. Moisture Content Plot for A-6 Soil Specimens

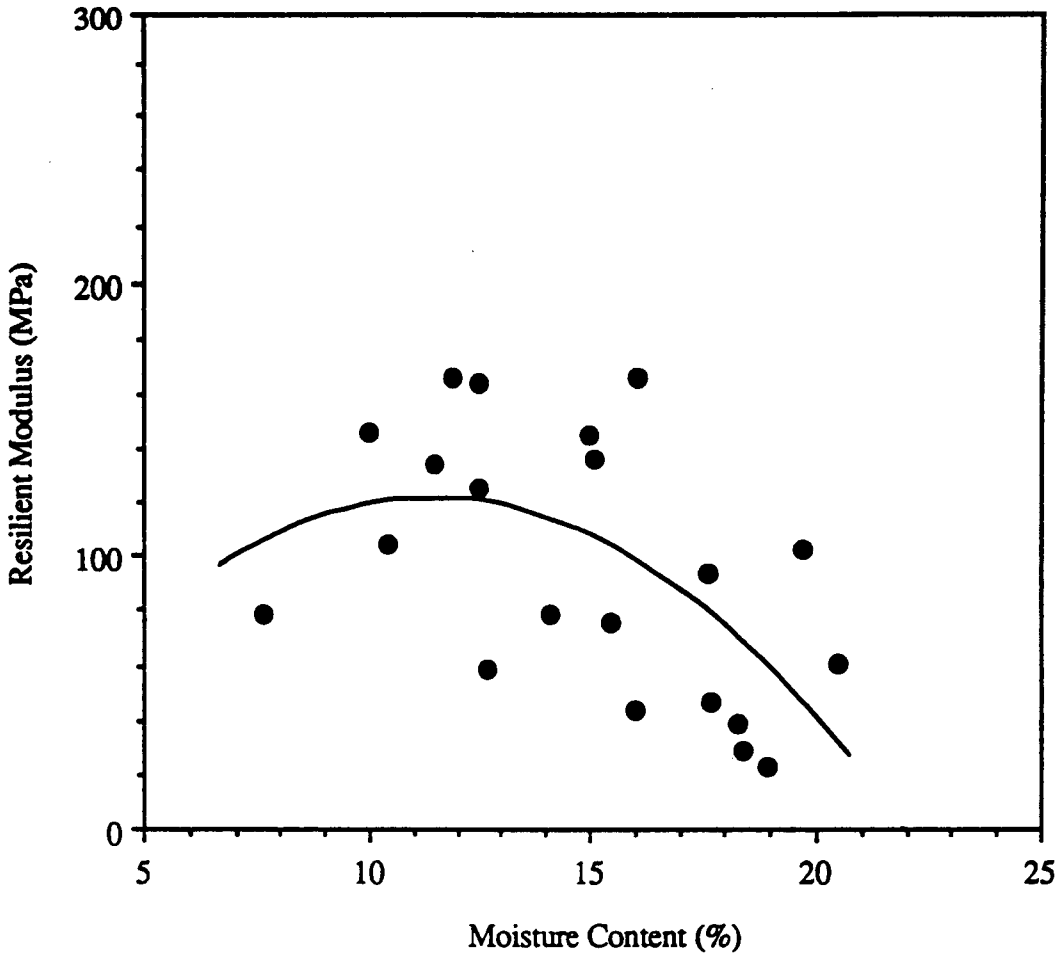

Figure 5.5.(b): Resilient Modulus Vs. Moisture Content Plot for A-6 Soil Specimens (Deviator Stress = 13.8 kPa)

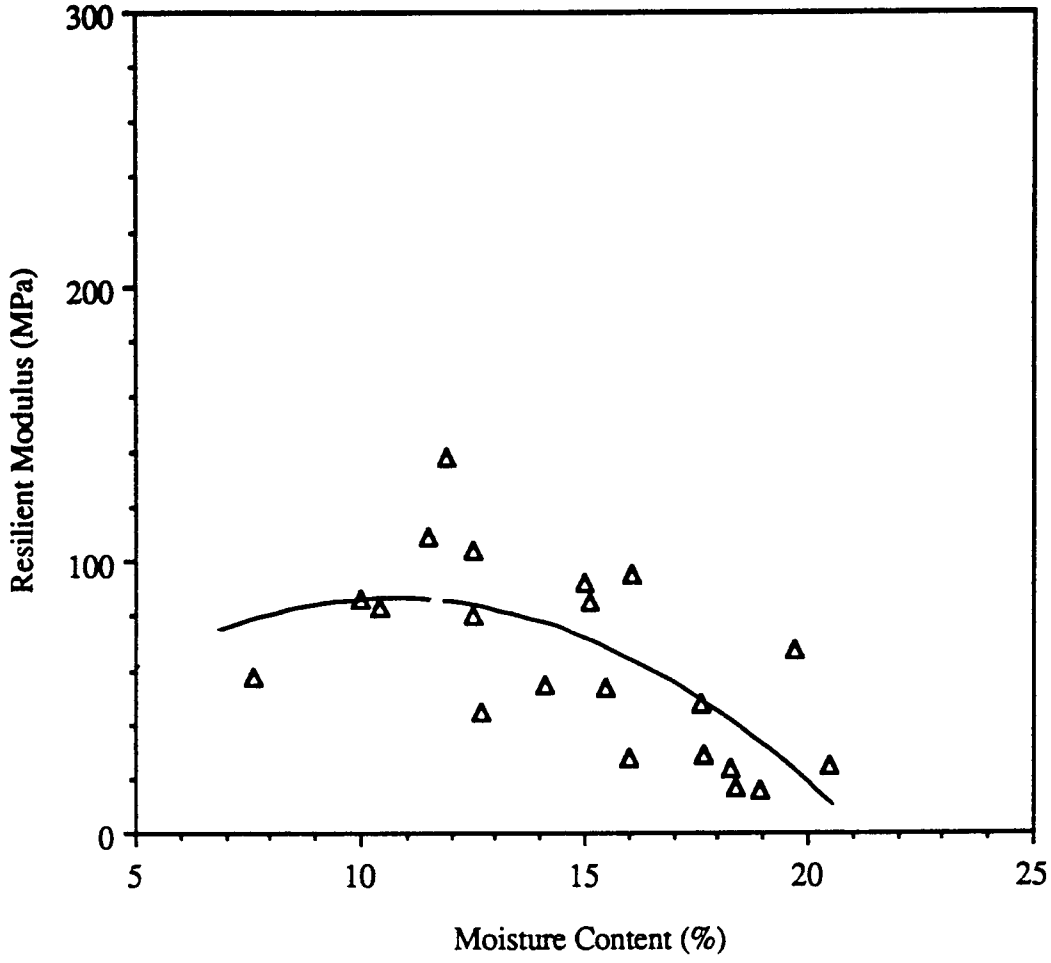

Figure 5.5.(c): Resilient Modulus Vs. Moisture Content Plot for A-6 Soil Specimens (Deviator Stress = 27.6 kPa)

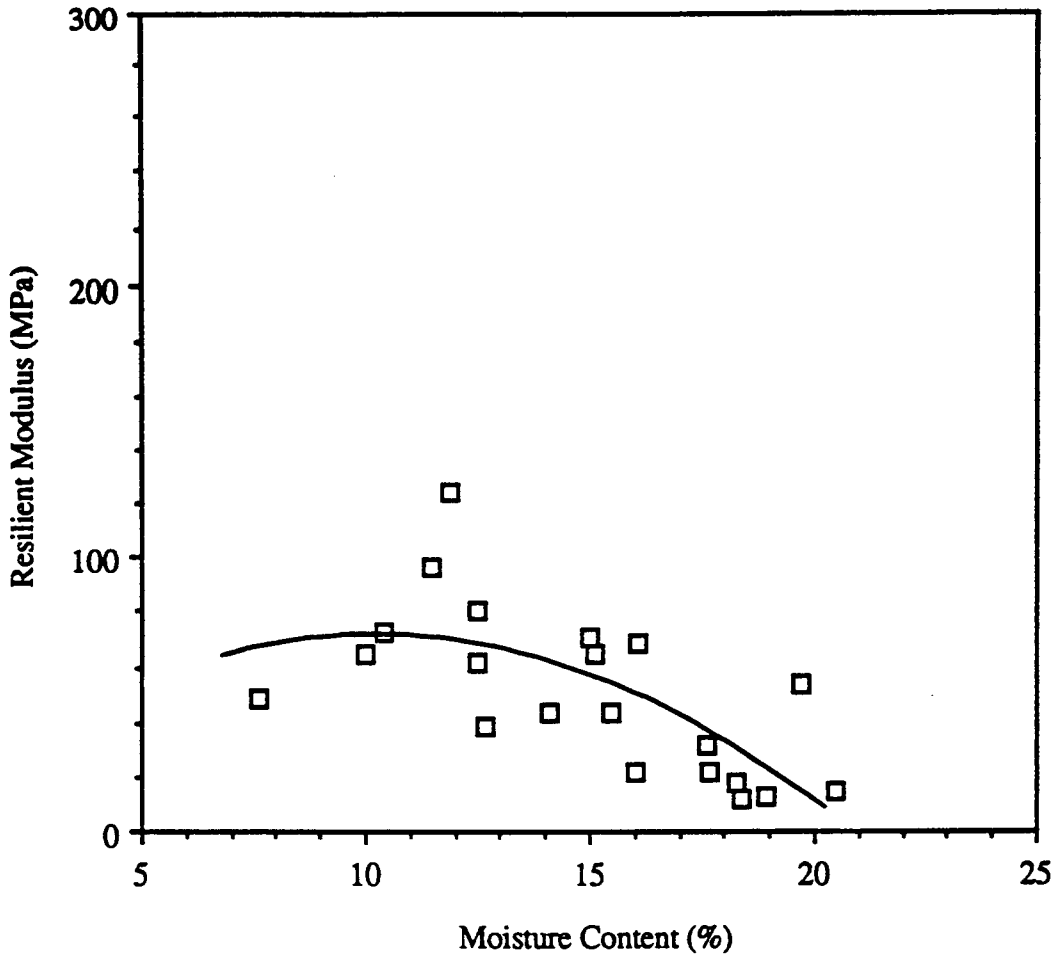

Figure 5.5.(d): Resilient Modulus Vs. Moisture Content Plot for A-6 Soil Specimens (Deviator Stress = 41.4 kPa)

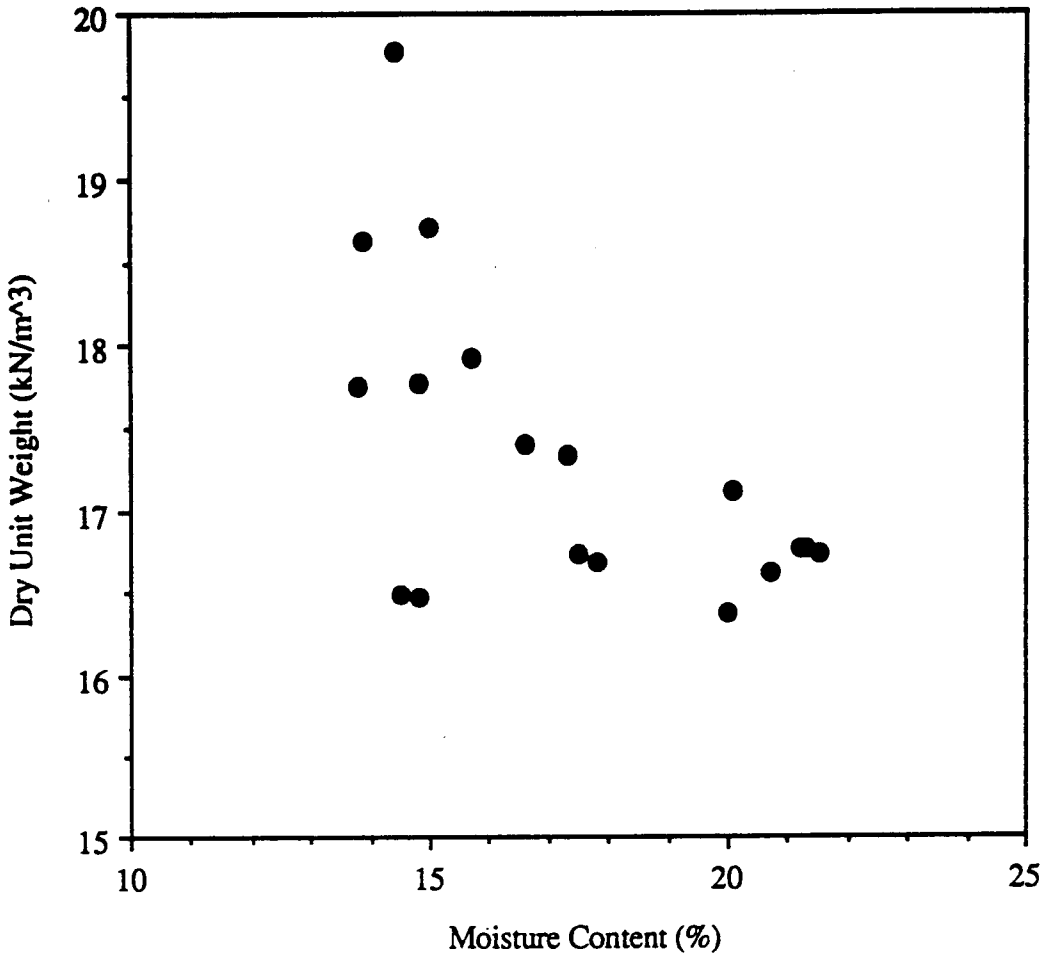

Figure 5.6.(a): Dry Unit Weight Vs. Moisture Content Plot for A-4 Soil Specimens

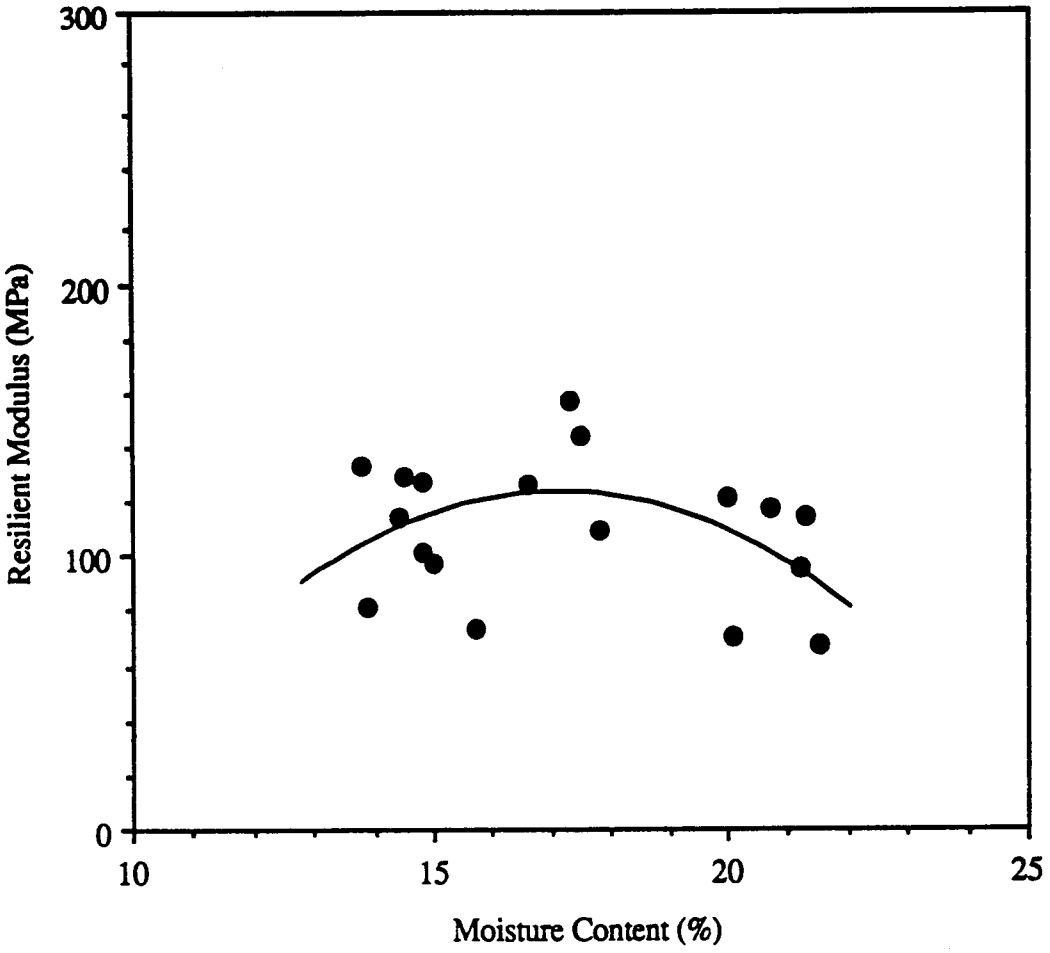

Figure 5.6.(b): Resilient Modulus Vs. Moisture Content Plot for A-4 Soil Specimens (Deviator Stress = 13.8 kPa)

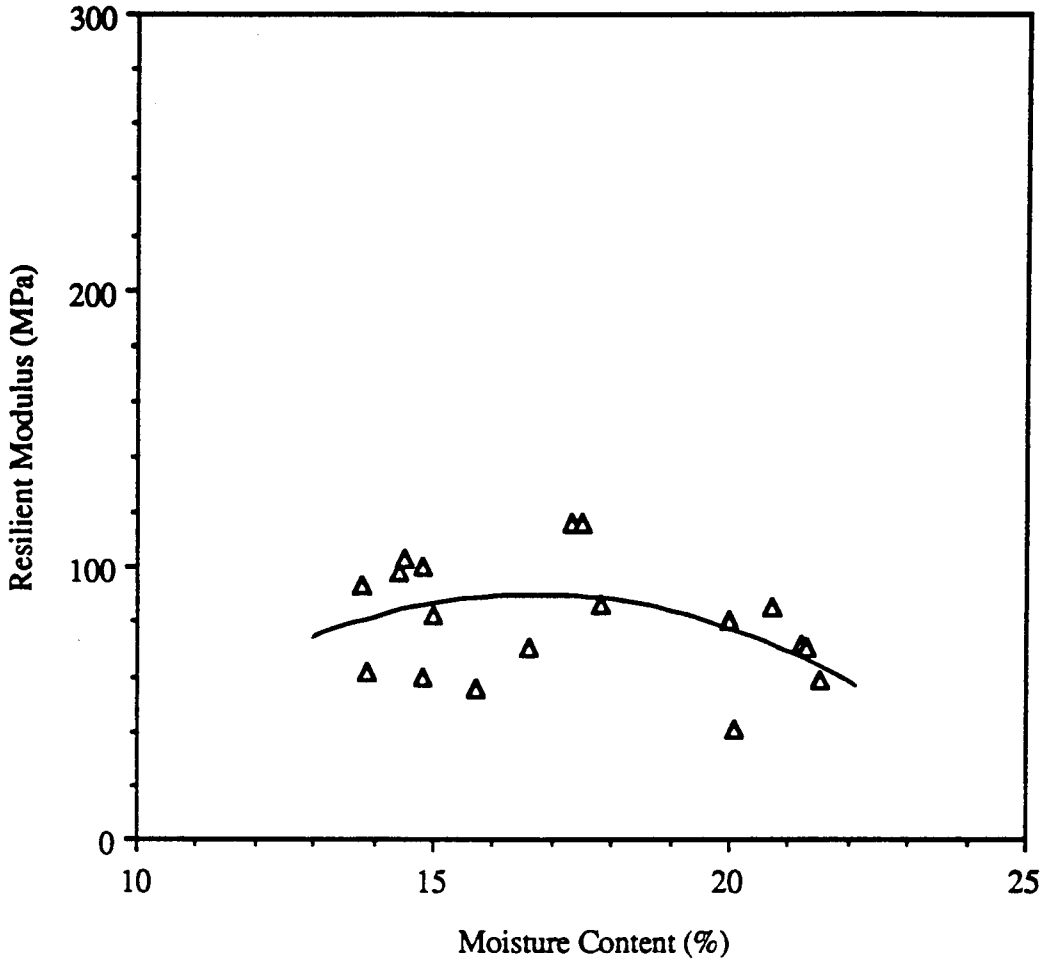

Figure 5.6.(c): Resilient Modulus Vs. Moisture Content Plot for A-4 Soil Specimens (Deviator Stress = 27.6 kPa)

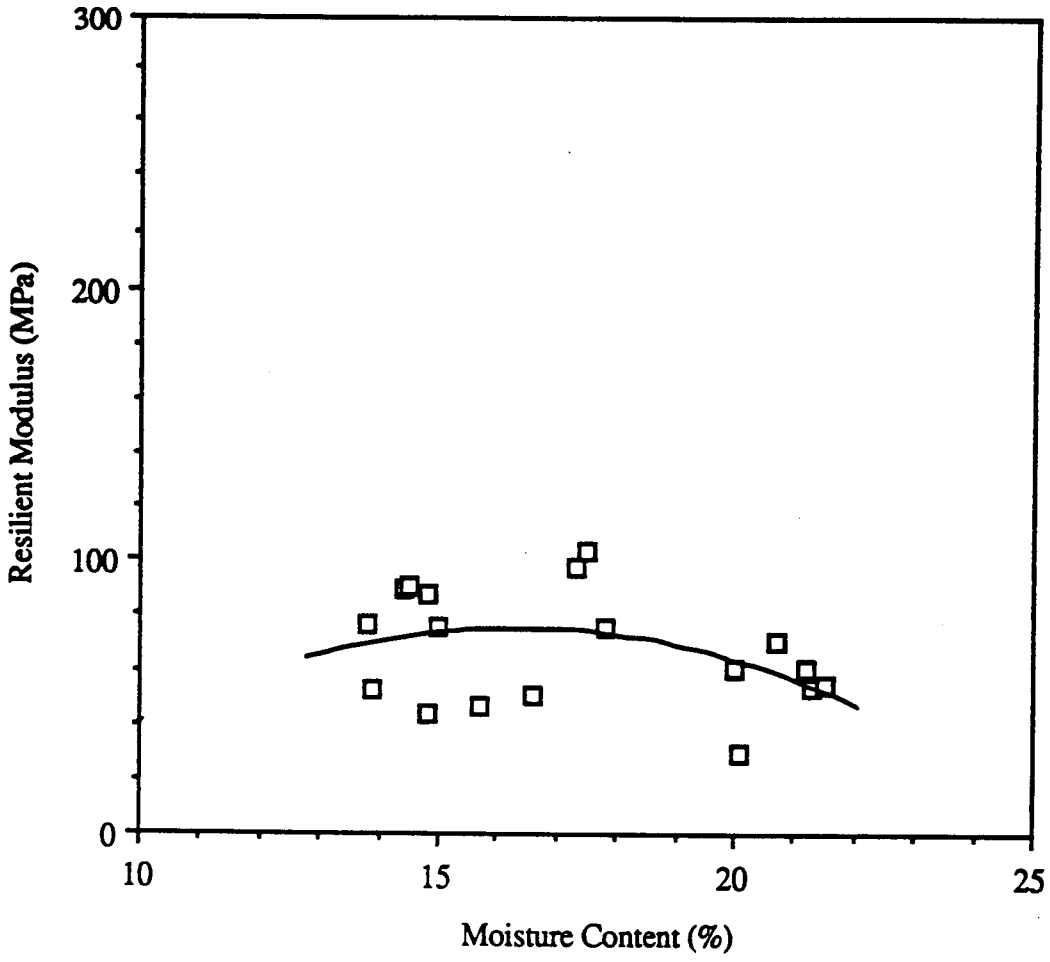

Figure 5.6.(d): Resilient Modulus Vs. Moisture Content Plot for A-4 Soil Specimens (Deviator Stress = 41.4 kPa)

between Test Nos. 3 and 4, 6 and 11, 7 and 11, 8 and 11, 26 and 58, and 37 and 59 provide additional support to this trend.

Another consistent trend is seen for the soil group A-6, which is that an increased dry unit weight leads to a higher resilient modulus at low moisture contents but to a lower resilient modulus at high moisture contents. Supporting evidences for this can be found in comparisons between Test Nos. 21 and 23, 22 and 36, 28 and 33, and 24 and 35. Soil specimens belonging to the soil group A-4 did not exhibit this trend clearly.

Based on observations of resilient modulus vs. moisture content for the three soil types, it is noted that the A-7-6 soil exhibited the greatest reduction in resilient modulus with increasing moisture content. The resilient modulus of the A-6 soil showed somewhat more sensitivity to moisture than the A-4 soil. These observations suggest that soils with a higher clay content exhibit a greater sensitivity to moisture.

Chapter 6

Case Study of Section 390101

6.1 Introduction

Data currently available and additional data obtained in the future as various test sections on the Ohio SHRP Test Road begin to fail will be used to develop a procedure, based on non-destructive testing, to evaluate the quality of subgrade compaction and improve uniformity throughout highway projects. A forensic study was performed on Section 390101 to obtain critical data relevant to the cause of premature rutting and fatigue cracking over a portion of this test section. Non-destructive testing performed on this section during construction and during the forensic study were used to analyze pavement performance and help determine the causes of failure.

6.2 Section Description

Section 390101 was an undrained test section consisting of 17.78 centimeters (7 inches) of asphalt concrete and 20.32 centimeters (8 inches) of dense graded aggregate base over a compacted A-6 subgrade. It was replaced after being opened to traffic for about 10 weeks because a portion of the section experienced premature rutting and fatigue cracking. The remainder of the test section experienced some rutting but not as severe. Transverse profiles were measured with a dipstick at 15.24-meter (50-foot) increments in the driving lane to determine the extent of rutting. Table 6.1 is a summary of maximum rutting found in each wheel path. This test section was initially predicted to last two to three years based on the design assumptions; however, after two and one-half months of service, distress reached such a level that traffic was diverted from the test road and the section was replaced.

Table 6.1: SHRP Section 390101, Rutting.

SHRP Station	Rutting, Right Wheel Path (mm)	Rutting, Left Wheel Path (mm)
0+00	24.6	11.43
0+50	20.8	16.51
1+00	22.1	16.51
1+50	10.7	13.5
2+00	10.4	5.8
2+50*	26.4	17.3
3+00	13.9	5.6
3+50	16.8	9.9
4+00	14.9	4.1
4+50	17.0	6.1
5+00	14.9	8.9

[Note] At Station 2+50, rutting shown in the table is not as significant as it appeared in the field due to the fatigue cracking and overall deterioration of this portion of the test section.

6.3 Falling Weight Deflectometer Testing

FWD tests were conducted according to LTPP protocol after completion of the subgrade, base, and asphalt concrete layers. The data was made available to the Ohio Research Institute for Transportation and the Environment (ORITE) team for correlation with distresses observed in the test section. Figures 6.1 through 6.5 present the FWD data obtained from Section 390101.

6.4 Dynamic Cone Penetrometer Testing

A series of dynamic cone penetrometer tests were performed along the test section. Based on the results of FWD testing and transverse profiles, three trenches were excavated. Trench one (SHRP Station 1+50) was made where the pavement exhibited average distress. Trench two (SHRP Station 2+65) was excavated in the most distressed region, while trench three (SHRP Station 4+00) was excavated in the least distressed region. Results of the DCP tests at these three trenches are plotted in Figures 6.6 through 6.11.

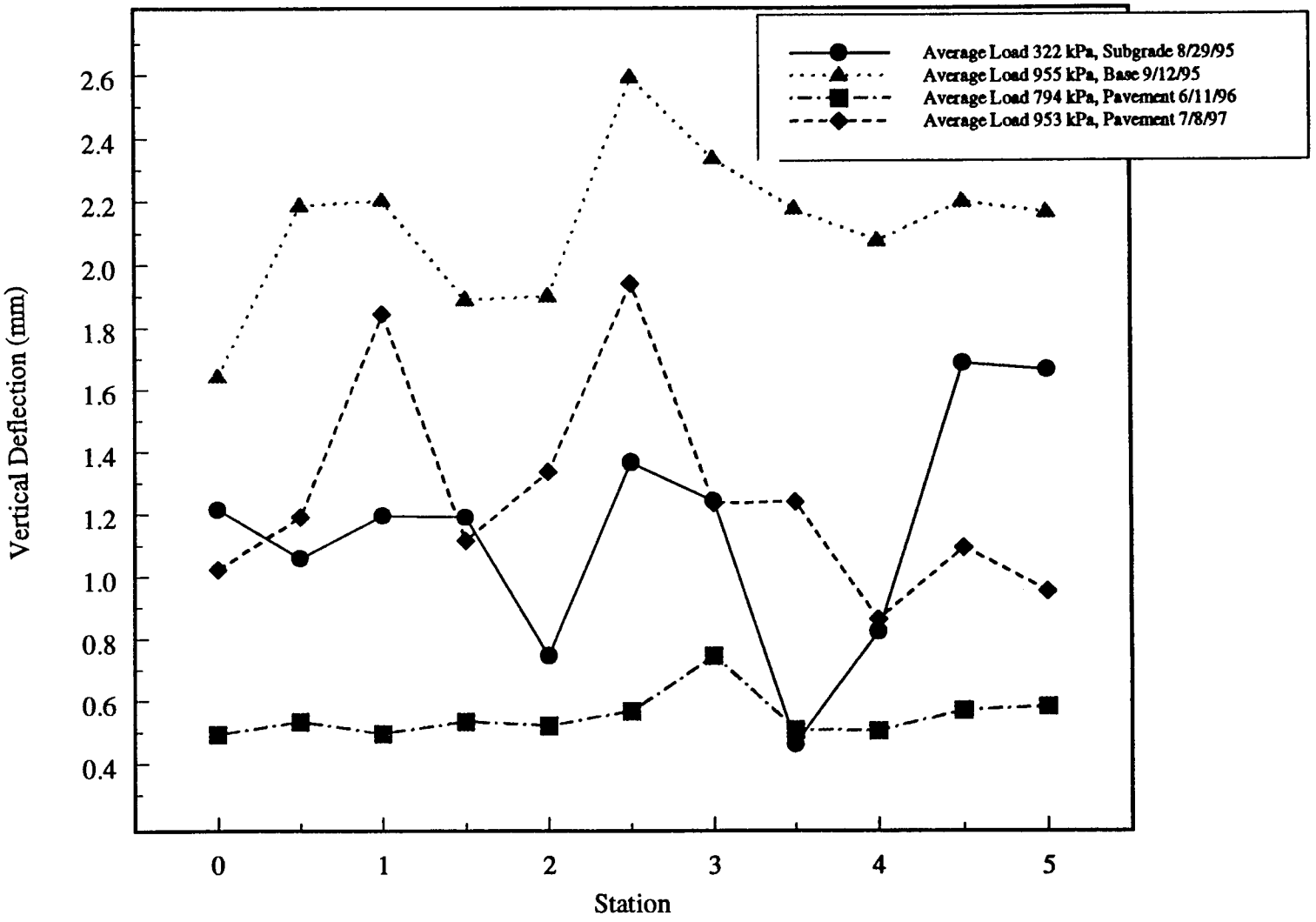

Figure 6.1: SHRP Section 390101. Falling Weight, Wheel Path.

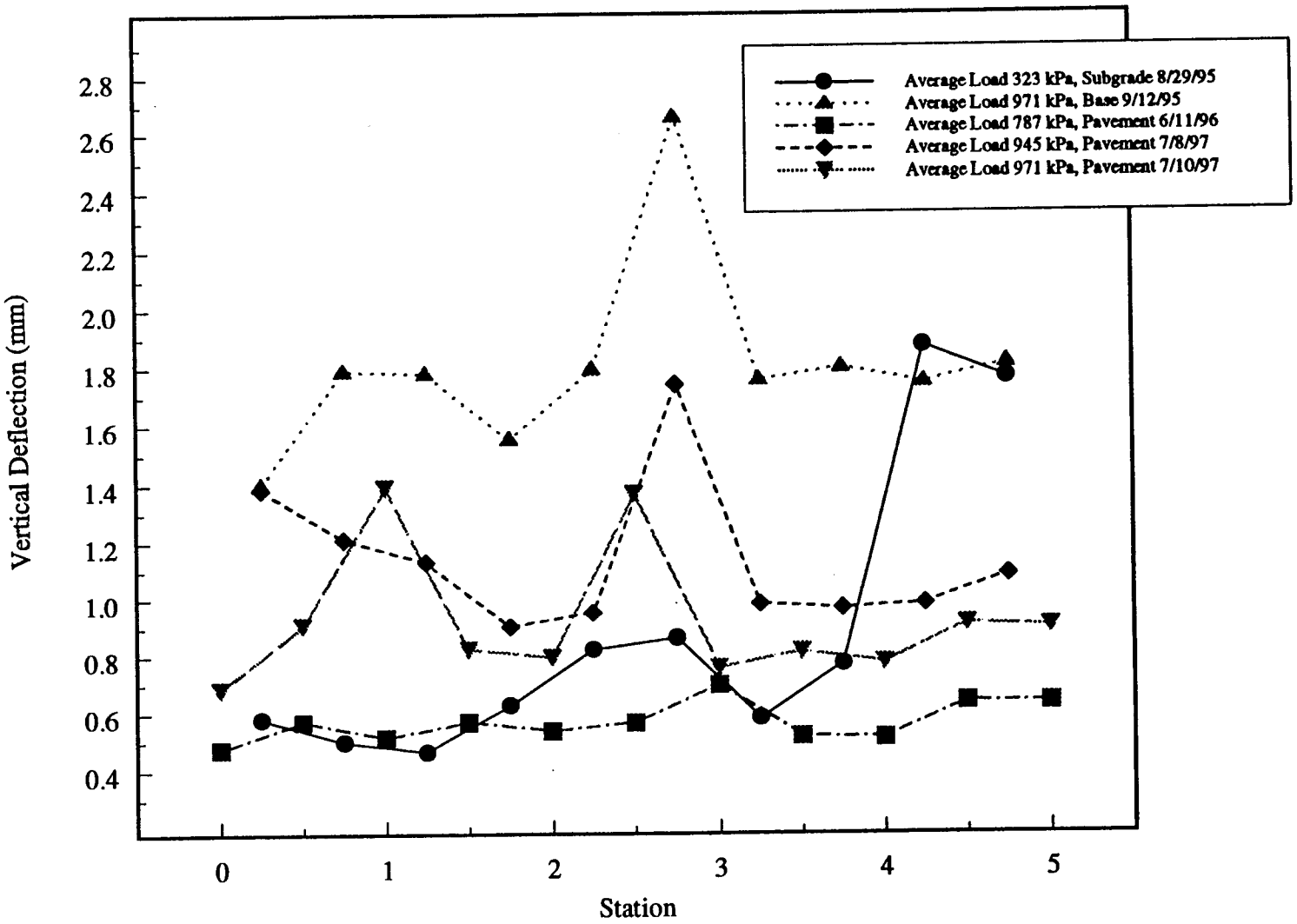

Figure 6.2: SHRP Section 390101. Falling Weight, Midlane.

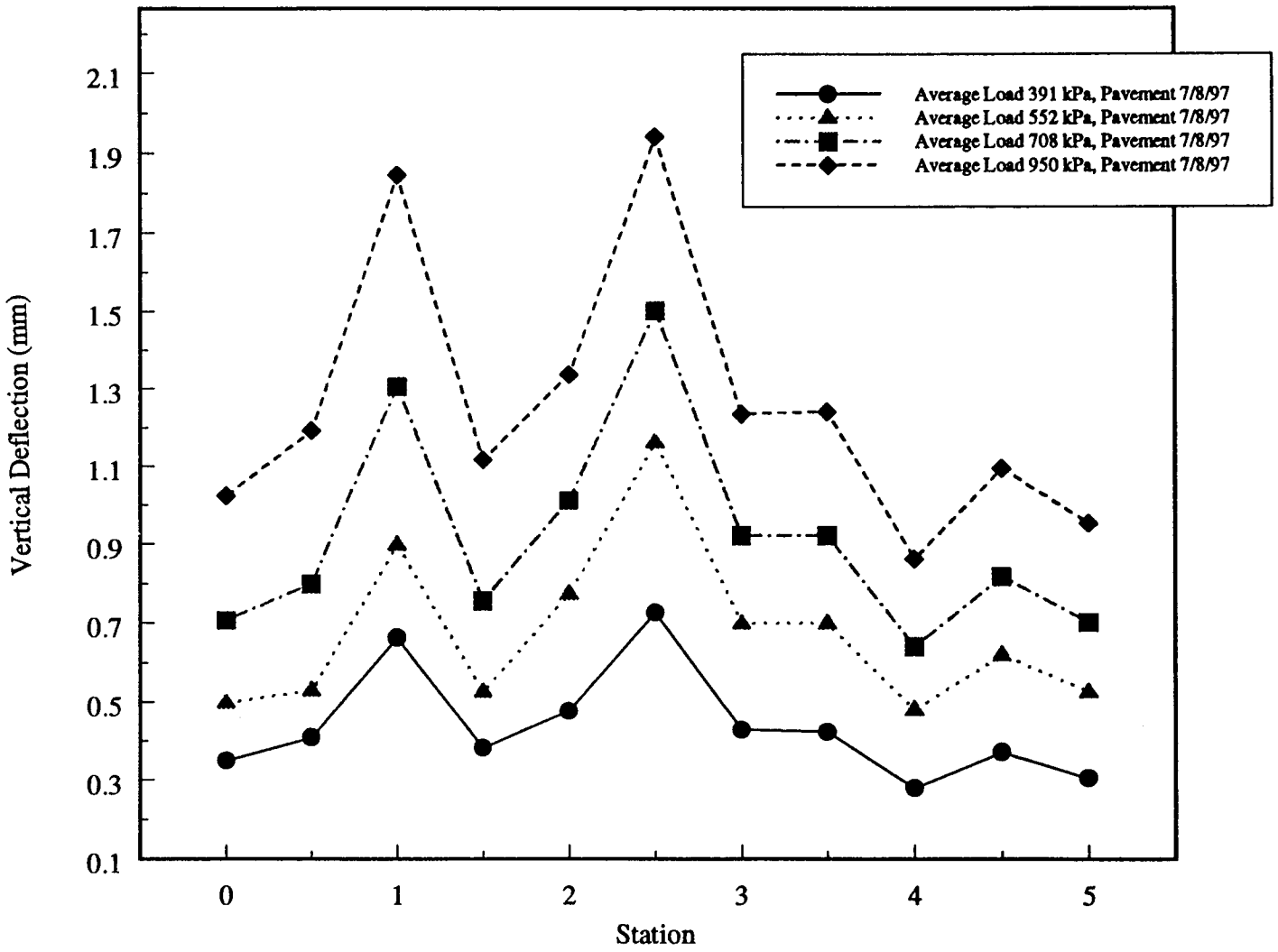

Figure 6.3: SHRP Section 390101. Falling Weight, Wheel Path, Pavement, 7/8/97.

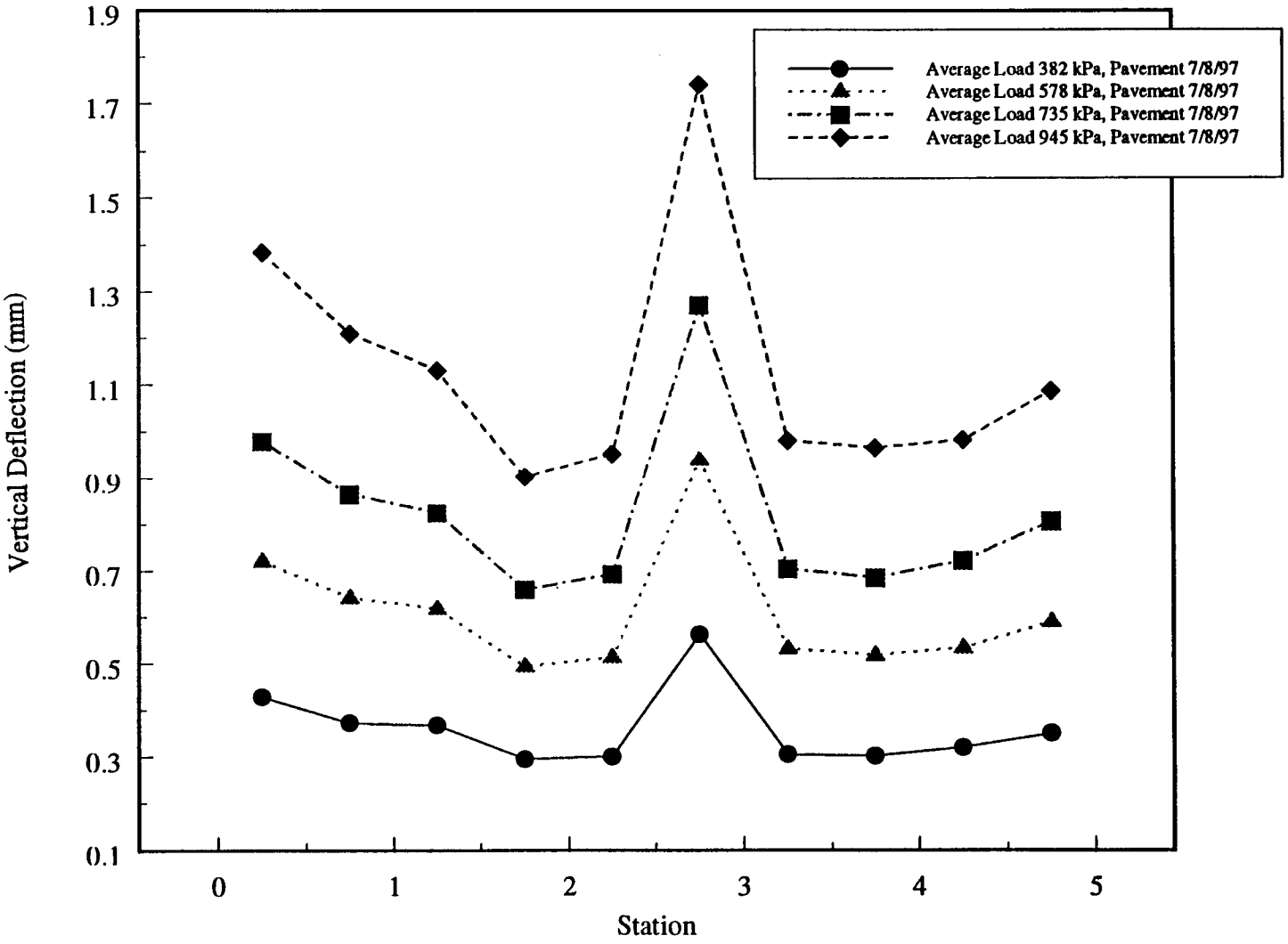

Figure 6.4: SHRP Section 390101. Falling Weight, Midlane, Pavement, 7/8/97.

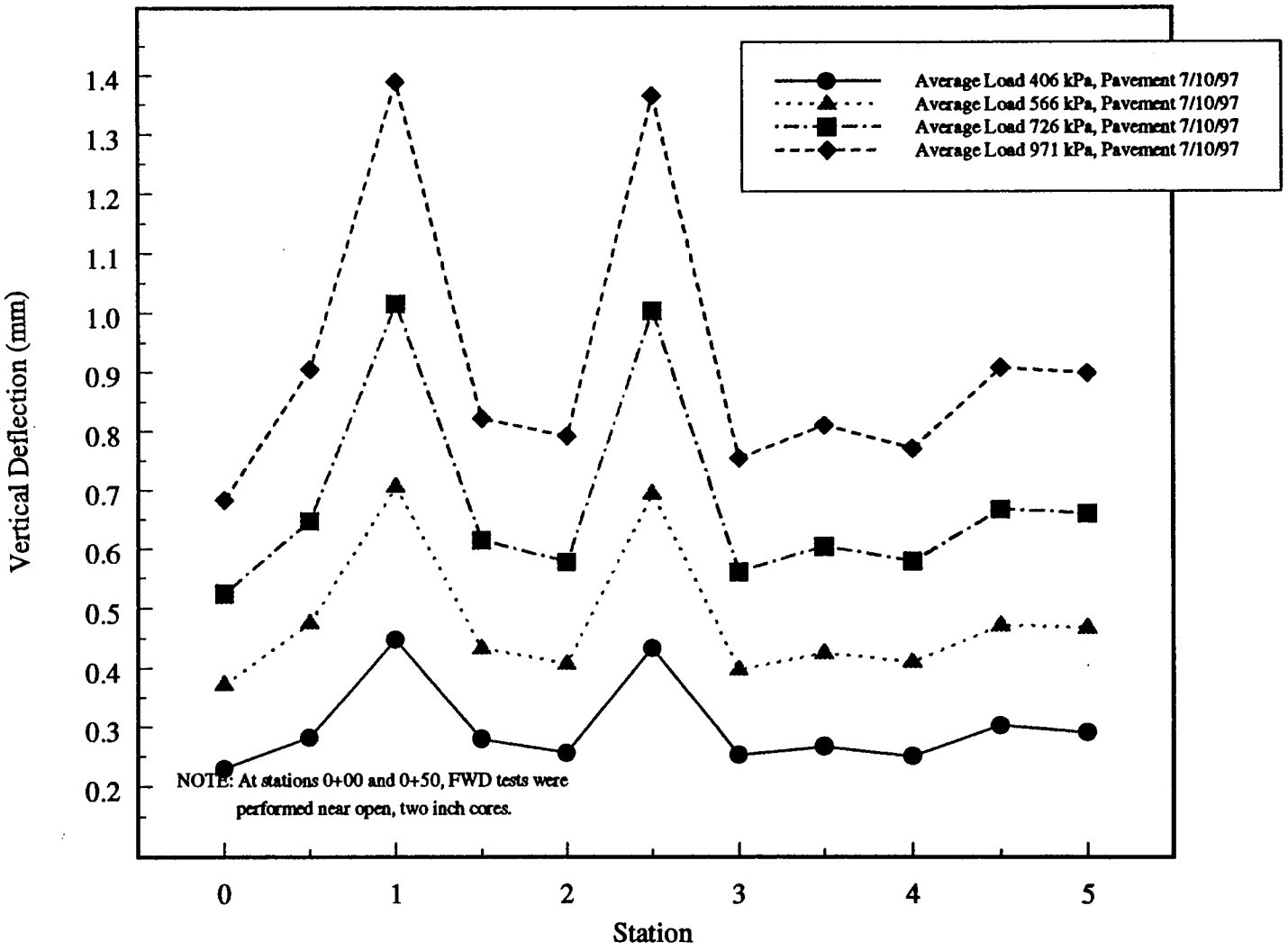

Figure 6.5: SHRP Section 390101. Falling Weight, Midlane, Pavement, 7/10/97.

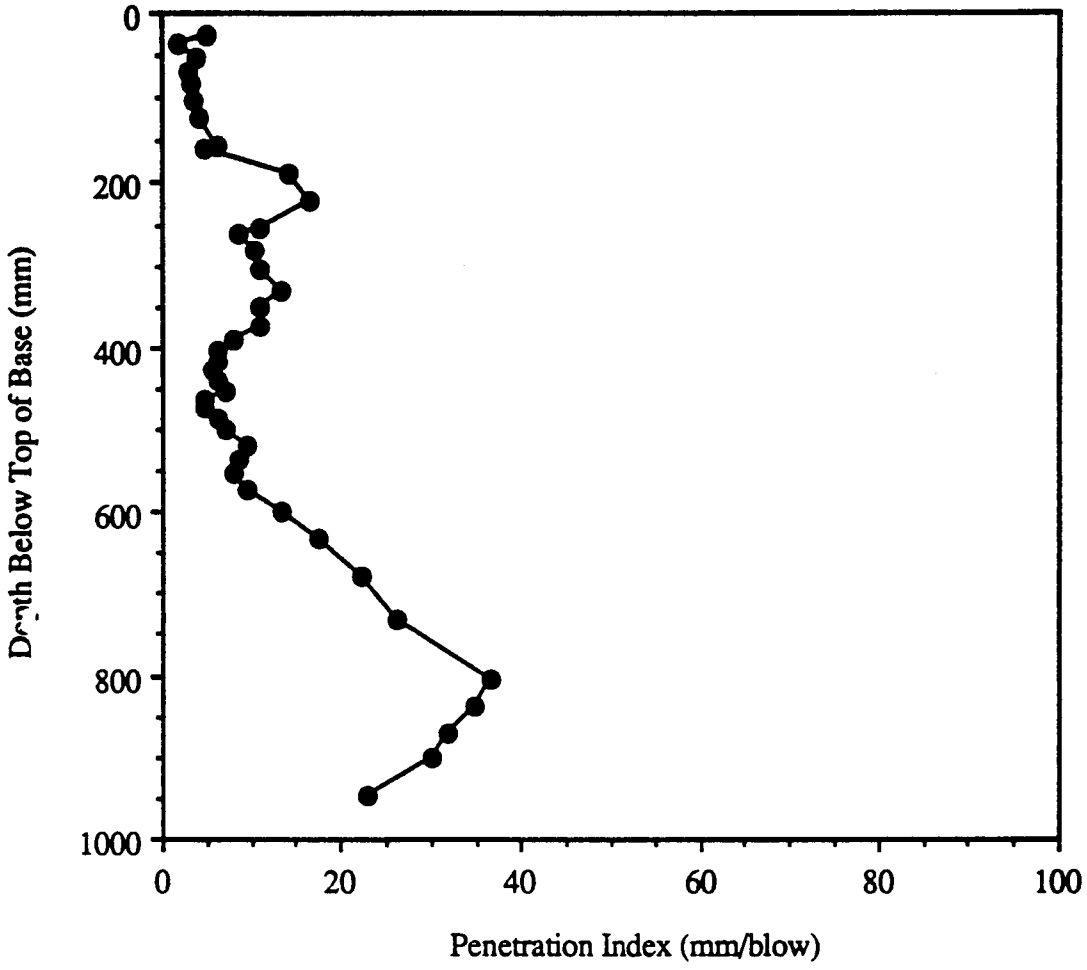

Figure 6.6: Result of DCP Test at Station 1+50 (Outer Wheel Path)

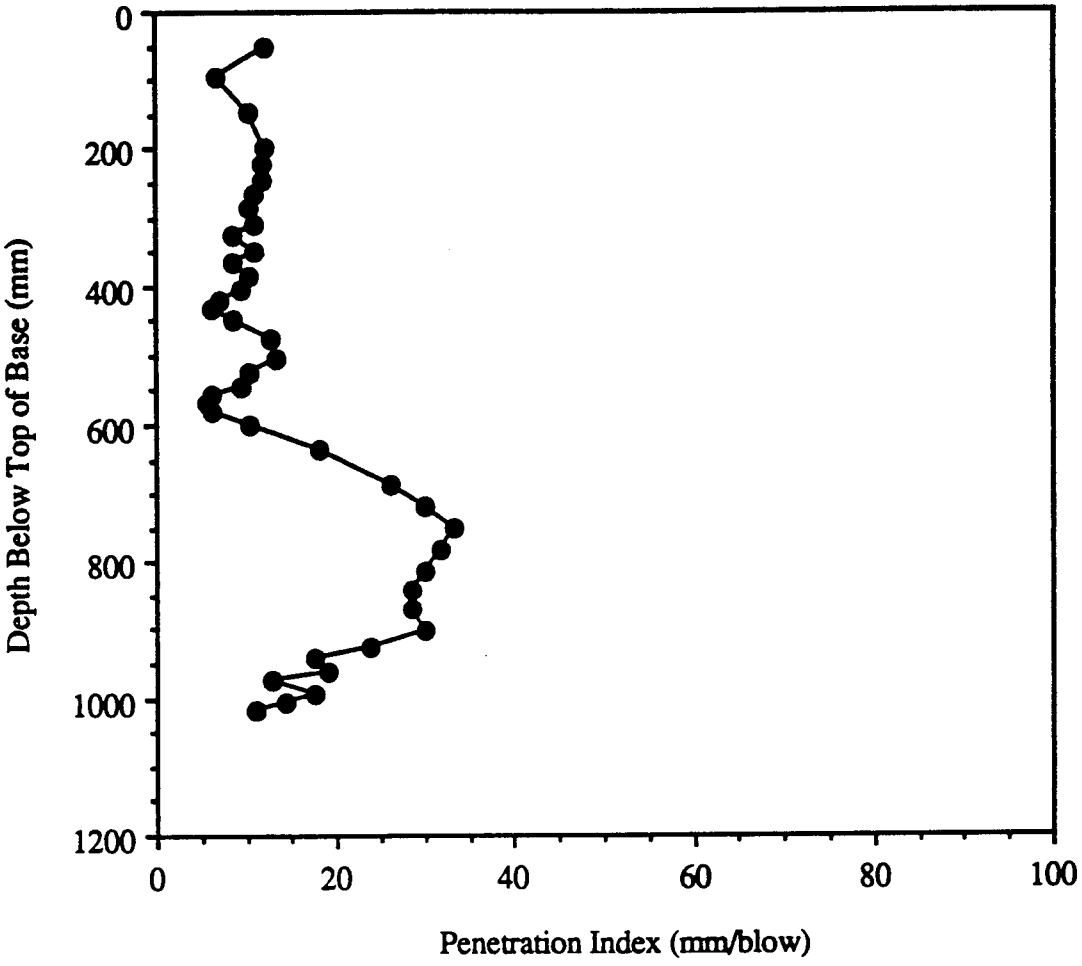

Figure 6.7: Result of DCP Test at Station 1+50 (Centerline)

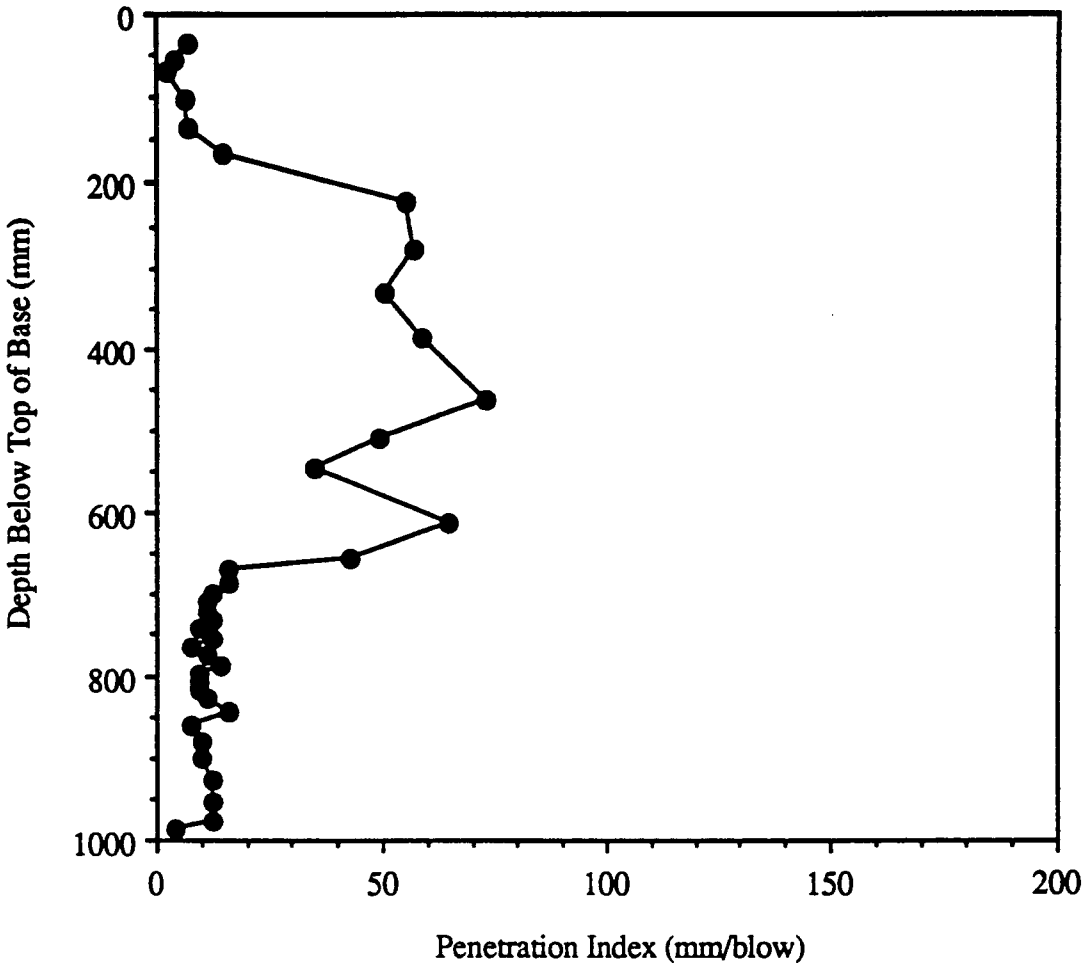

Figure 6.8: Result of DCT Test at Station 2+65 (Outer Wheel Path)

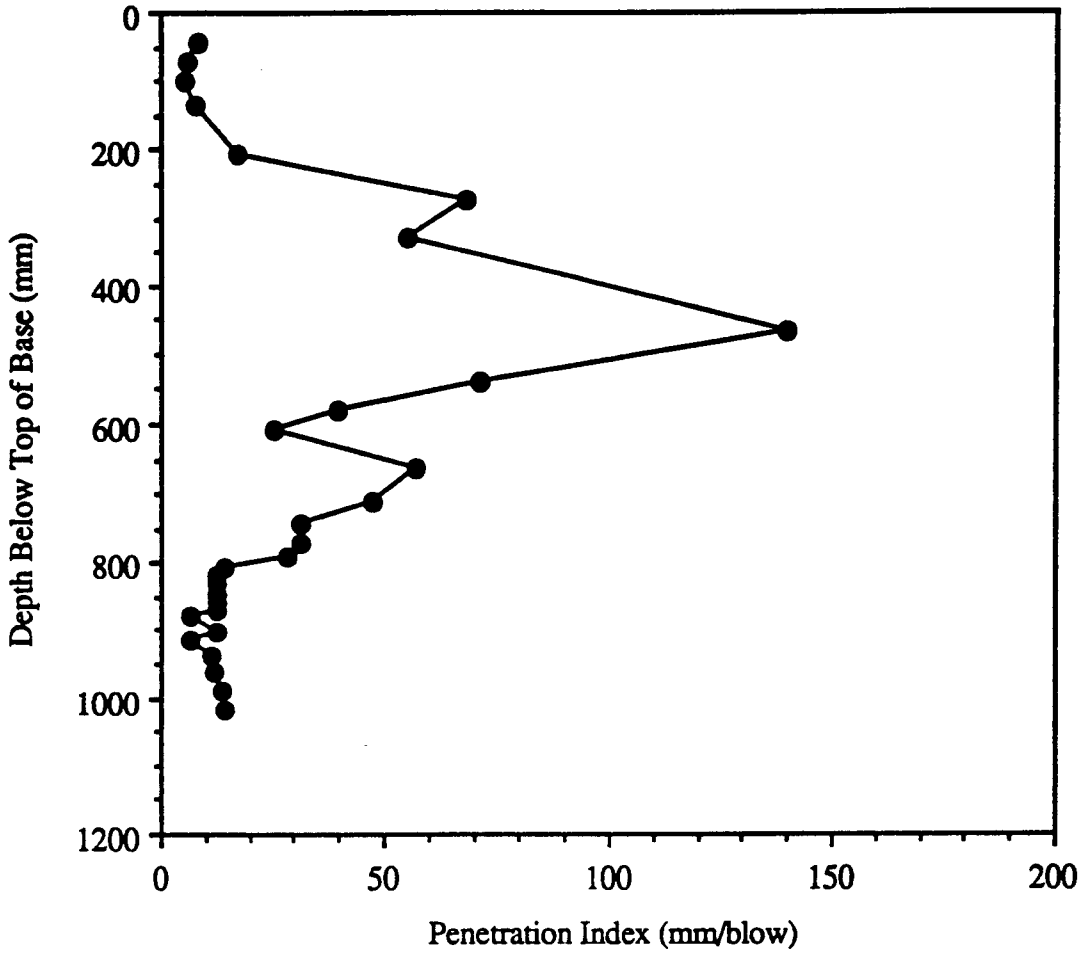

Figure 6.9: Result of DCP Test at Station 2+65 (Centerline)

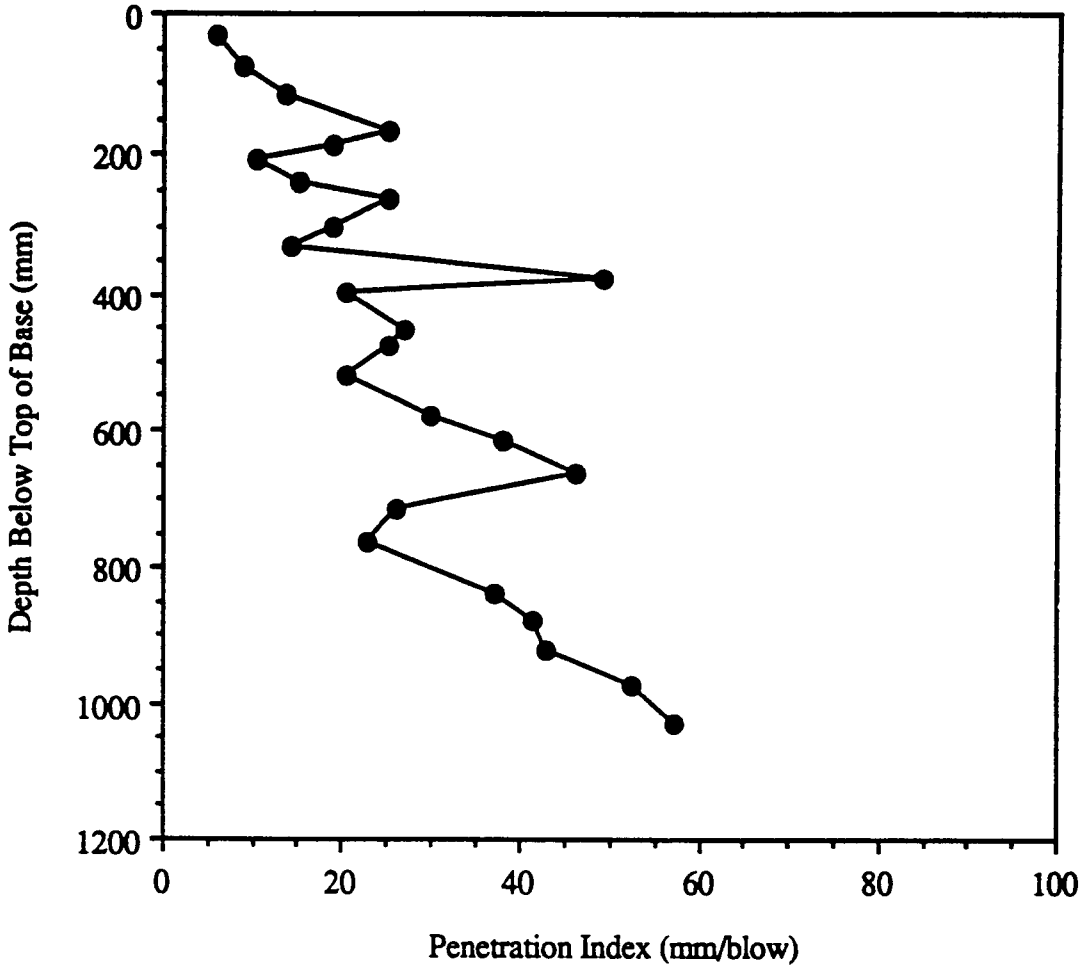

Figure 6.10: Result of DCP Test at Station 4+00 (Outer Wheel Path)

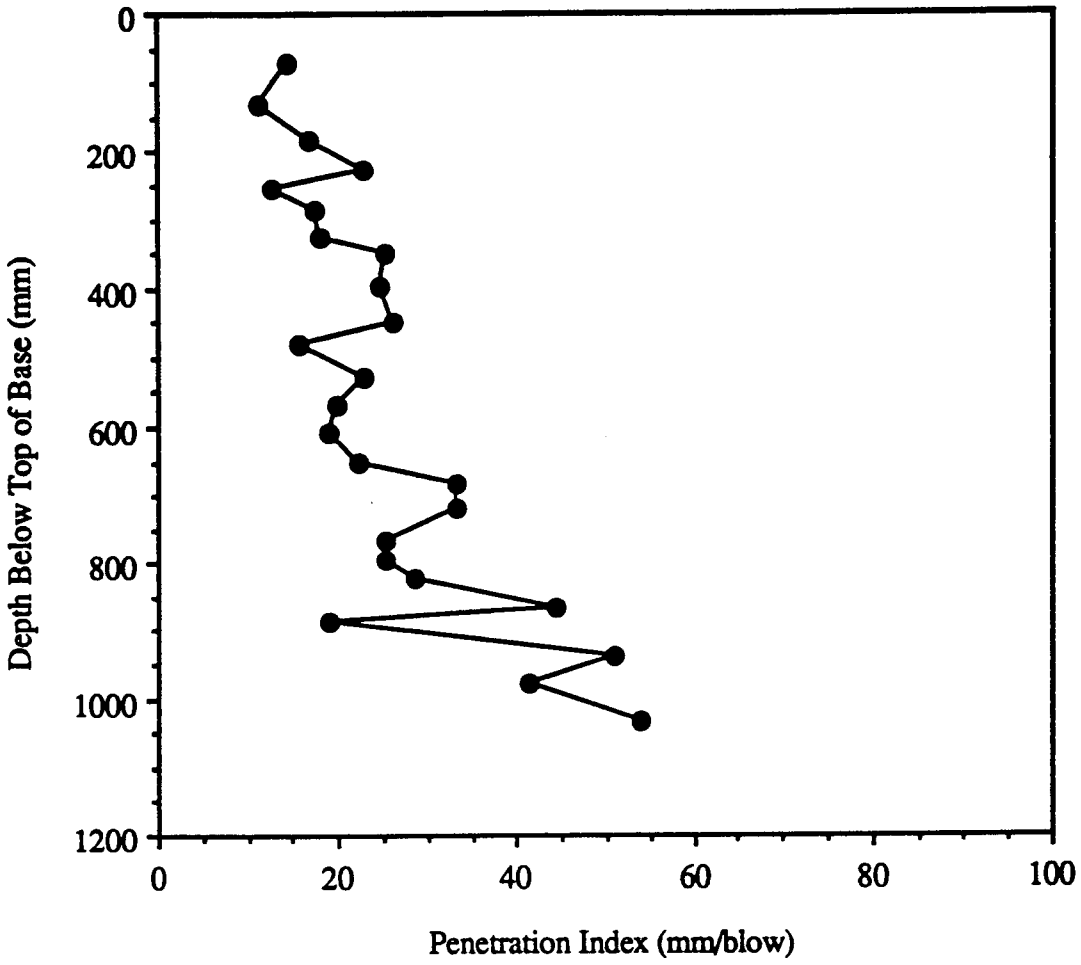

Figure 6.11: Result of DCP Test at Station 4+00 (Centerline)

6.5 Analysis of Section 390101

Section 390101 was analyzed separately. Figures 6.12, 6.13, and 6.14 show the best-fit moduli, the RMS deviations, and a histogram of subgrade modulus values for that section. Figure 6.15 is a plot of the pressure and deflection data from the location having the worst RMS deviation, Station 354+50. Figure 6.16 is an analogous plot for the location having the best RMS deviation, Station 351+75. A typical location, Station 353+25, is represented in Figure 6.17. It should be observed in Figures 6.15 and 6.17 that the linearity is excellent in the typical case and is not excessively poor in the worst. Figures 6.12 and 6.14, however, illustrate the great variability in subgrade modulus, even within a single section.

Referring to Figures 6.1 through 6.5, results of the Falling Weight Deflectometer on the subgrade, base, and asphalt concrete clearly indicate the stiffness of the pavement system varies significantly along the section length. These figures also show the pavement system had more deflection and less stiffness between SHRP Stations 2 and 3 than the rest of this 152.4-meter (500-foot) long section. These high deflections occurred in the same area (SHRP Station 2+65) where the premature fatigue cracking and rutting occurred. This behavior could be explained by poor layer compaction and/or excessive moisture, both of which affect structural integrity of the pavement system. The DCP results indicate non-uniformity throughout the section, with higher Penetration Indices being measured at SHRP Stations 2+50 and 2+65. Data from the statistical analysis, FWD, and DCP all agree with one another and clearly indicate that the subgrade around SHRP Station 2+65 had potential problems.

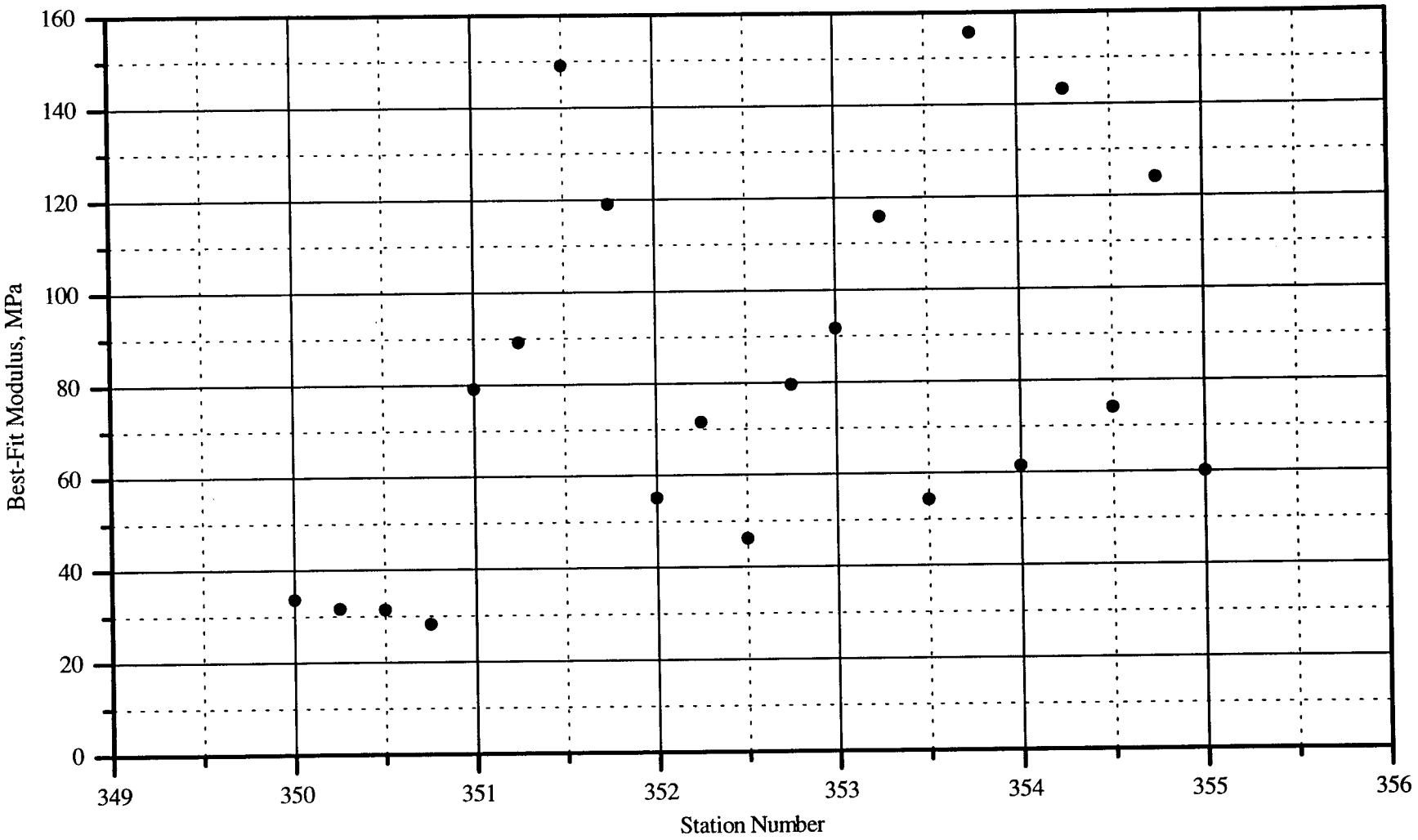

Figure 6.12: Best-fit modulus at each FWD test location for Section 390101.

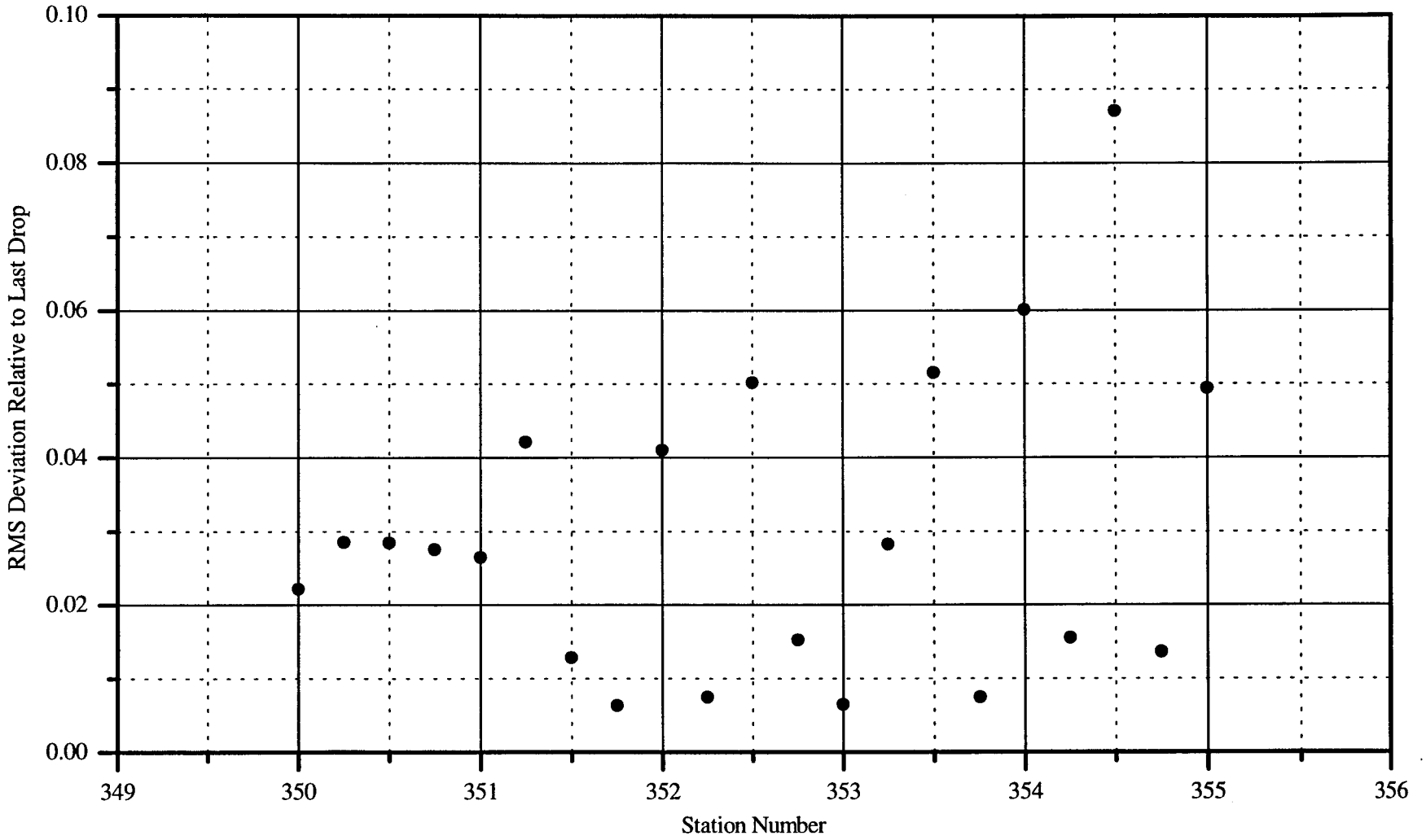

Figure 6.13: RMS deviation from the best-fit line at each FWD test location on Section 390101, as a fraction of the pressure and deflection for the last drop.

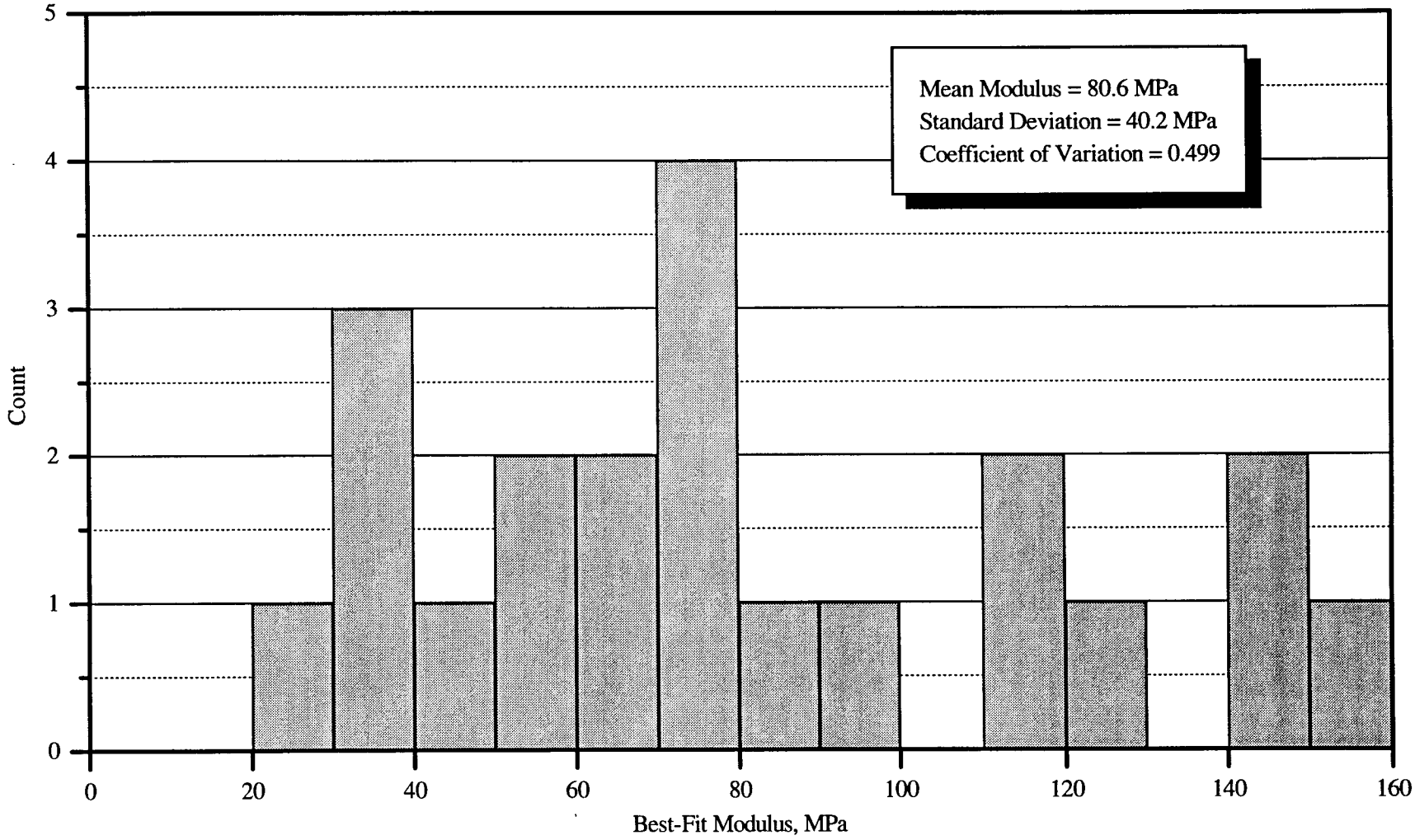

Figure 6.14: Histogram of best-fit moduli from Section 390101.

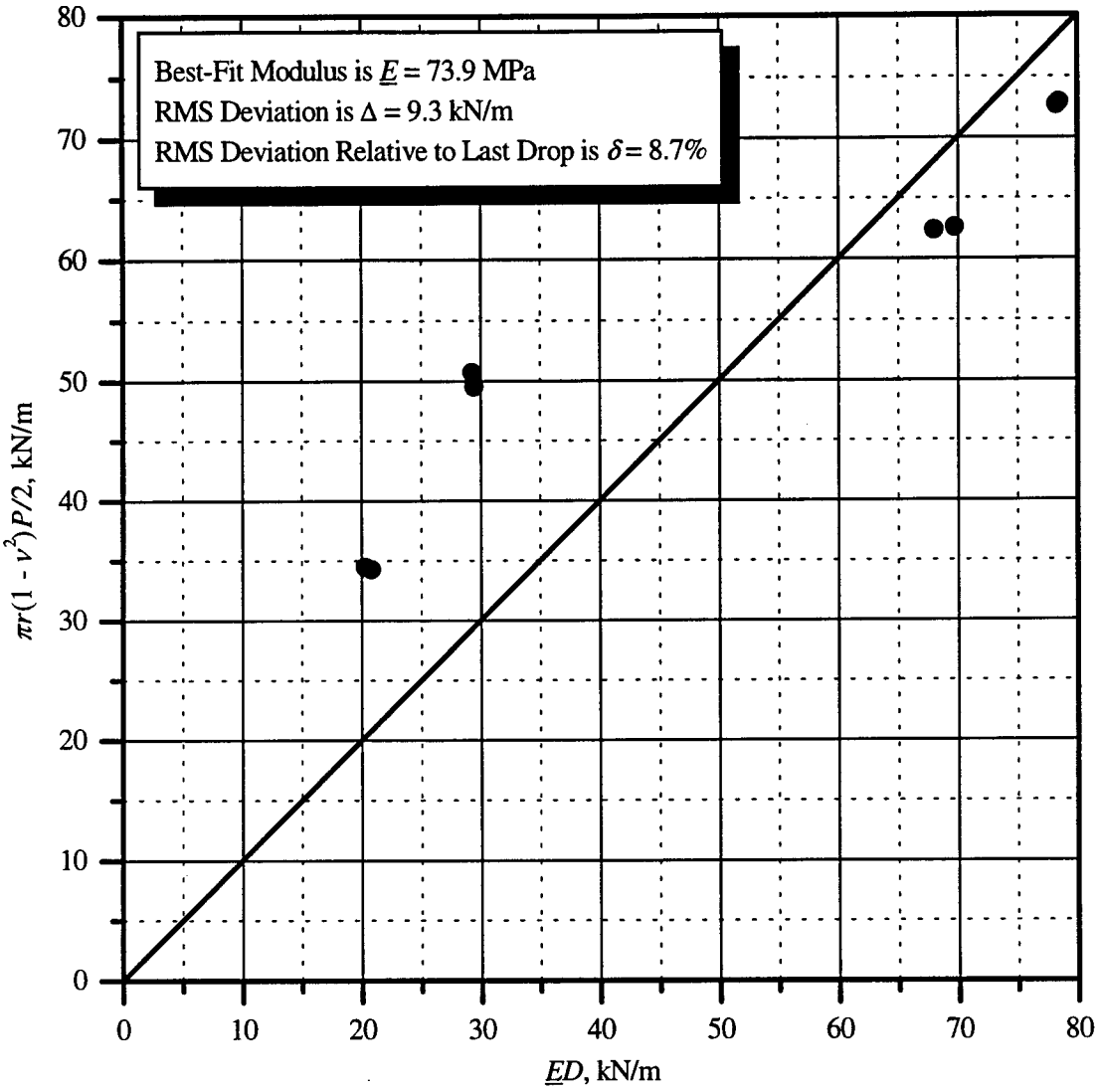

Figure 6.15: Pressure and deflection data and best-fit line for Station 354+50 southbound, the location with the worst RMS deviation on Section 390101.

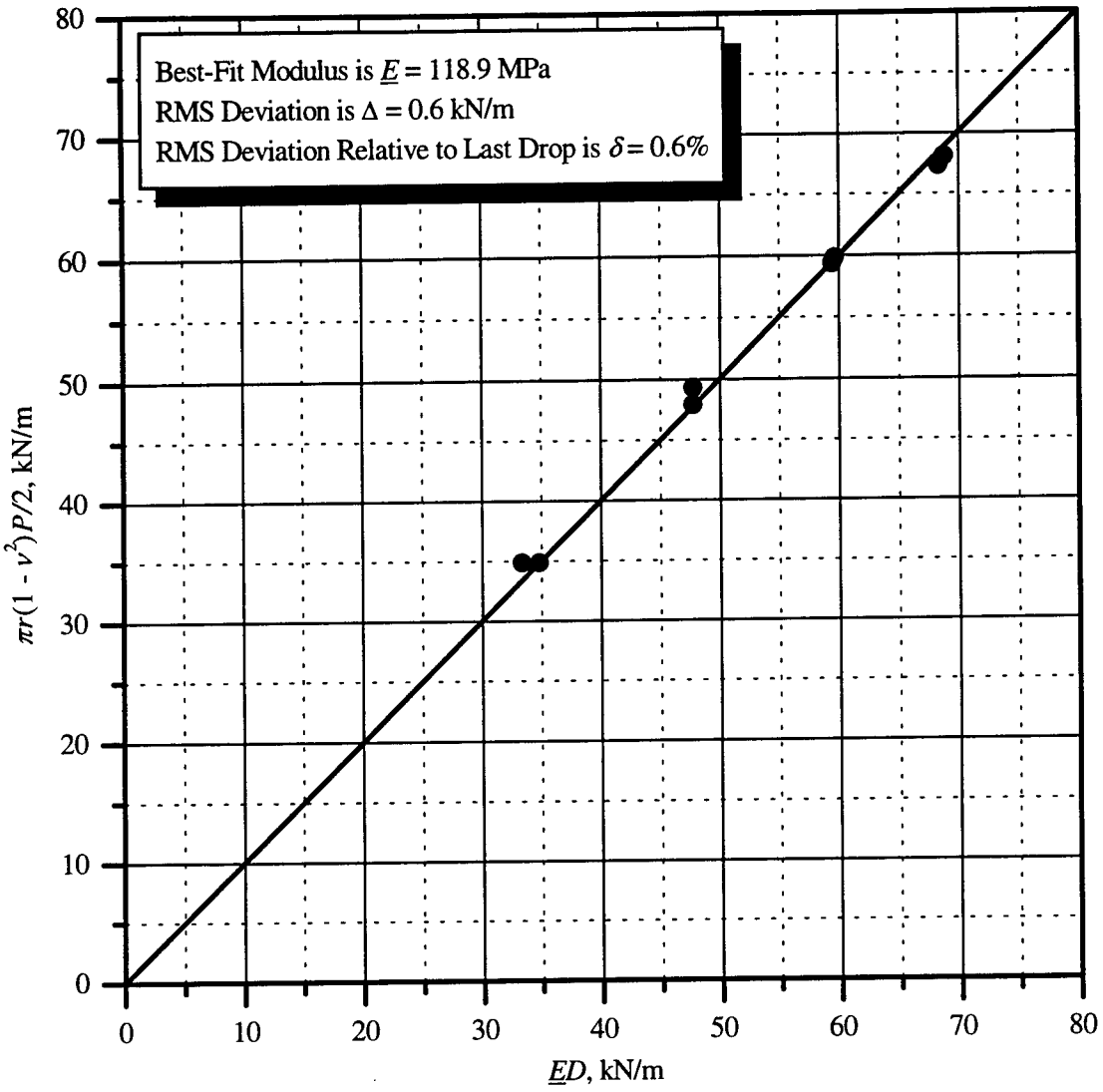

Figure 6.16: Pressure and deflection data and best-fit line for Station 351+75 southbound, the location with the best RMS deviation on Section 390101.

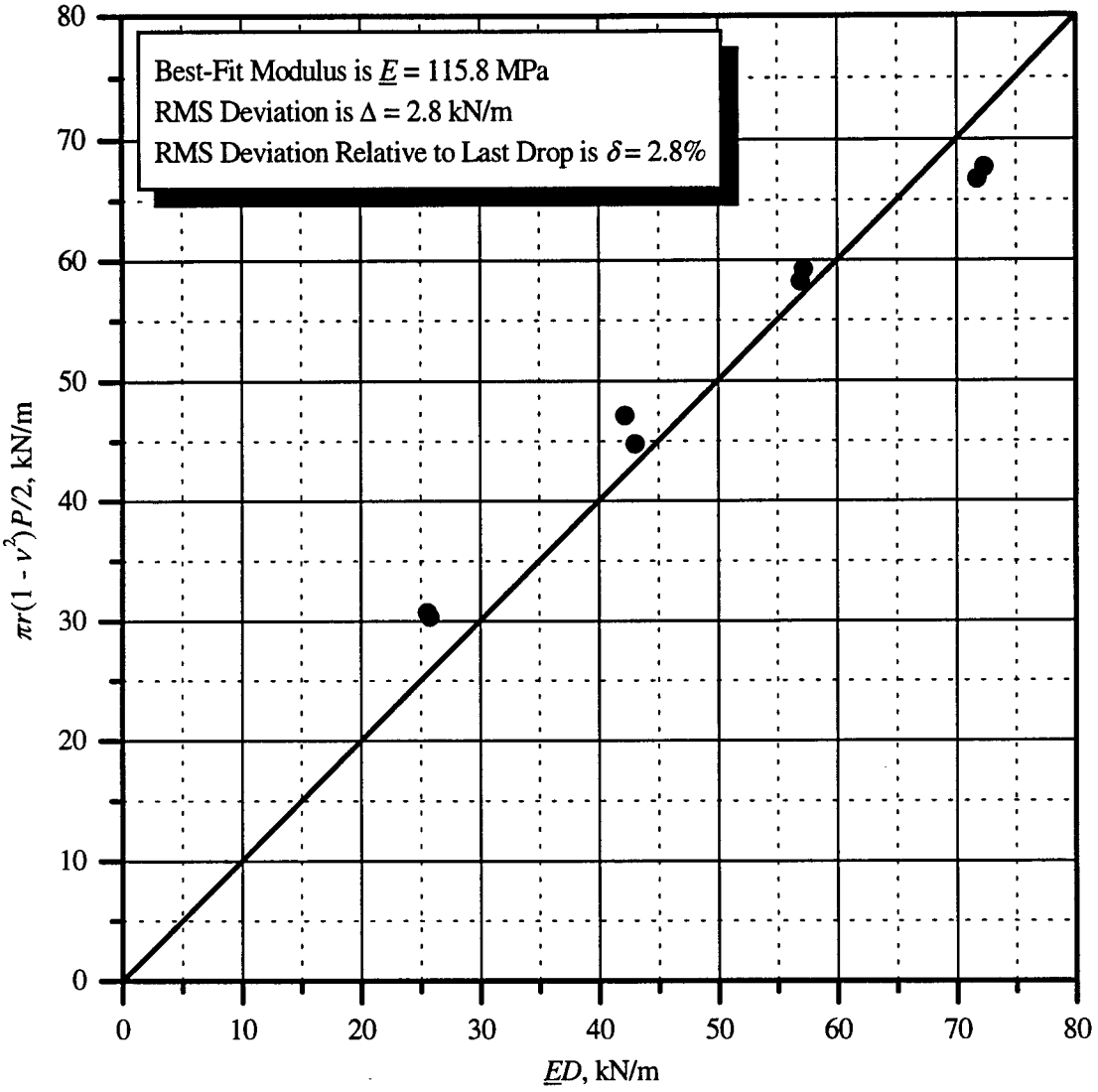

Figure 6.17: Pressure and deflection data and best-fit line for Station 353+25 southbound, a location having a typical RMS deviation on Section 390101.

Chapter 7

Improving Subgrade Uniformity

7.1 Background

Field and laboratory data presented earlier indicate a wide variation in subgrade stiffness within individual test sections and between test sections throughout the 3.5-mile length of the Ohio-SHRP Test Road on U.S. 23 north of Delaware. These results were rather surprising considering the high profile this project received and the following circumstances surrounding it:

1. The project was located in an area of very flat topography.
2. Preliminary borings suggested a relatively uniform soil classification along the 3.5-mile project length.
3. The project was part of a national experiment, and ODOT and SHRP placed a strong emphasis on the importance of having a uniform subgrade to prevent premature failures and possible skewing of the experiment.
4. Provisions were made to replace any subgrade material that failed to meet the construction specifications.
5. Extensive sampling and testing were performed throughout each phase of construction.

7.2 Construction Monitoring of Subgrade

During excavation for this test pavement, unsuitable subgrade material was removed, occasionally to a depth of several feet, and replaced with borrow from a pit adjoining the project. Under standard ODOT specifications used on the U.S. 23 project, moisture and density were monitored as the excavated areas were built up to grade. Acceptance of the finished subgrade was based on the unit weight or density achieved during compaction with a steel wheel roller, and final proof rolling. Approximately three density measurements were taken with a nuclear density gauge in each 500-foot test section, which represents a very small percentage of the total area being evaluated. Subsequently, the sections were proof rolled to further identify areas of weakness where corrective action might be required. Proof rolling certainly is a more comprehensive test

of the entire subgrade surface, but it is subjective, it is somewhat unreliable as evidenced by the variations noted, and its use is not always feasible, especially on small projects.

7.3 Pavement Design Methodology

When designing a highway pavement, engineers establish a period of time over which they expect it to carry an estimated volume of traffic before requiring major rehabilitation. Using a variety of different analytical procedures, a series of material layers are then selected to comprise a pavement structure which will provide the necessary stiffness and durability to meet this life expectancy. Generally, layers placed close to the pavement surface are stiffer, more resistant to environmental fluctuations, better able to resist high stresses imposed by heavy traffic loads and capable of distributing these loads over less stiff layers lower in the structure.

In elastic theory, the stiffness of each pavement layer is quantified by assigning it a modulus of elasticity based upon known characteristics of the material in that layer. The layered structure is then modeled as a composite structure, with internal stresses, strains, and deflections being determined under standard wheel loading. By correlating these results with fatigue characteristics of the various materials being proposed, the functional life of the pavement can be estimated. A structural deficiency in any of the layers, especially the subgrade which supports the entire structure, can seriously affect the overall performance of the pavement.

During construction, stiffness of the pavement layers is not monitored in a manner consistent with the way they were modeled or the way they will carry traffic. Subgrade stiffness is typically correlated to density, with higher density being indicative of higher stiffness. While this premise is generally true, actual in-situ layer stiffness cannot be determined directly from density measurements. Also, density tests are limited in effectiveness by infrequent spacing throughout projects and the localized area being tested around the nuclear gauge. They are particularly limited in testing density with depth.

7.4 Nondestructive Testing Techniques

Nondestructive testing (NDT) with the Falling Weight Deflectometer (FWD) or Dynaflect is a viable option for testing the in-situ stiffness of pavement layers in a manner more consistent with pavement geometry and traffic loading. In NDT, a dynamic load is applied to the uppermost pavement layer in place at the time of testing, and surface deflections are measured in the basin generated by the load. The shape of this basin is a function of the composite action of all layers in the structure to a depth of several feet. These data can then be used to backcalculate actual moduli of the various layers in the structure at that point in time and compare with the original design assumptions.

Objective measurements of structural integrity of the pavement can be obtained quickly, evaluated at the site, and recorded for future assessment. Raw deflection data can be used without the necessity of converting it to moduli. Maximum acceptable deflections can be established for each layer within the pavement structure as it is constructed, either to provide some minimal overall level of support or to identify areas which deviate beyond some acceptable level above the mean average deflection to reduce variability and improve uniformity.

While it is often necessary to convert deflection measurements to moduli for a better understanding of how layer stiffness impacts pavement performance, this conversion is not necessary in the field when in-situ stiffness is being evaluated with NDT techniques. Figure 7.1 shows how the Boussinesq equations relate surface deflection generated by a FWD to the modulus of a single uniform layer, as described in Chapter 4. Using this relationship for pavement subgrade, maximum acceptable deflections can be established for quality control during construction. Areas showing deflection higher than accepted limits can be marked for corrective action as the tests are being performed. When the measurements have been completed, data can be reviewed on site to identify additional areas where deflection may not exceed the established maximum limits, but may exceed an allowable deviation above the mean deflection. These areas also can be marked that same day for correction.

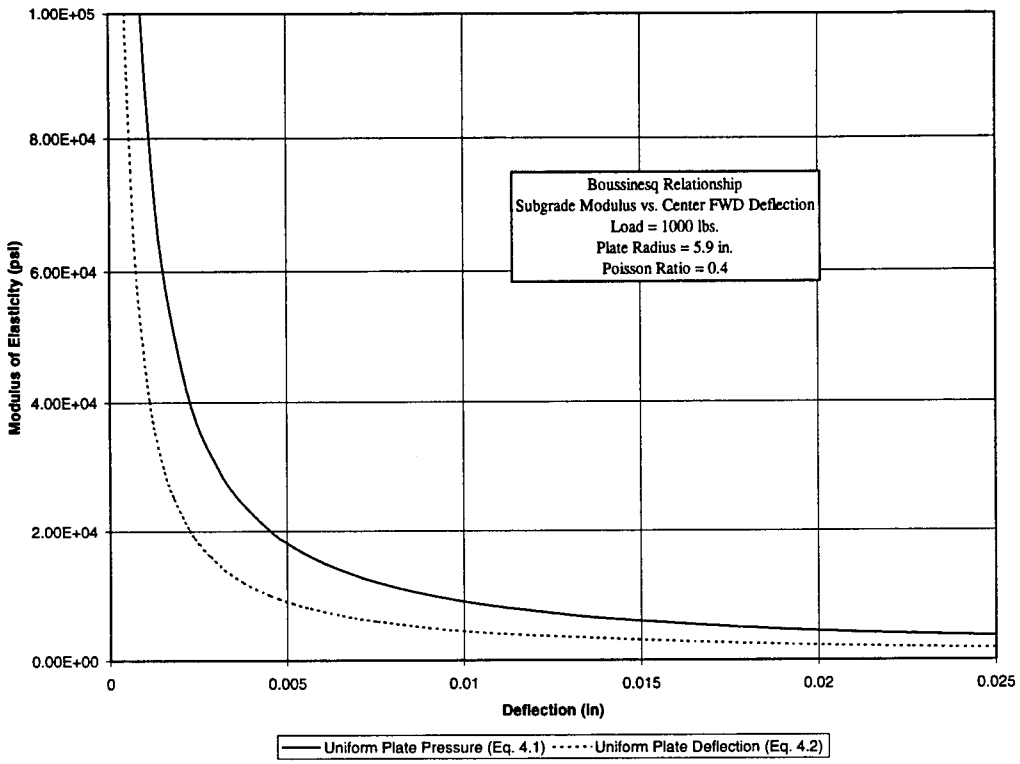

Figure 7.1(a): Subgrade Modulus vs. FWD Deflection. (English Units)

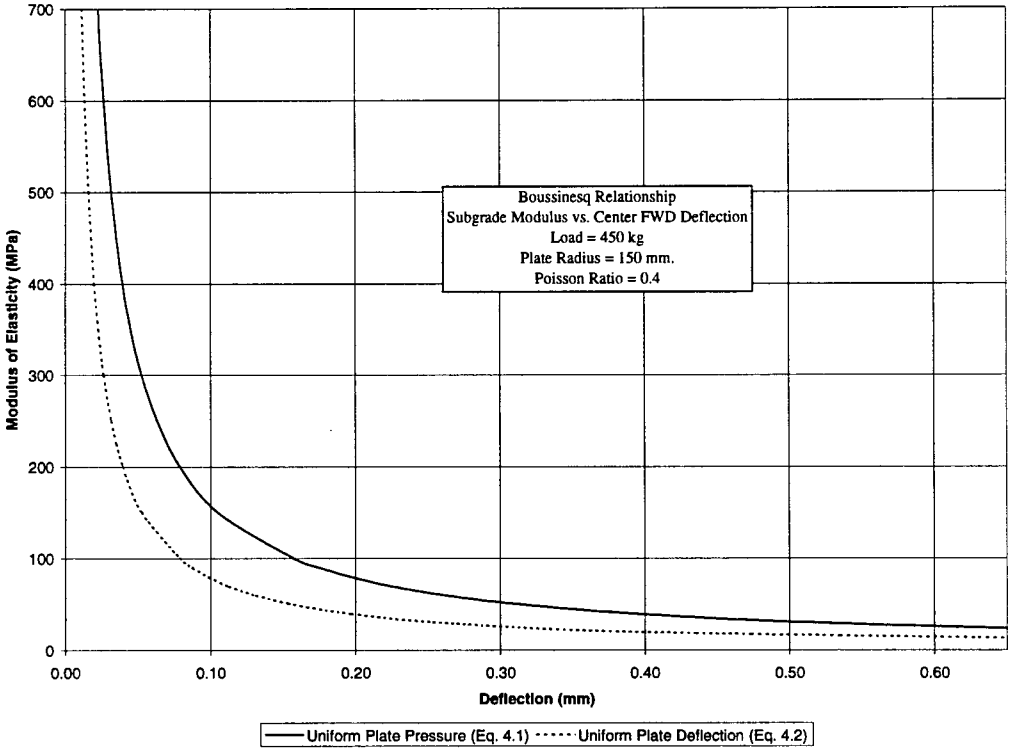

Figure 7.1(b): Subgrade Modulus vs. FWD Deflection. (Metric Units)

Because subgrade stiffness can fluctuate dramatically with moisture content, some attention must be given to this parameter. NDT measurements should be taken at about the same time nuclear measurements or proof rolling would be performed and not when the subgrade is unusually wet. This is reasonable from the standpoint of getting the equipment on the subgrade and having it operate properly. In the Midwest, once subgrades are covered over with additional pavement layers, they tend to retain more moisture and provide less support throughout much of the year than NDT readings obtained during construction might indicate. This factor can be accounted for by reducing allowable deflections at the time of construction.

While the FWD and Dynaflect test pavements in a similar manner, the load and sensor geometry are different. The FWD applies haversine loads of up to about 1,385 kPa (22,000 lbs.) and has the option of placing seven sensors at selected distances (up to several feet away with a remote sensor) from the center of a 300 mm (11.8 in.) diameter load plate. Traditionally, ODOT uses a sensor spacing of 0, 203, 305, 457, 610, 914, and 1524 mm (0, 8, 12, 18, 24, 36, and 60 in.) on the FWD. The Dynaflect is more fixed in load application and sensor spacing. A total of 63 kPa (1000 lbs.) is applied sinusoidally through two rigid wheels spaced 20 in. apart. The first sensor is midway between the wheels at 254 mm (10 in.), while the four remaining sensors are distributed outward across the basin to a distance of about 1.2 m (4 ft).

On occasion, the accuracy of data obtained at the center or edge of the FWD load plate appears to be questionable when deflections do not increase to the center of the plate as would normally be expected. In these situations, a sensor away from the load plate may be used for evaluating the subgrade. This approach may also be useful when correlating data from the FWD and Dynaflect, since the Dynaflect does not measure deflection under or at the edge of the loaded area.

To eliminate the problem of dealing with different loads for nondestructive evaluation, deflections in Figure 7.1 are shown for a load of 4,400 N (1,000 lbs.). An earlier ODOT study and subsequent deflection measurements on the completed U.S. 23 pavement showed a clear correlation between the FWD and the Dynaflect when loads are normalized to 4,400 N (1000 lbs.). Therefore, either device could be used to monitor

subgrade stiffness. It requires about one minute of time to obtain data at a given point with the FWD or Dynaflect.

7.5 Dynamic Cone Penetrometer

Another piece of equipment that offers some potential benefits in measuring subgrade stiffness is the Dynamic Cone Penetrometer (DCP). The DCP applies a standard amount of energy to a rod as it is driven into the subgrade. The rate of penetration is continuously monitored so stiffness can be evaluated in the subgrade with depth. While resistance to a driven rod may not be a direct indication of how layers within a composite structure carry load, it is a measure of stiffness and specific layers of weakness within the subgrade structure can be identified quickly. NDT tests can be used to show areas of reduced stiffness, but they do not readily identify the depth to the problem. Corrective action may be required during construction when the DCP rate of penetration exceeds some established criteria. It requires approximately five minutes to test the subgrade to a depth of 1.2-m (4 ft) at a given point.

Chapter 8

Summary and Conclusions

From Tables 4.1and 4.2, the average subgrade modulus calculated for the 19 test sections on the northbound side of the Ohio SHRP Test Road was 100.8 Mpa, with a range of 34.3 to 205.3 Mpa. From Tables 4.1 and 4.3, the average modulus calculated for the 17 test sections on the southbound side was 108.9 Mpa, with a range of 39.8 to 186.0 Mpa. The sections with the lowest modulus on each side of the pavement were constructed a year later than the other sections and were noted to have much higher moisture content at the time the FWD measurements were obtained. According to the ODOT Design Manual, the average modulus associated with A-6, A-4 and A-7-6 soils is 49.7 Mpa. With the exception of the two sections with unusually low moduli, the condition of the subgrade at the time the FWD measurements were taken was relatively dry, and stiffnesses calculated then would be expected to be higher than average design values assumed for the entire year. As the base and pavement layers were added, and as moisture migrates into the subgrade, these in-situ moduli would be expected to drop significantly as suggested by laboratory tests. They may even remain below the assumed value of 49.6 Mpa for much of the year. This could result in a reduced service life for these pavement sections

Variability of subgrade stiffness can be a significant cause of premature localized distress in the pavement system. This variability can be caused by deviations in moisture content, density of the material, and inconsistencies during construction. Construction specifications generally require that the subgrade be compacted to a designated density. Even if uniform density is achieved in the field, it does not guarantee the subgrade stiffness will be uniform since density alone is not a reliable parameter to describe the mechanical properties of subgrade. In addition, the monitoring of density in the field is time consuming and labor intensive. An alternative approach to density specifications for subgrade compaction is the utilization of stiffness.

Soil stiffness can be determined from non-destructive testing devices such as the Falling Weight Deflectometer, and Dynaflect, or with the Dynamic Cone Penetrometer. Generally, non-destructive testing can be conducted in a short period of time, thereby allowing a more comprehensive sampling of the surface area. Recently, a new device (Humbold Stiffness Gauge) has been introduced. This device also measures in-place stiffness at the rate of one test per minute, but only to a depth of six inches.

On the Ohio SHRP Test Road, subgrade stiffness was quantified as back-calculated moduli using data from the FWD. Here it is shown that a linear model can be employed with reasonable accuracy. It was revealed that stiffness varied greatly along individual test sections and throughout the entire project. Because stiffness is determined from one sensor under the FWD load plate, it can be evaluated directly from the deflection measured by this sensor.

Employing a nuclear gauge, subgrade density and moisture were monitored in the field 300-mm (12 in.) below the surface at three locations in each test section. In this study, it was illustrated that it is difficult to achieve uniform moisture or density through the entire project. In addition, a good correlation between moisture and density with stiffness cannot be established. One of the main reasons is that moisture and density are monitored at a specific depth where, in the computation of stiffness, the influence of the entire thickness of soil mass is incorporated.

A comprehensive laboratory study was conducted to determine the resilient modulus of subgrade for specific moisture, density, and stress levels for a range of soils present in the Ohio SHRP Test Road. The data indicated that the resilient modulus of the subgrade was very sensitive to the moisture content. The results from the laboratory study are necessary for accurate mathematical modeling of the pavement structure.

The laboratory study yields some valuable information for the resilient modulus of subgrade. As the deviator stress increased, the resilient modulus sharply decreased. The resilient modulus remained almost constant beyond a deviator stress of about 62-kPa (9-psi). The effect of confining stress was insignificant on the resilient properties of all soil types. The higher the clay content in the soil, the more sensitive its resilient modulus was

to changes in moisture content. An increase in the moisture content leads to a decline in the resilient modulus when the dry unit weight stays constant. An increased dry unit weight leads to a higher resilient modulus at low moisture contents but to a lower resilient modulus at high moisture contents.

Excessive rutting was observed at a limited number of locations in Section 390101. A forensic study of this section revealed that premature localized distress in the pavement occurred in areas of lowest subgrade or base stiffness. This reinforced the belief that stiffness of the subgrade and base should be monitored during construction. In this investigation, the dynamic cone penetrometer (DCP) provided valuable information on soil stiffness at various depths and confirmed conclusions drawn from the FWD data.

This study revealed that soil stiffness is a parameter that plays a key role in the quality control of pavement subgrade in the field. Any variability in subgrade support is very crucial to pavement performance, especially those constructed for limited service. Data from the Ohio SHRP Test Road and other test pavements around the U.S. could be used to establish minimum requirements for average subgrade stiffness and/or maximum acceptable deviations in the stiffness over a project length.

Appendix

Best-fit modulus and range at each falling-weight test location.

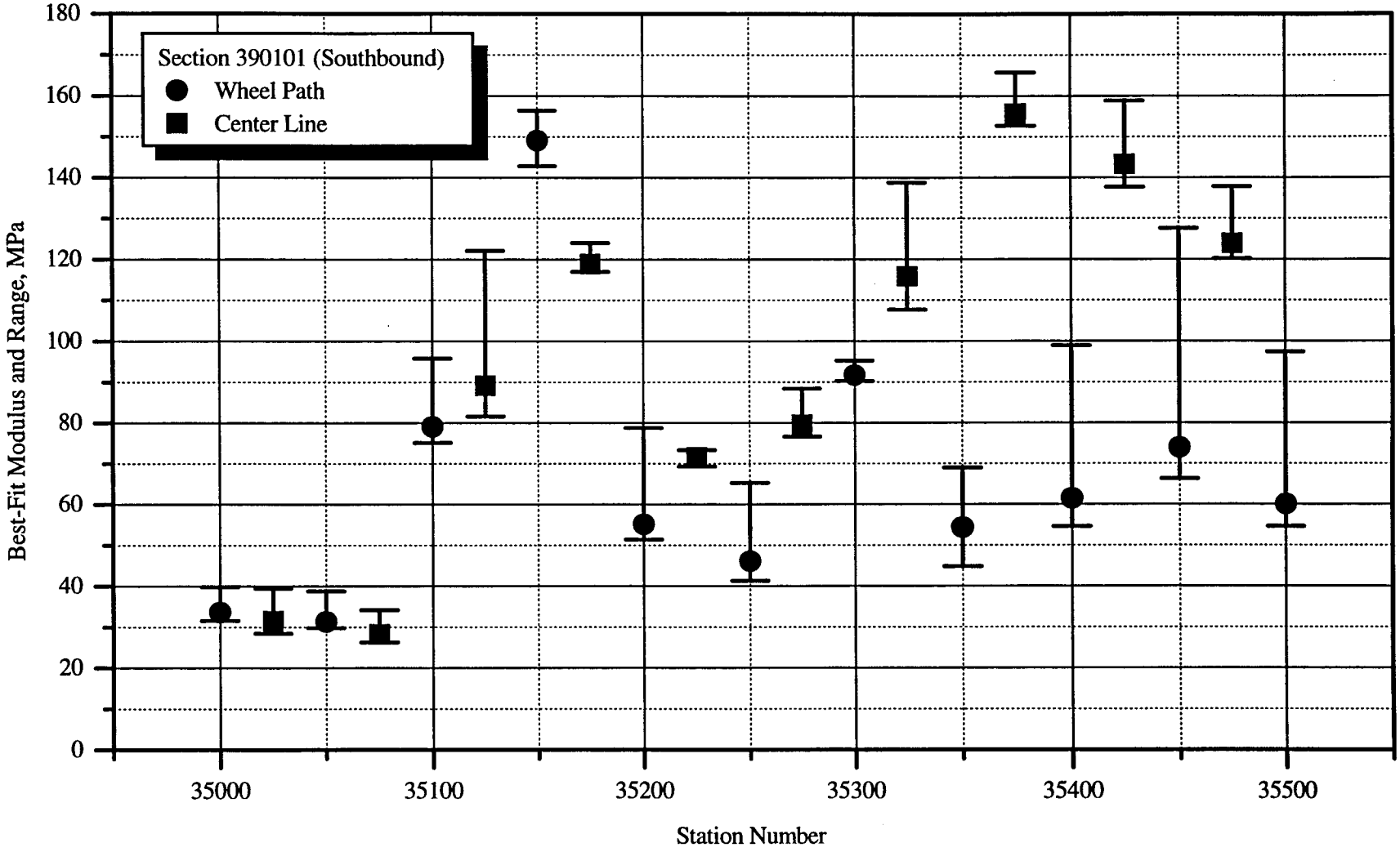

Figure A.1: Best-fit modulus and range at each falling-weight test location in section 390101.

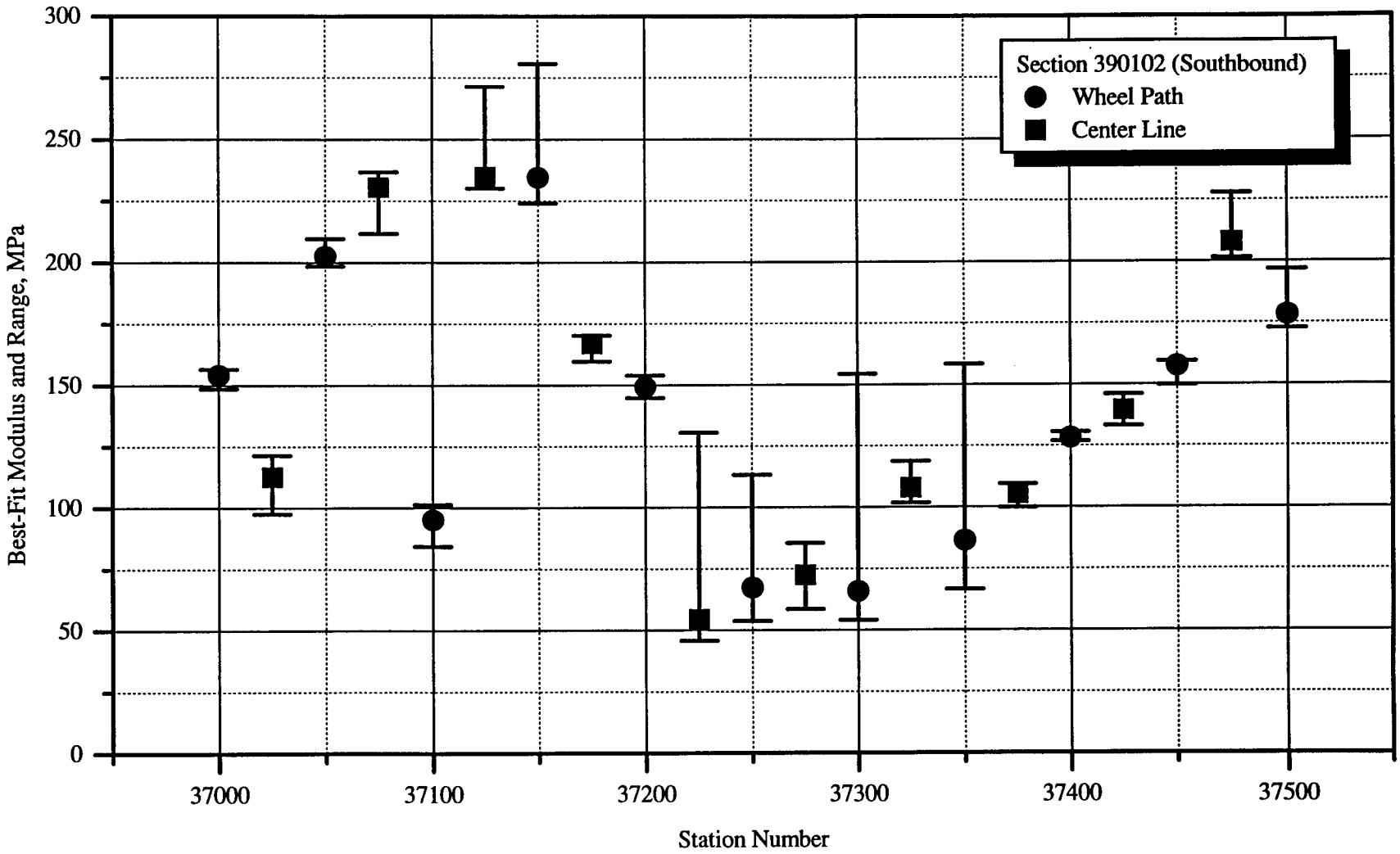

Figure A.2: Best-fit modulus and range at each falling-weight test location in section 390102.

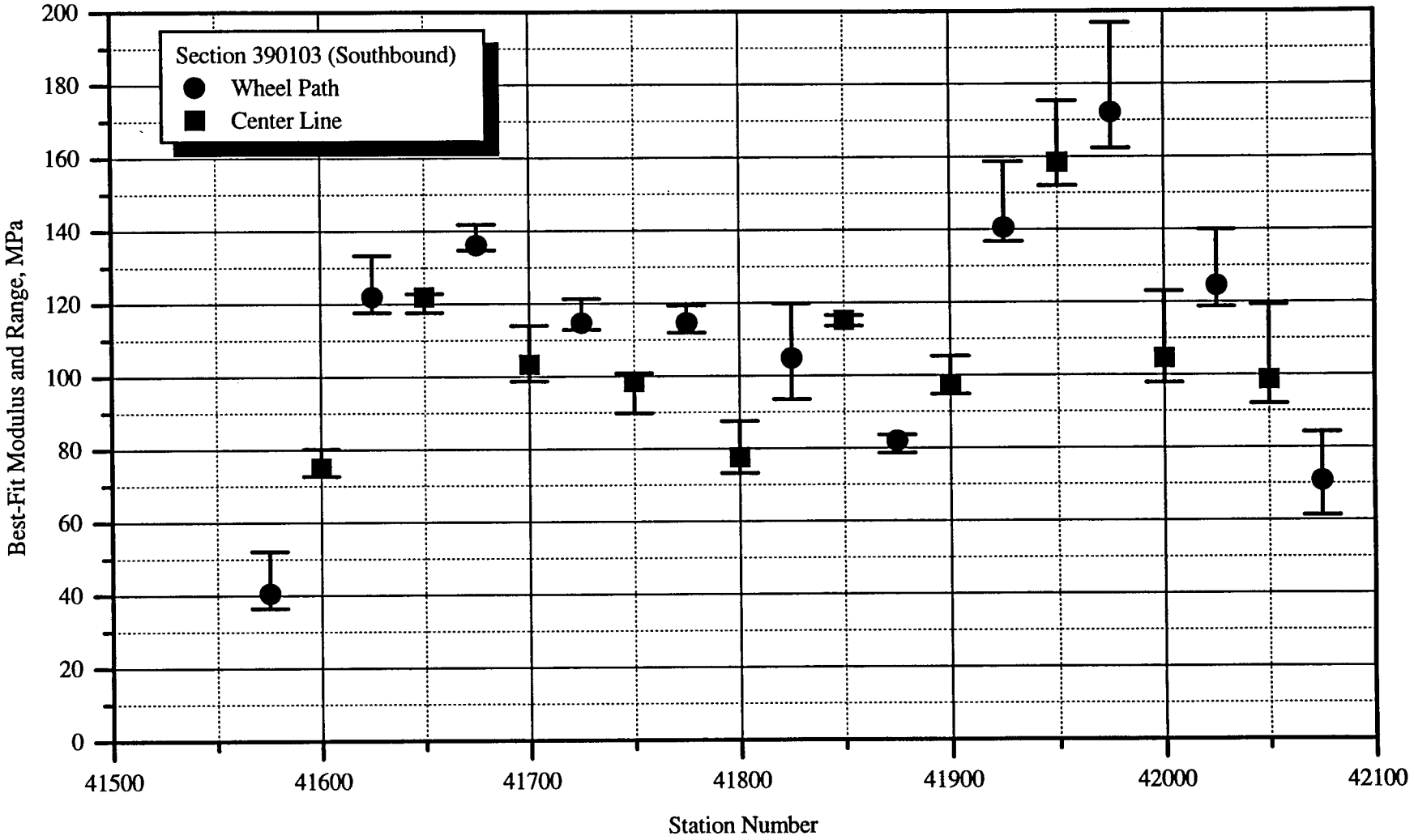

Figure A.3: Best-fit modulus and range at each falling-weight test location in section 390103.

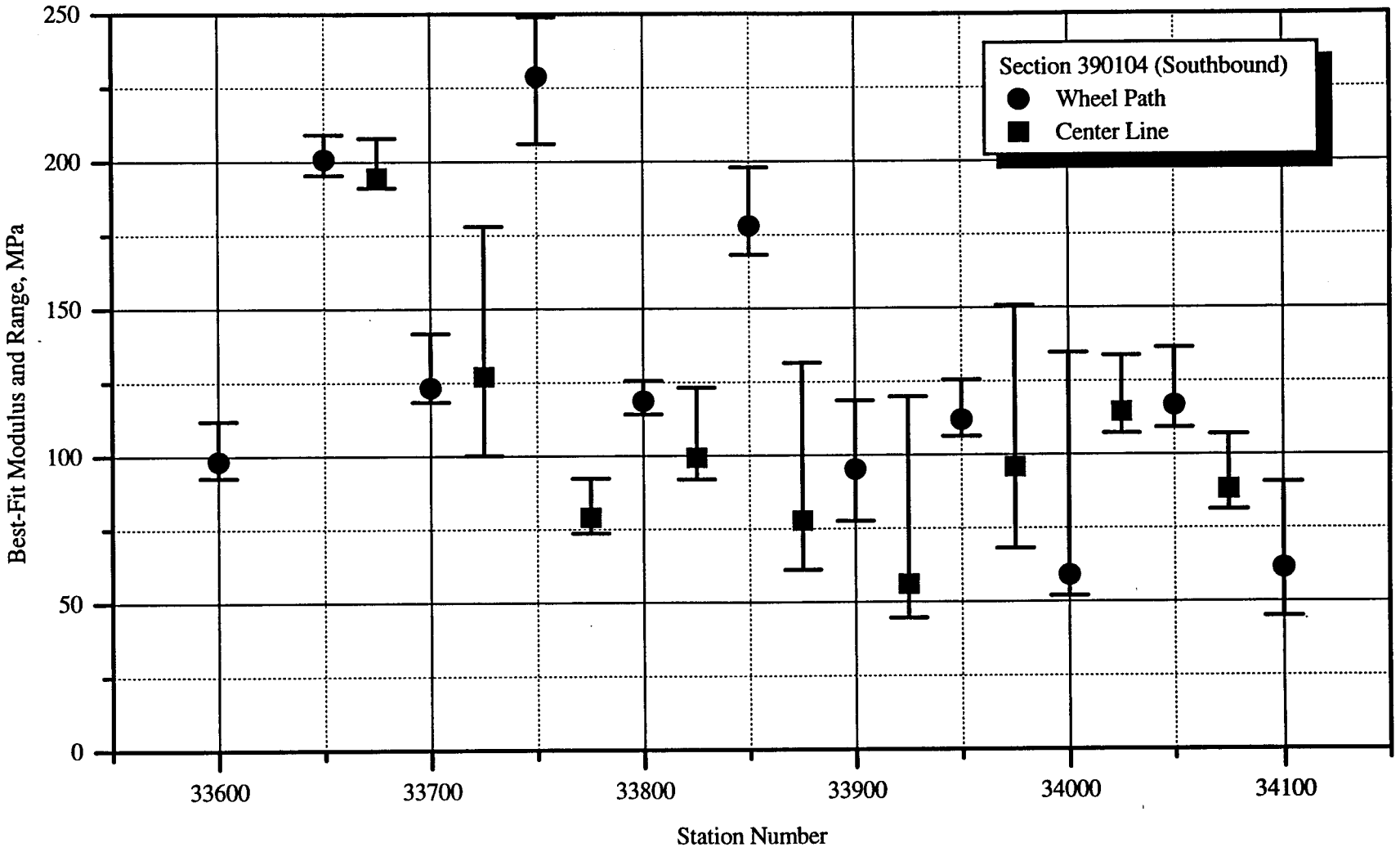

Figure A.4: Best-fit modulus and range at each falling-weight test location in section 390104.

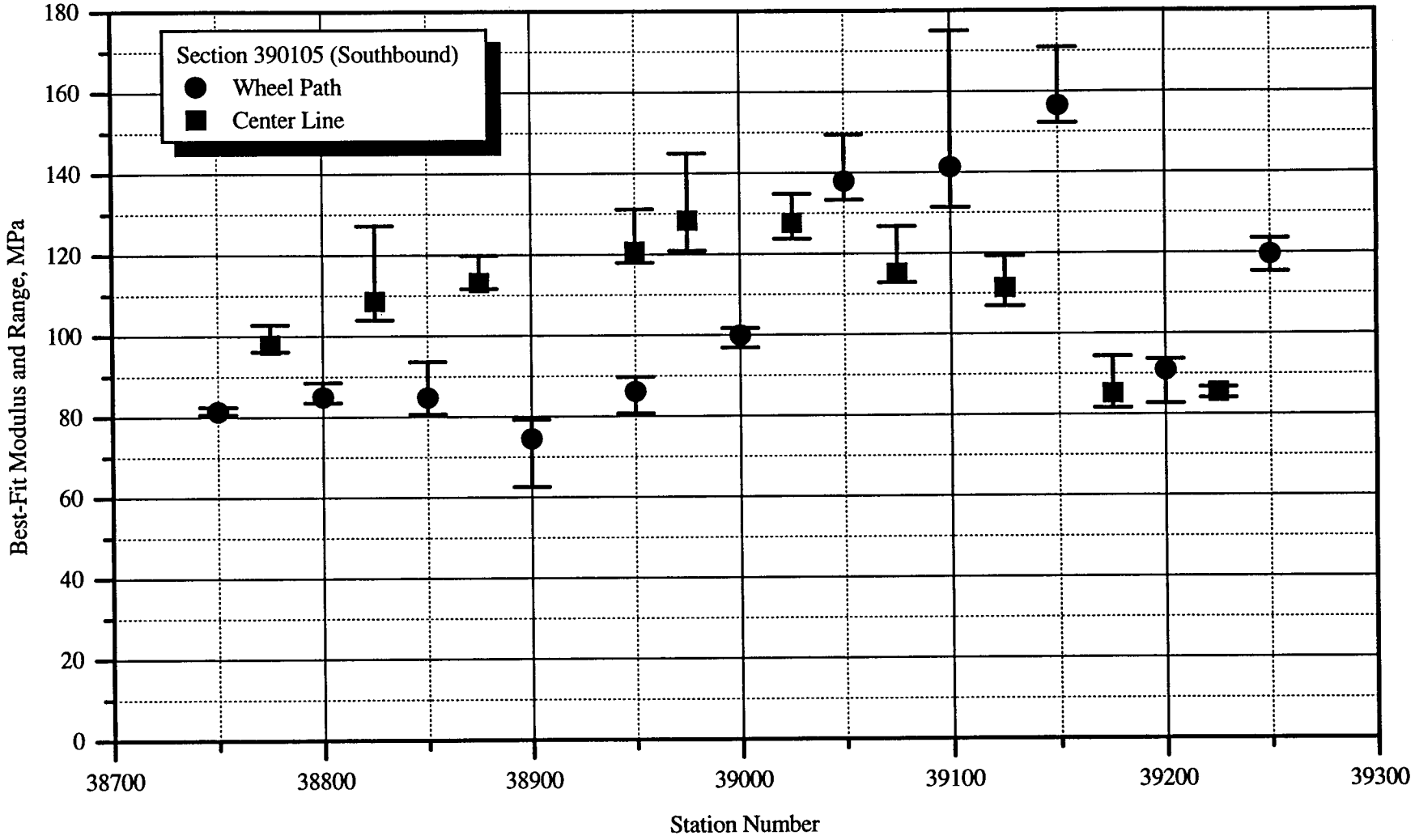

Figure A.5: Best-fit modulus and range at each falling-weight test location in section 390105.

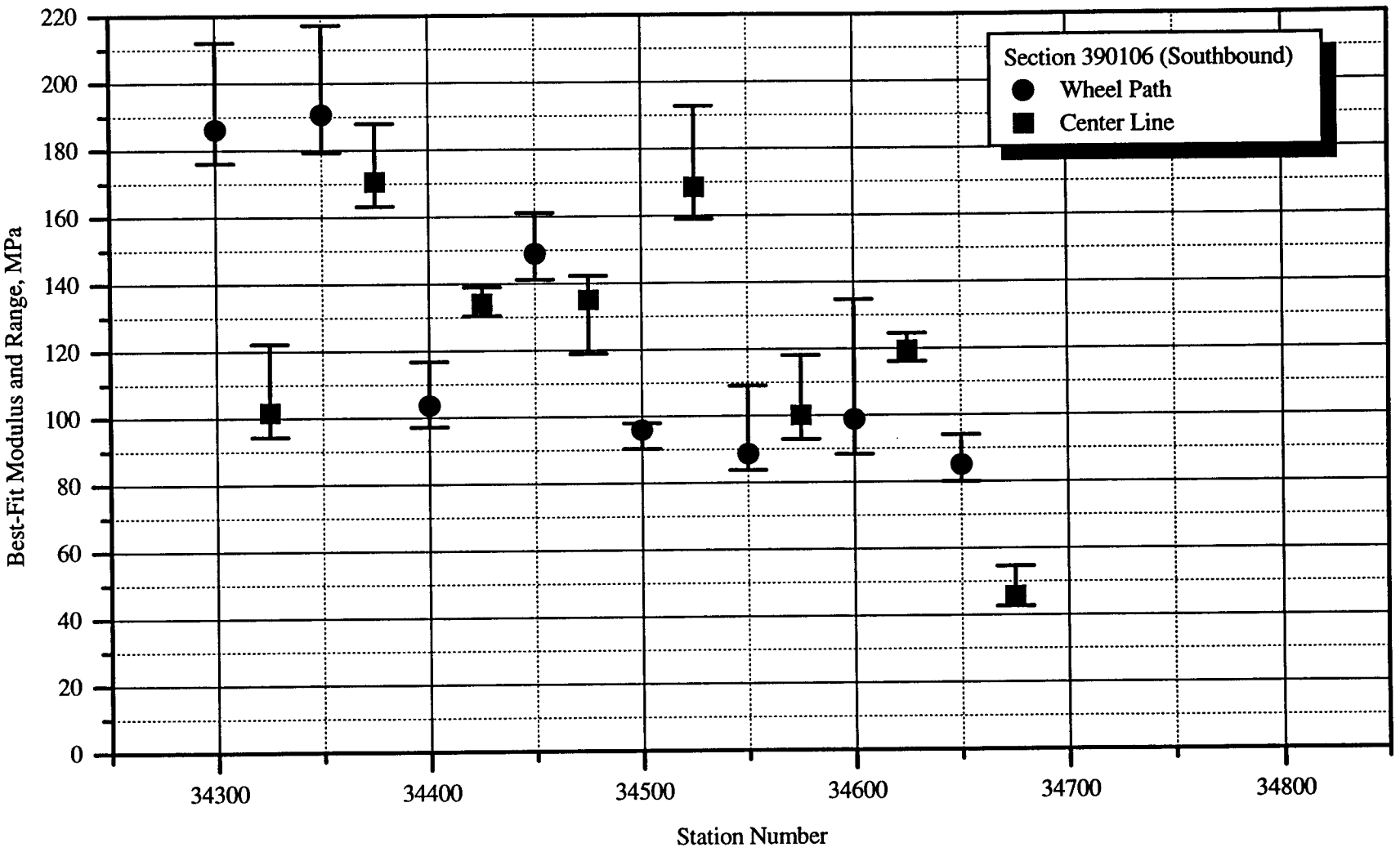

Figure A.6: Best-fit modulus and range at each falling-weight test location in section 390106.

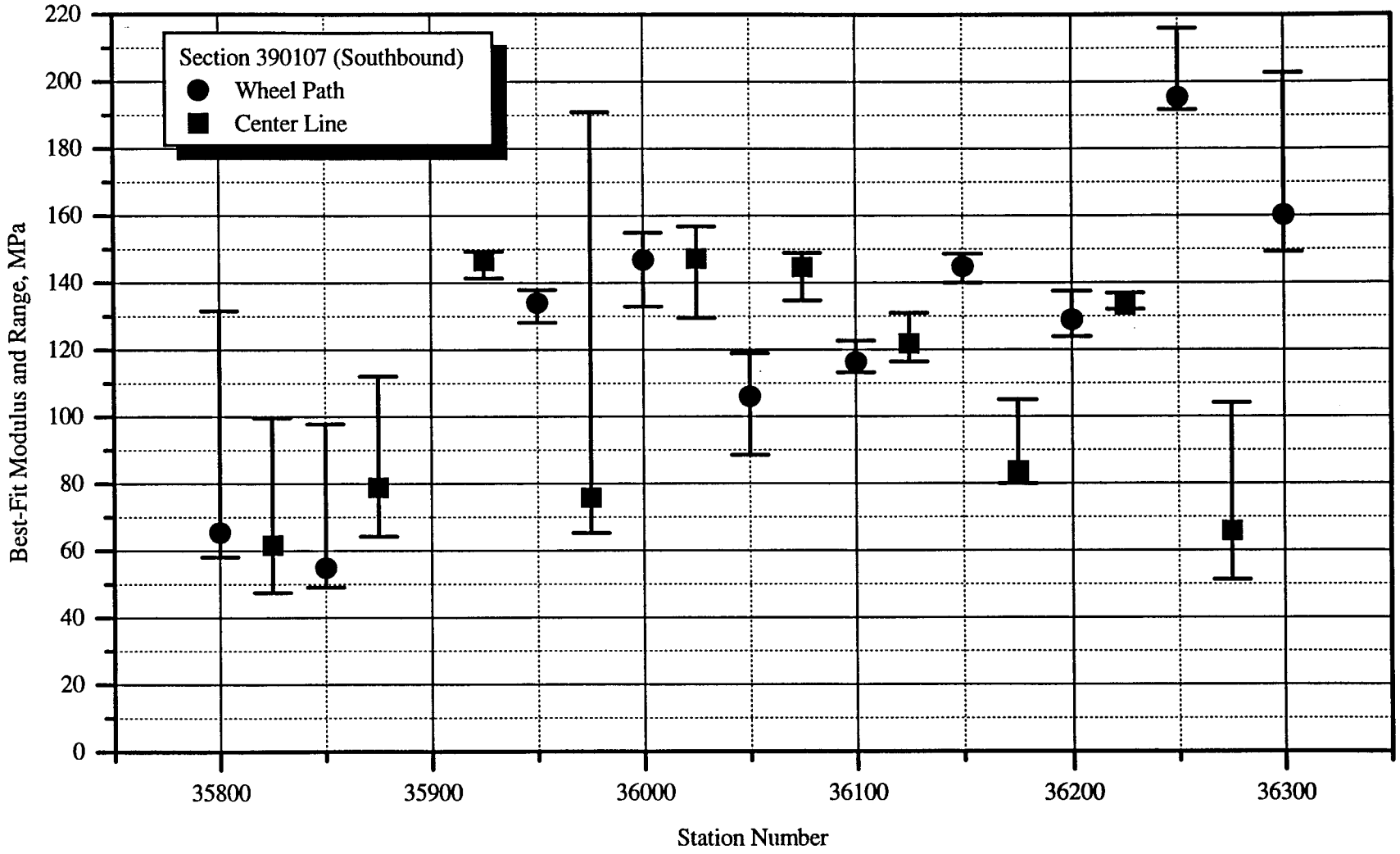

Figure A.7: Best-fit modulus and range at each falling-weight test location in section 390107.

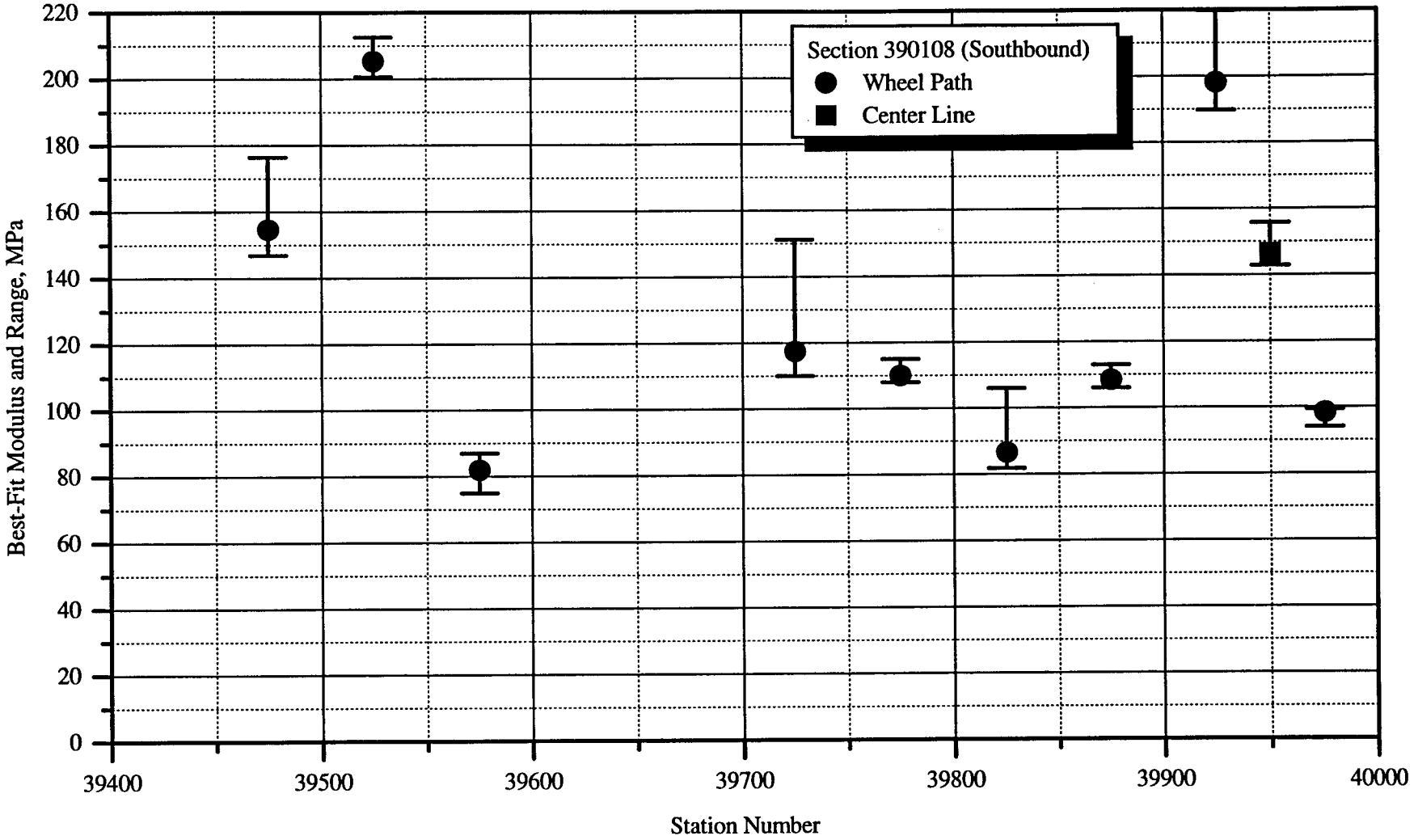

Figure A.8: Best-fit modulus and range at each falling-weight test location in section 390108.

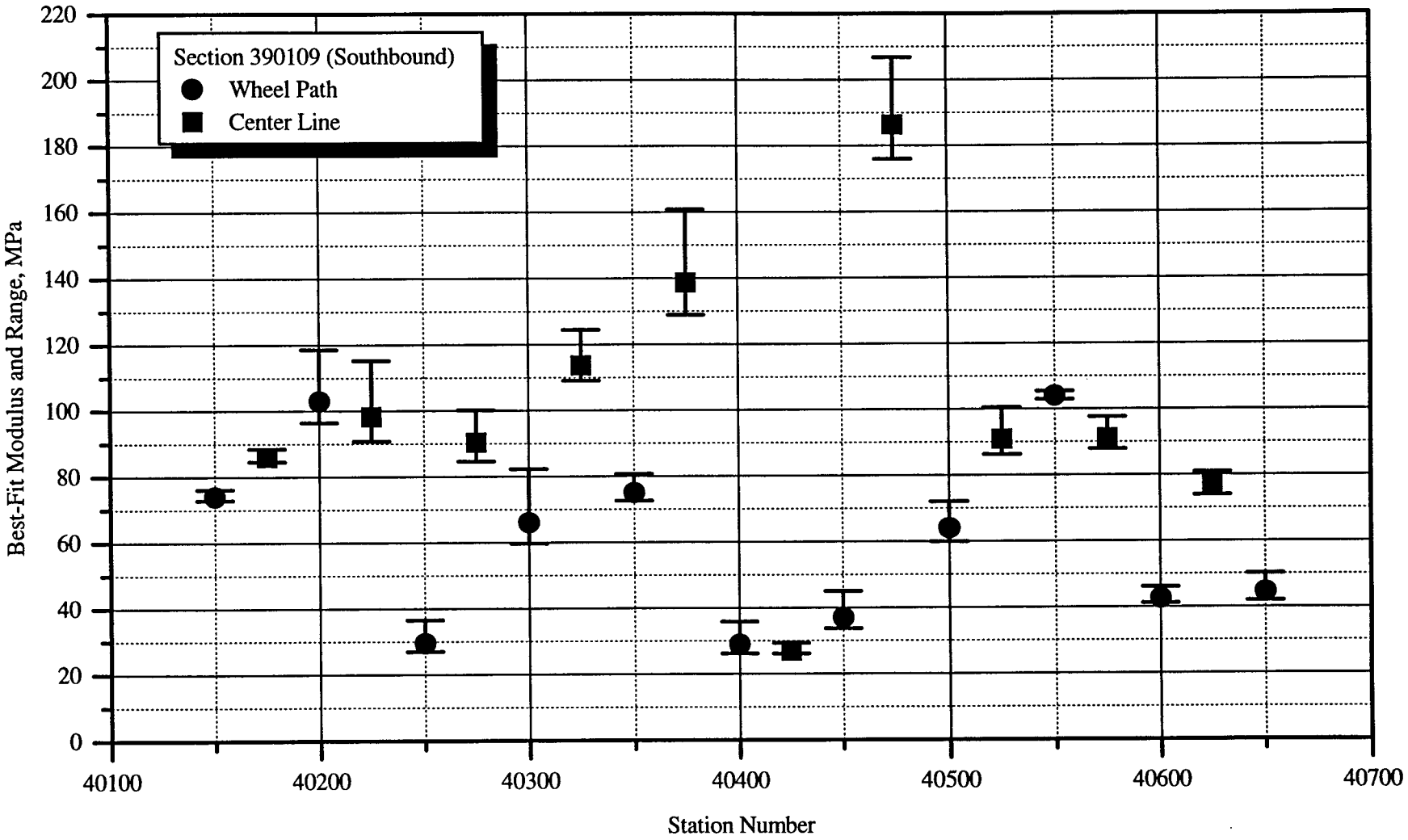

Figure A.9: Best-fit modulus and range at each falling-weight test location in section 390109.

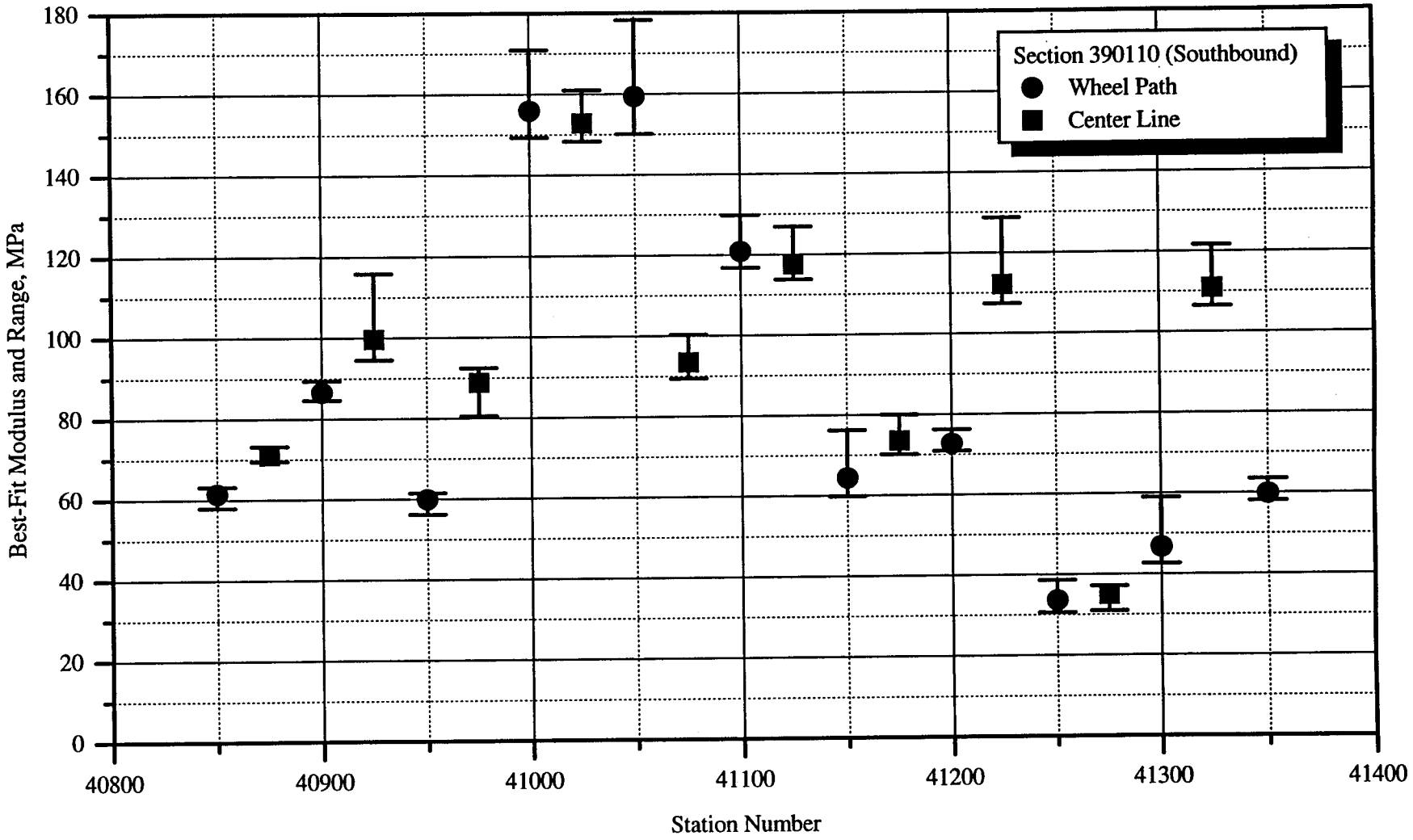

Figure A.10: Best-fit modulus and range at each falling-weight test location in section 390110.

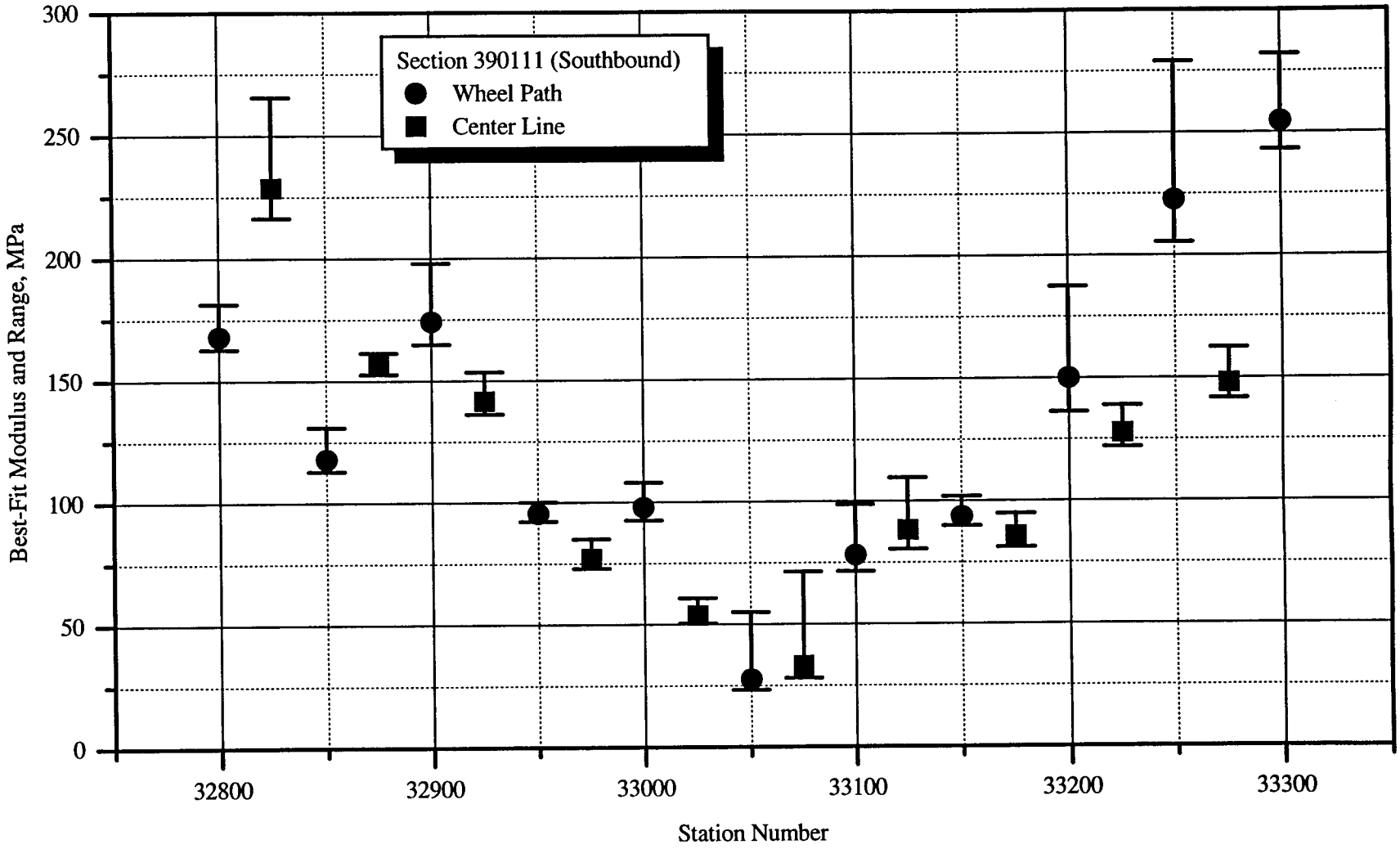

Figure A.11: Best-fit modulus and range at each falling-weight test location in section 390111.

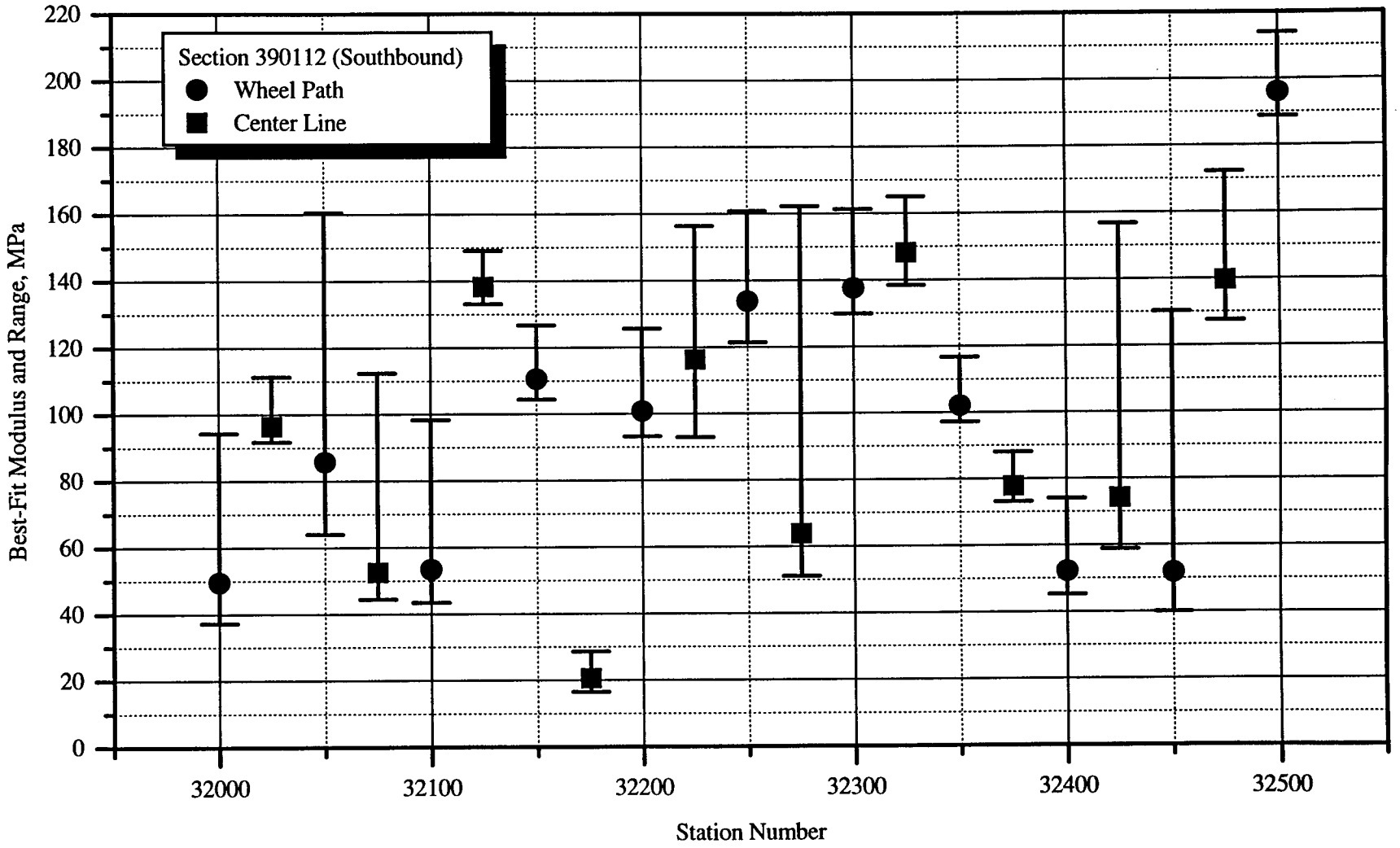

Figure A.12: Best-fit modulus and range at each falling-weight test location in section 390112.

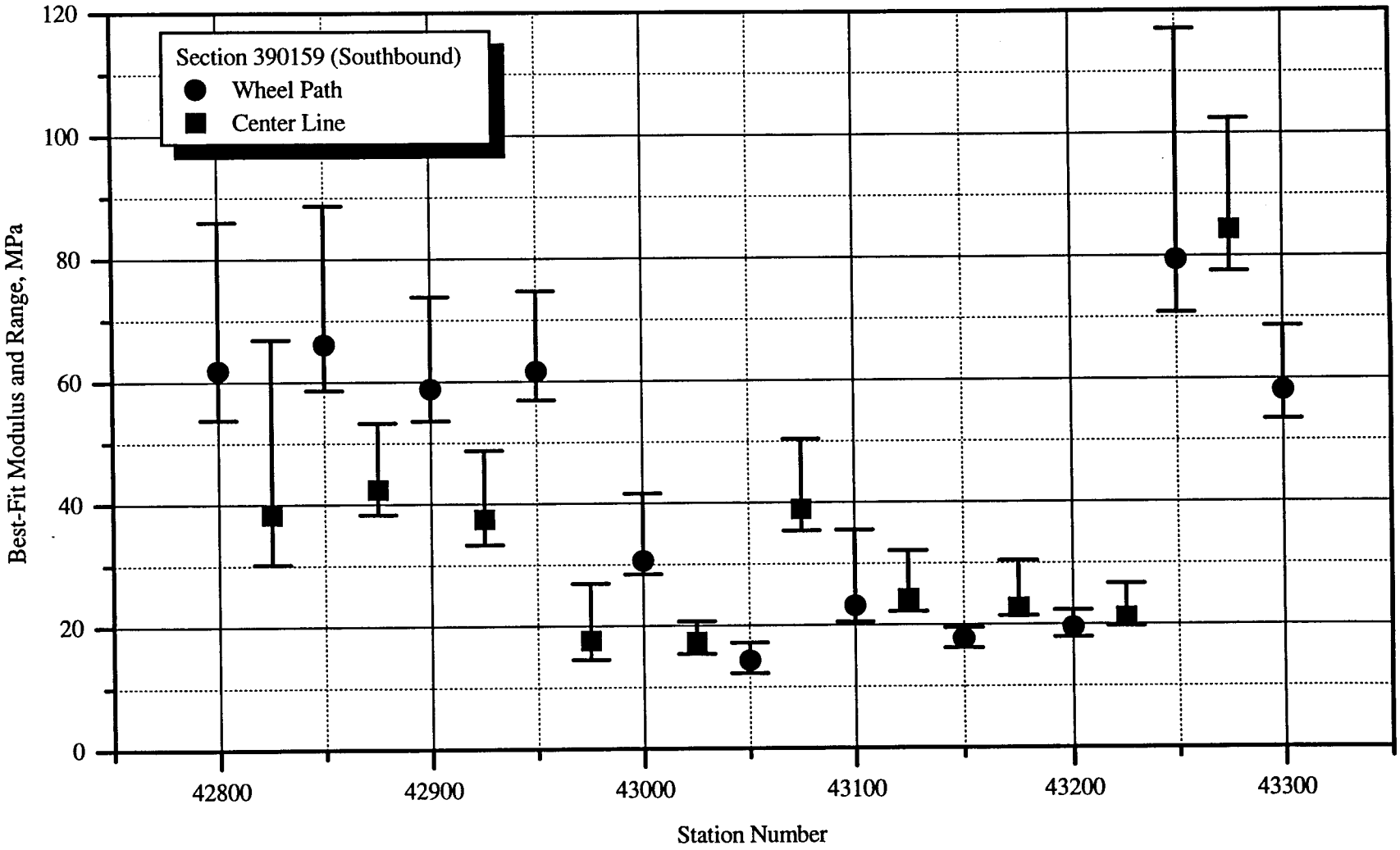

Figure A.13: Best-fit modulus and range at each falling-weight test location in section 390159.

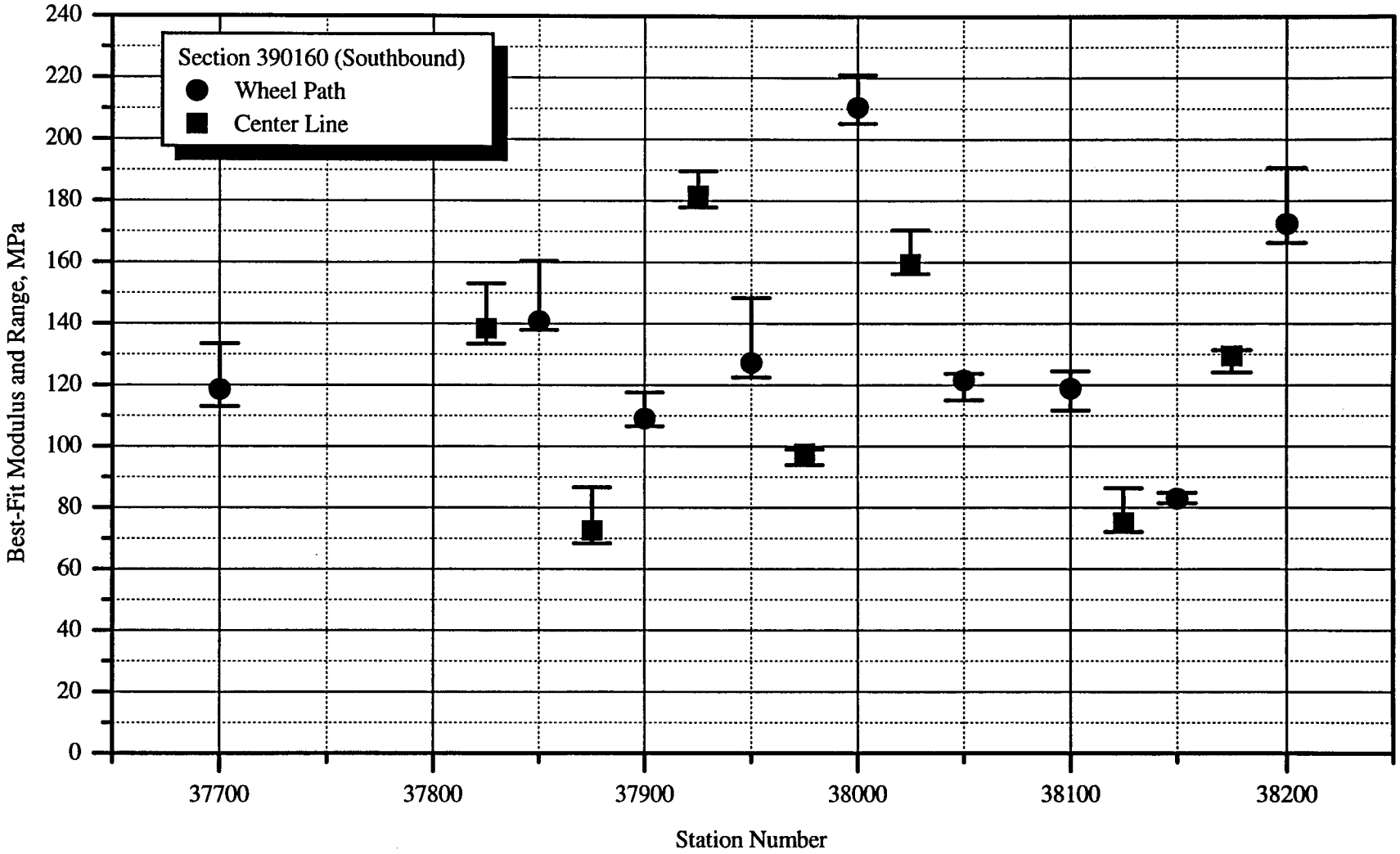

Figure A.14: Best-fit modulus and range at each falling-weight test location in section 390160.

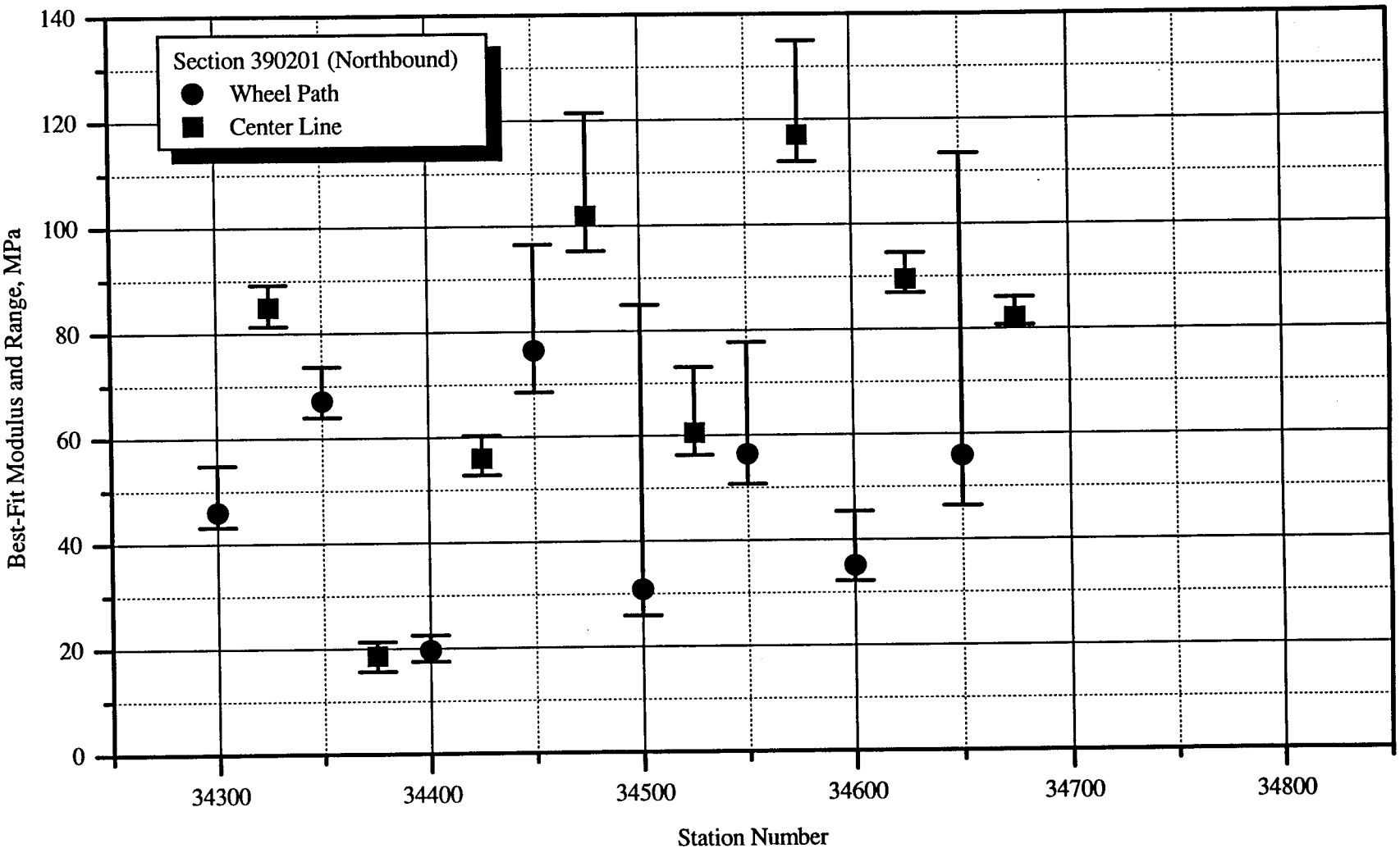

Figure A.15: Best-fit modulus and range at each falling-weight test location in section 390201.

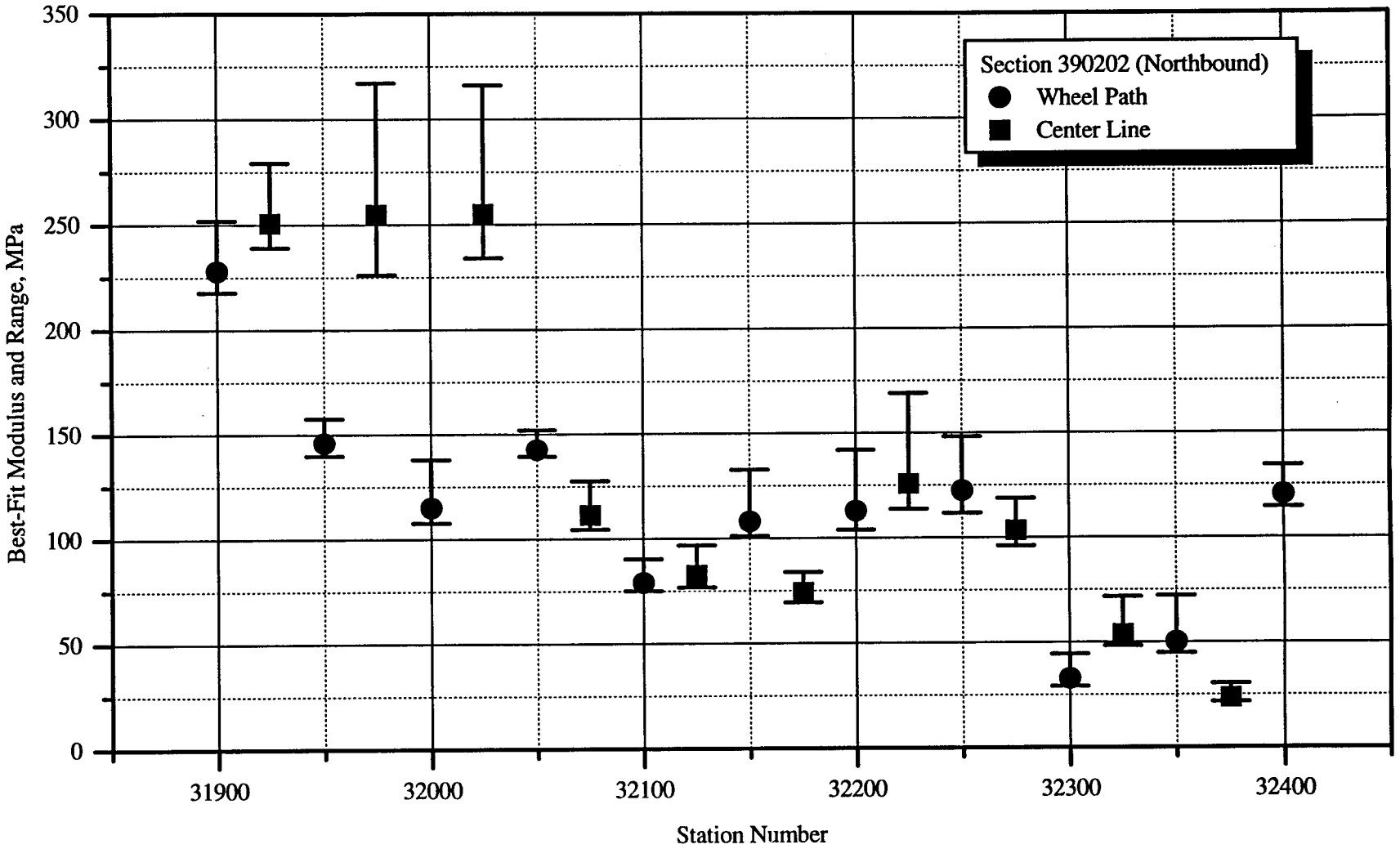

Figure A.16: Best-fit modulus and range at each falling-weight test location in section 390202.

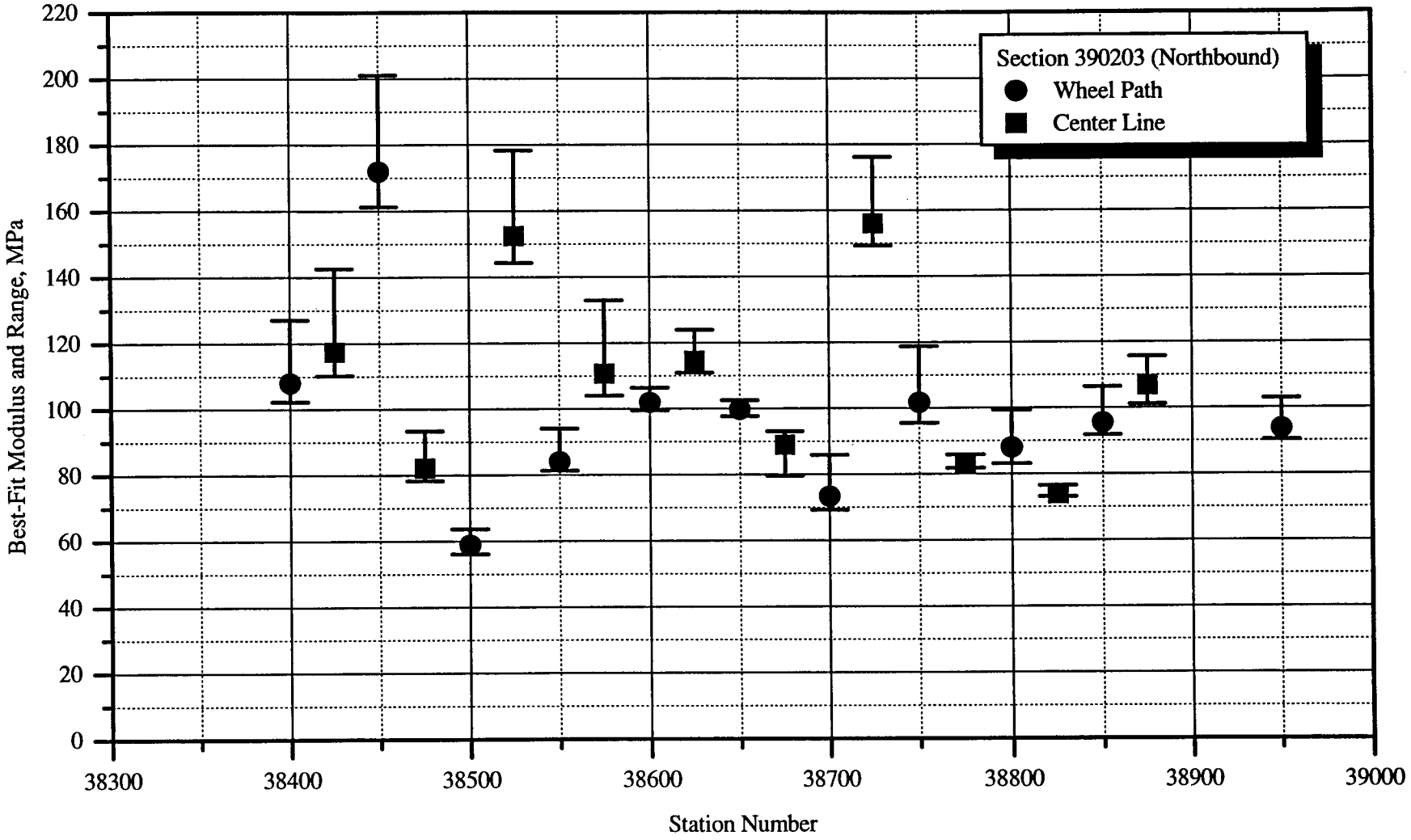

Figure A.17: Best-fit modulus and range at each falling-weight test location in section 390203.

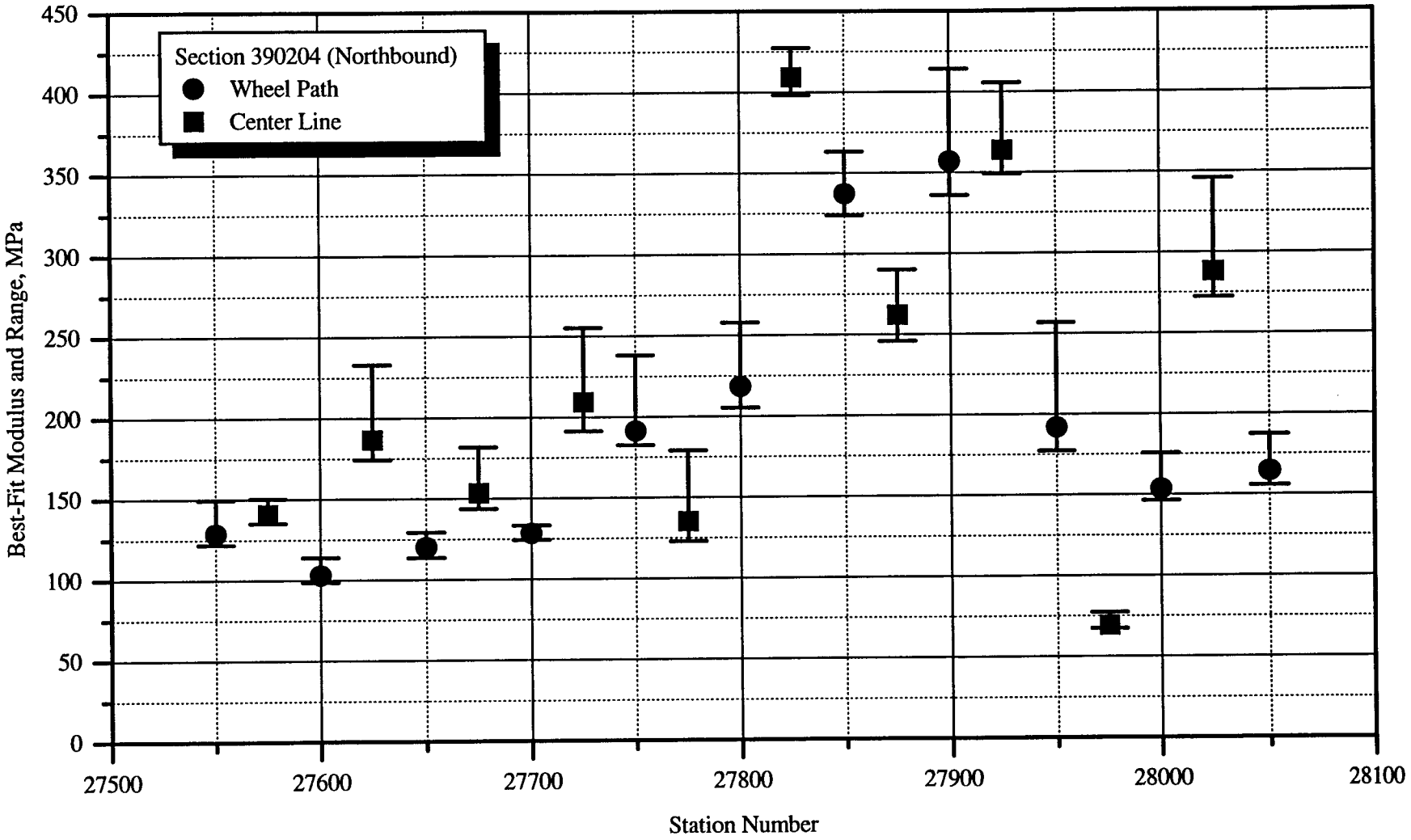

Figure A.18: Best-fit modulus and range at each falling-weight test location in section 390204.

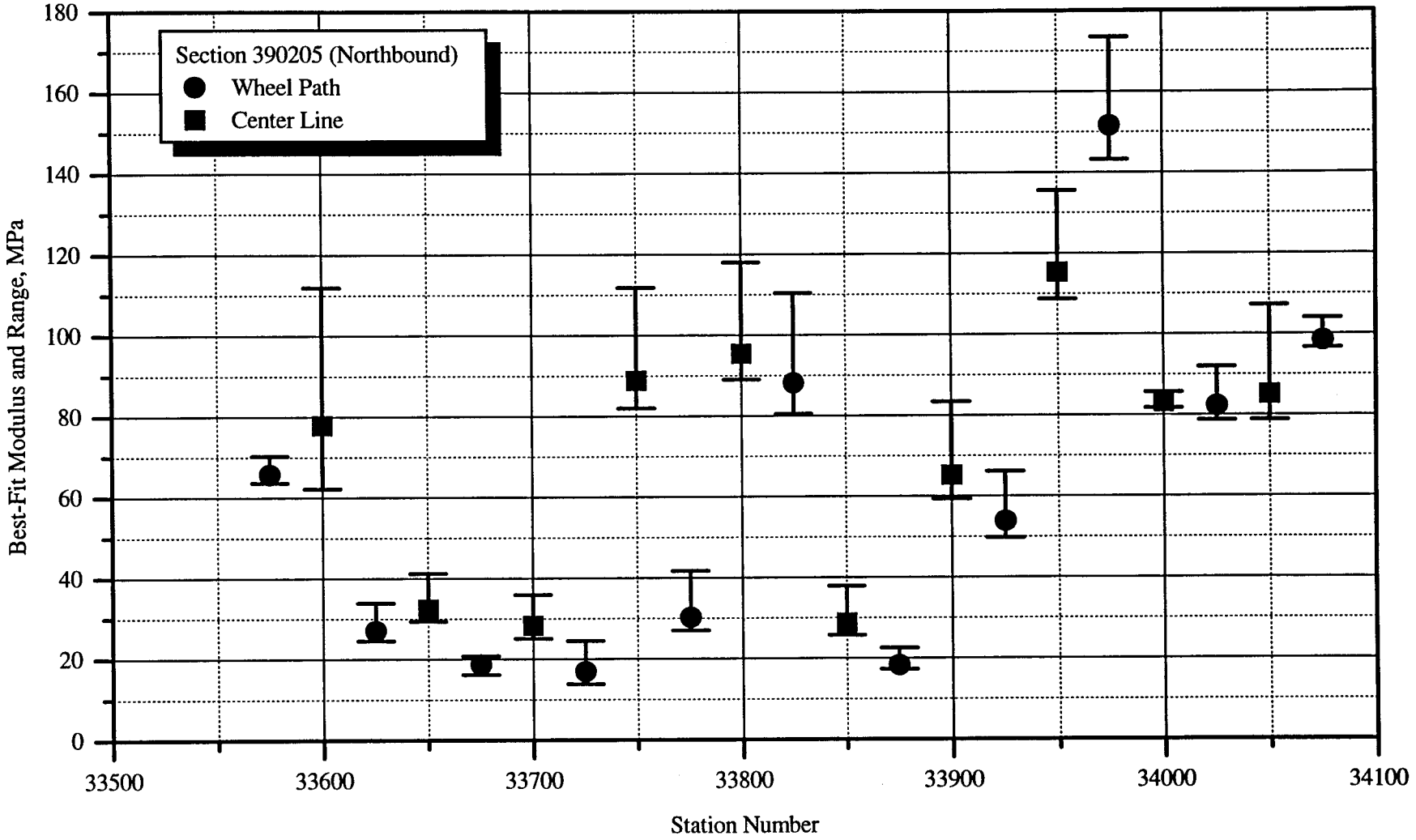

Figure A.19: Best-fit modulus and range at each falling-weight test location in section 390205.

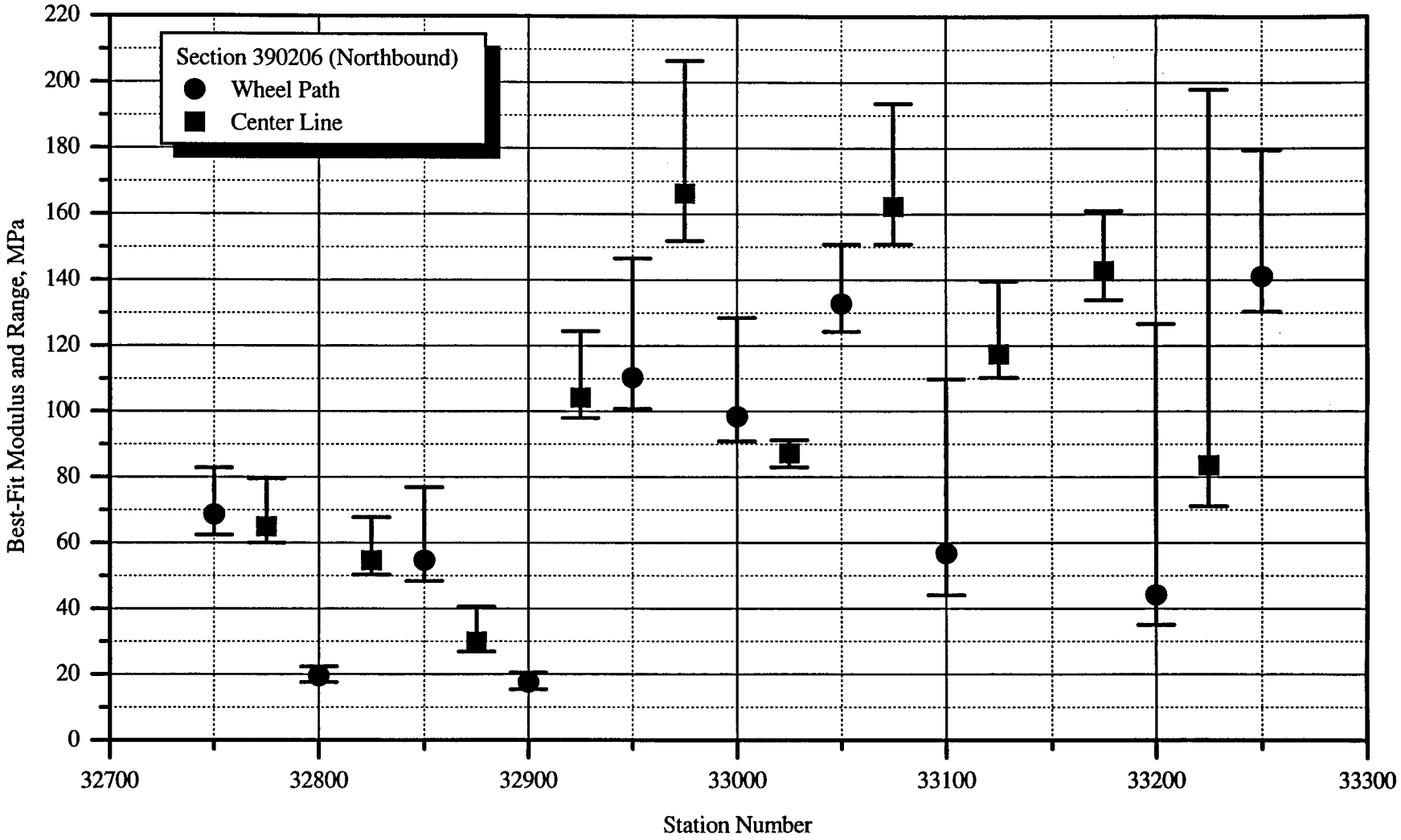

Figure A.20: Best-fit modulus and range at each falling-weight test location in section 390206.

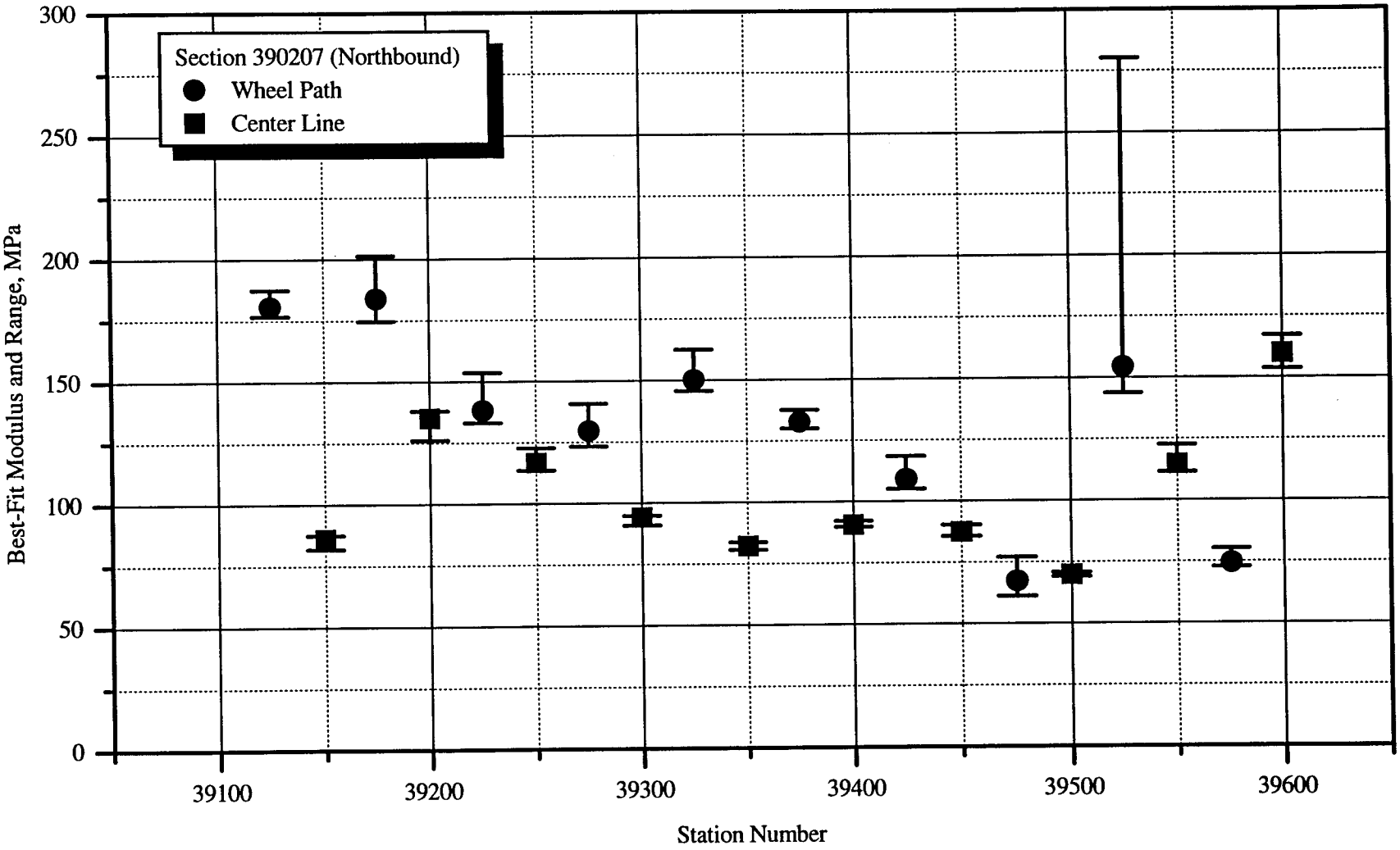

Figure A.21: Best-fit modulus and range at each falling-weight test location in section 390207.

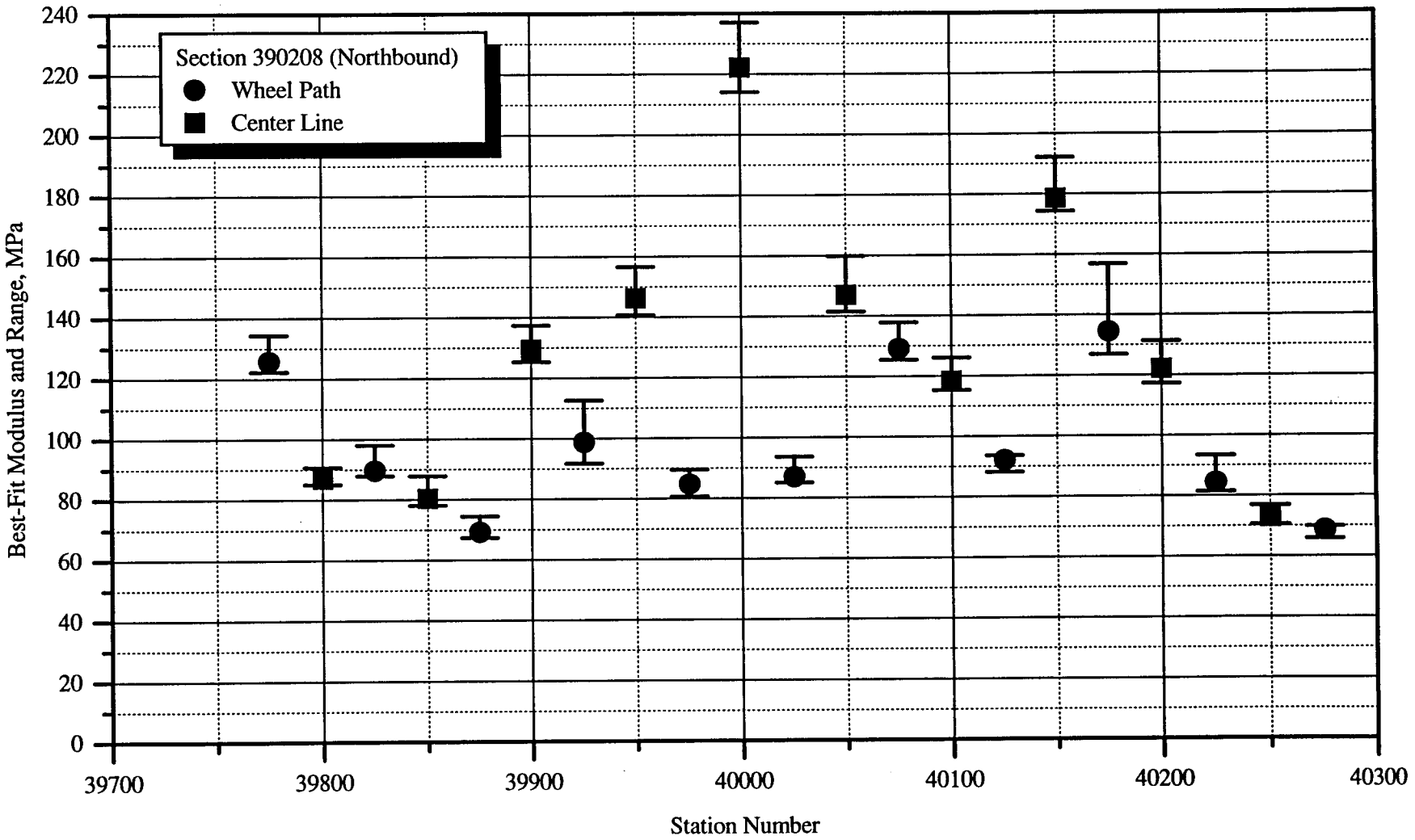

Figure A.22: Best-fit modulus and range at each falling-weight test location in section 390208.

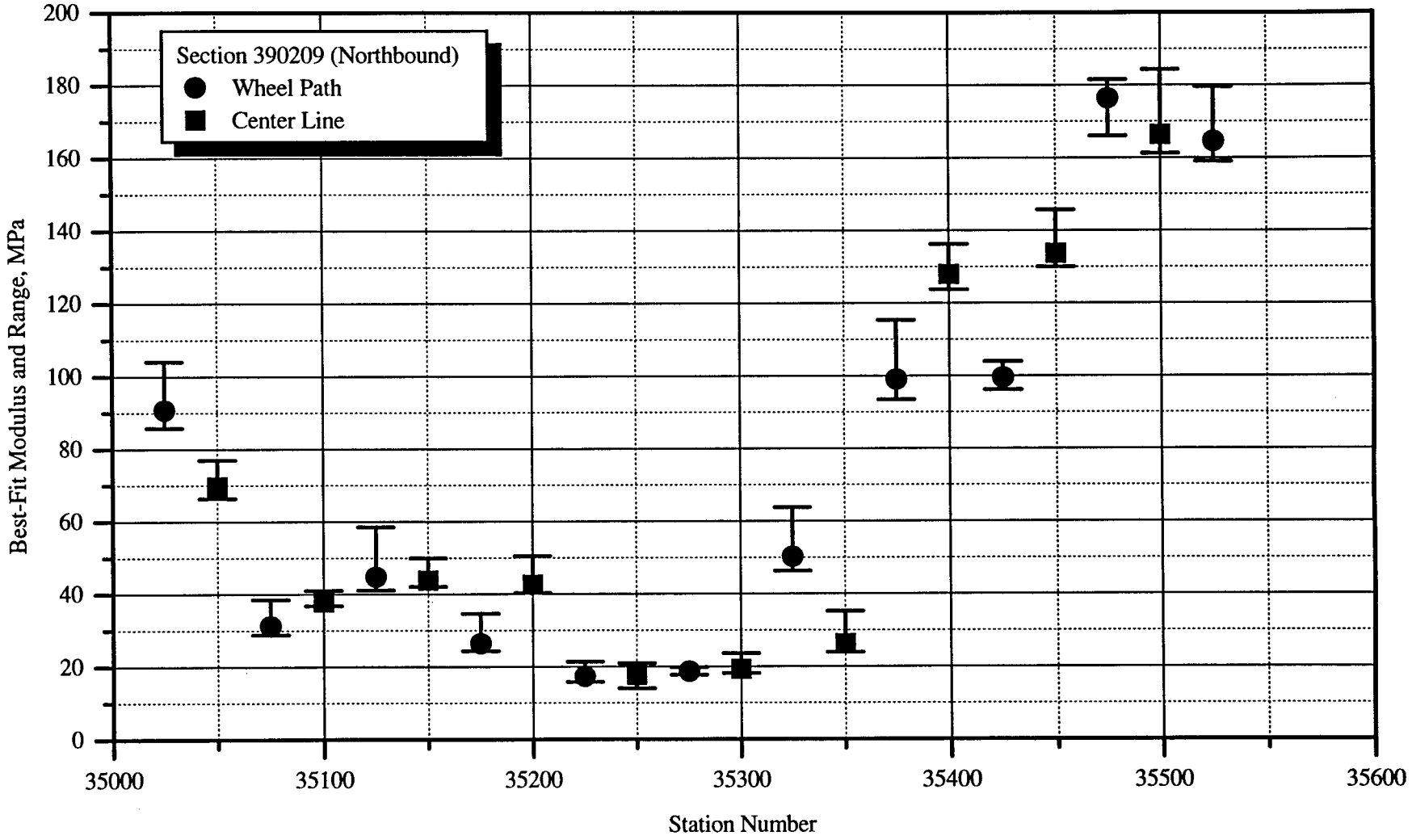

Figure A.23: Best-fit modulus and range at each falling-weight test location in section 390209.

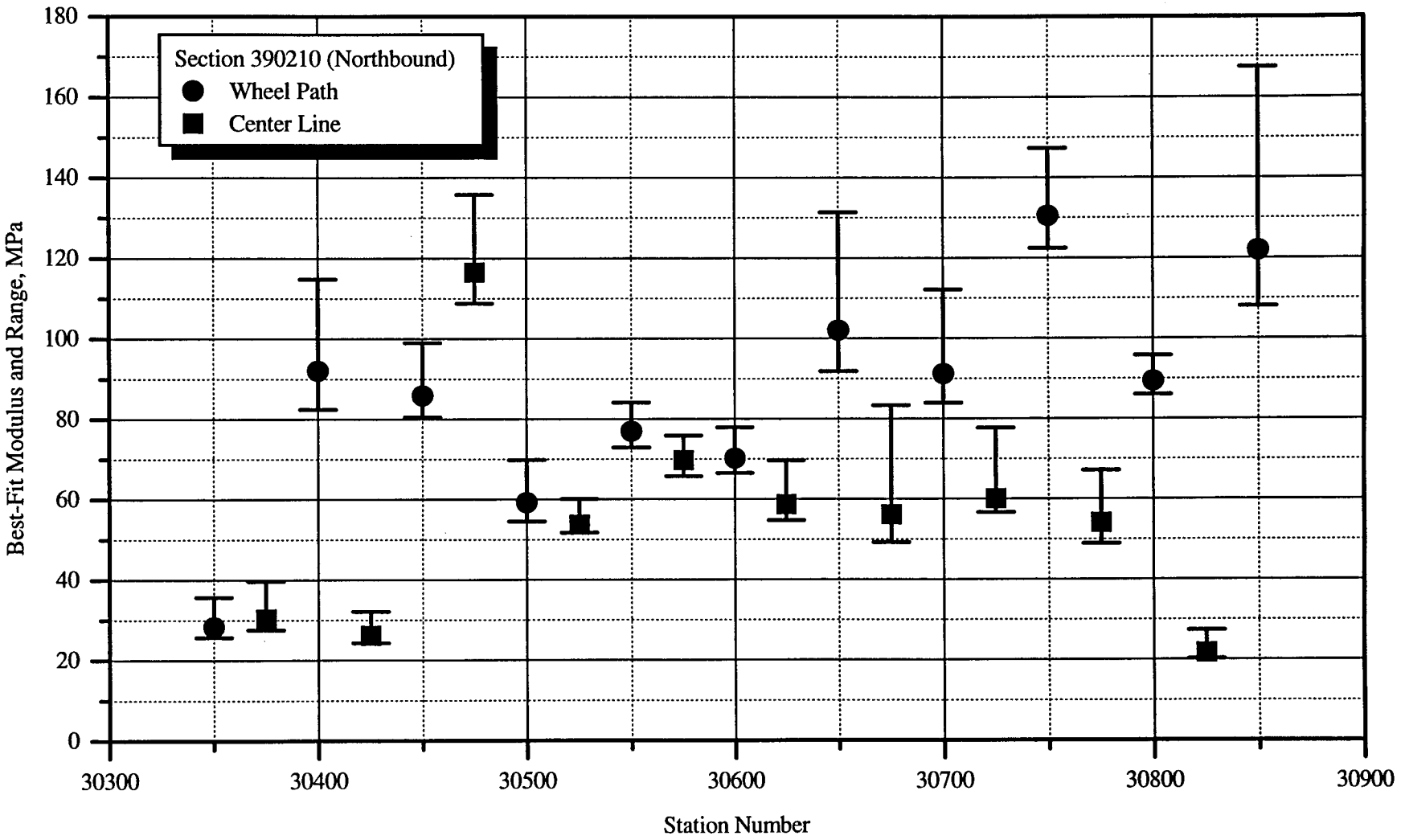

Figure A.24: Best-fit modulus and range at each falling-weight test location in section 390210.

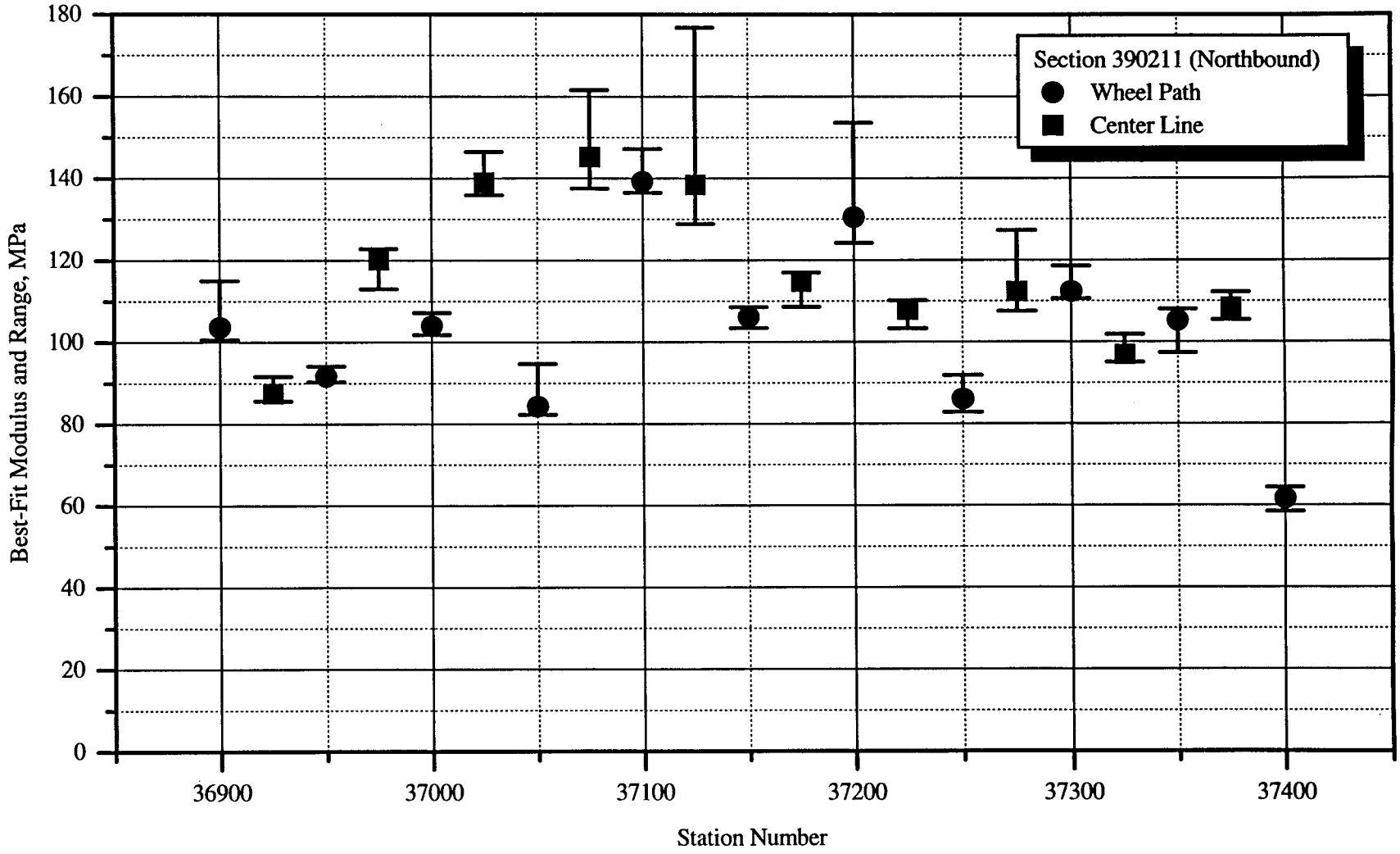

Figure A.25: Best-fit modulus and range at each falling-weight test location in section 390211.

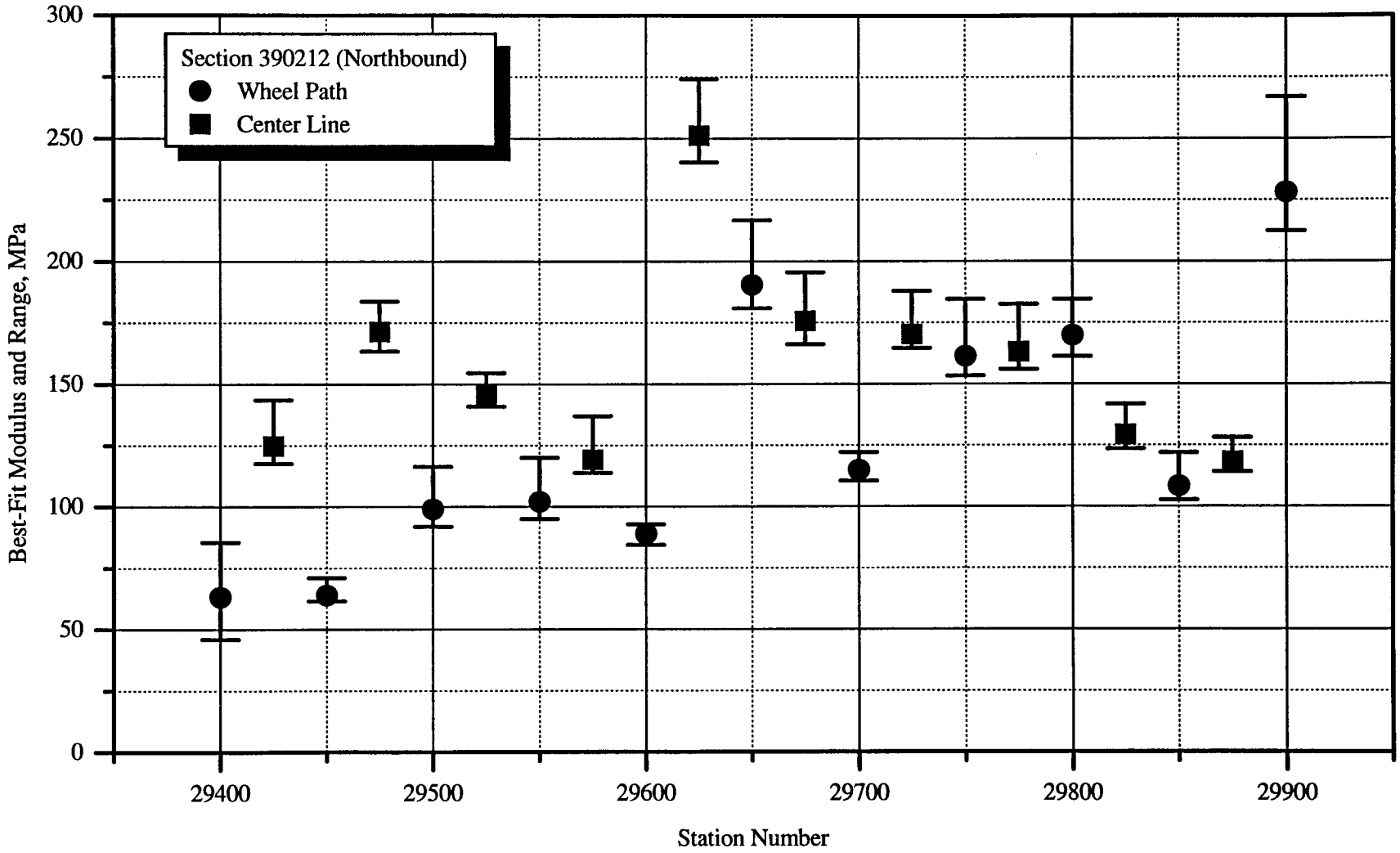

Figure A.26: Best-fit modulus and range at each falling-weight test location in section 390212.

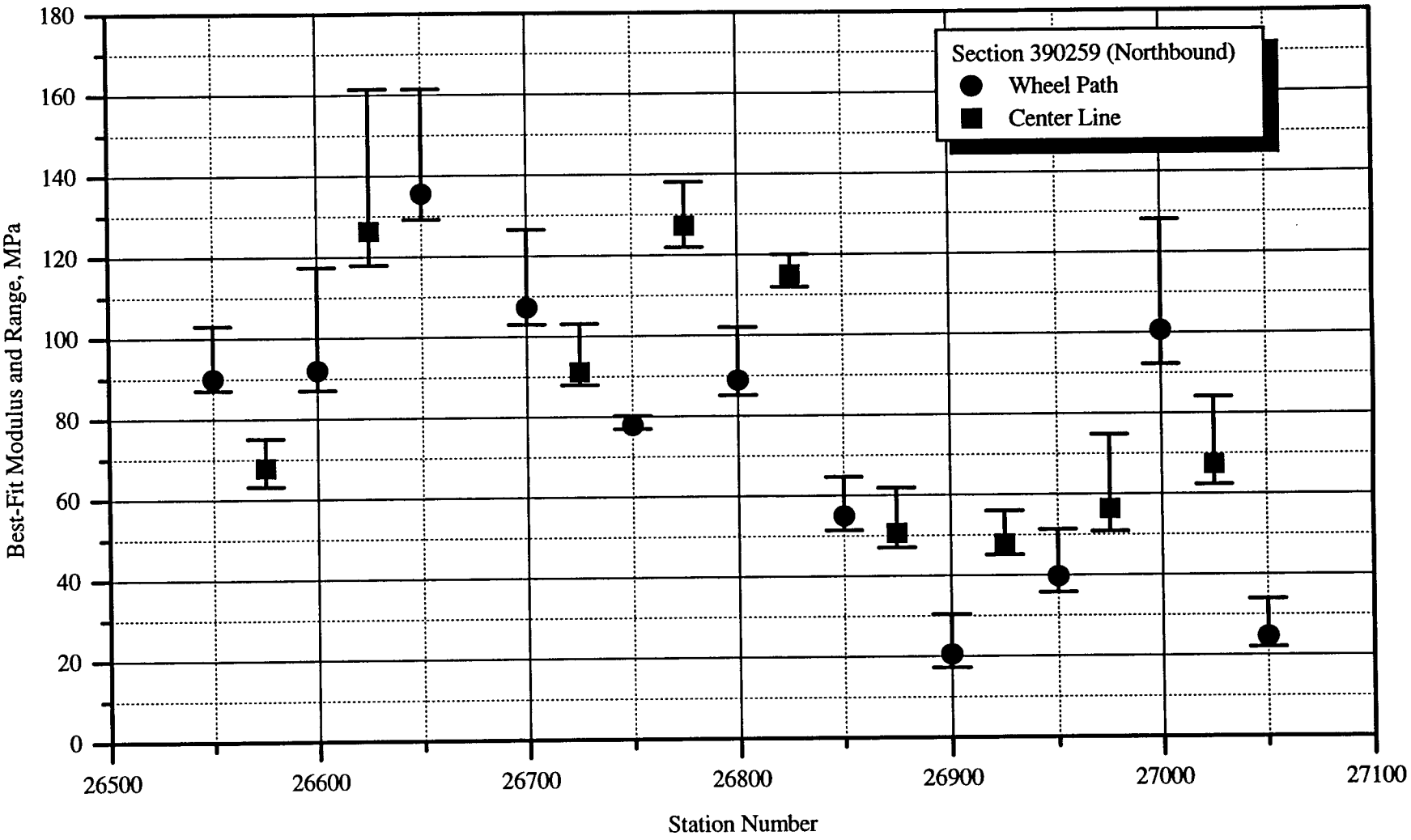

Figure A.27: Best-fit modulus and range at each falling-weight test location in section 390259.

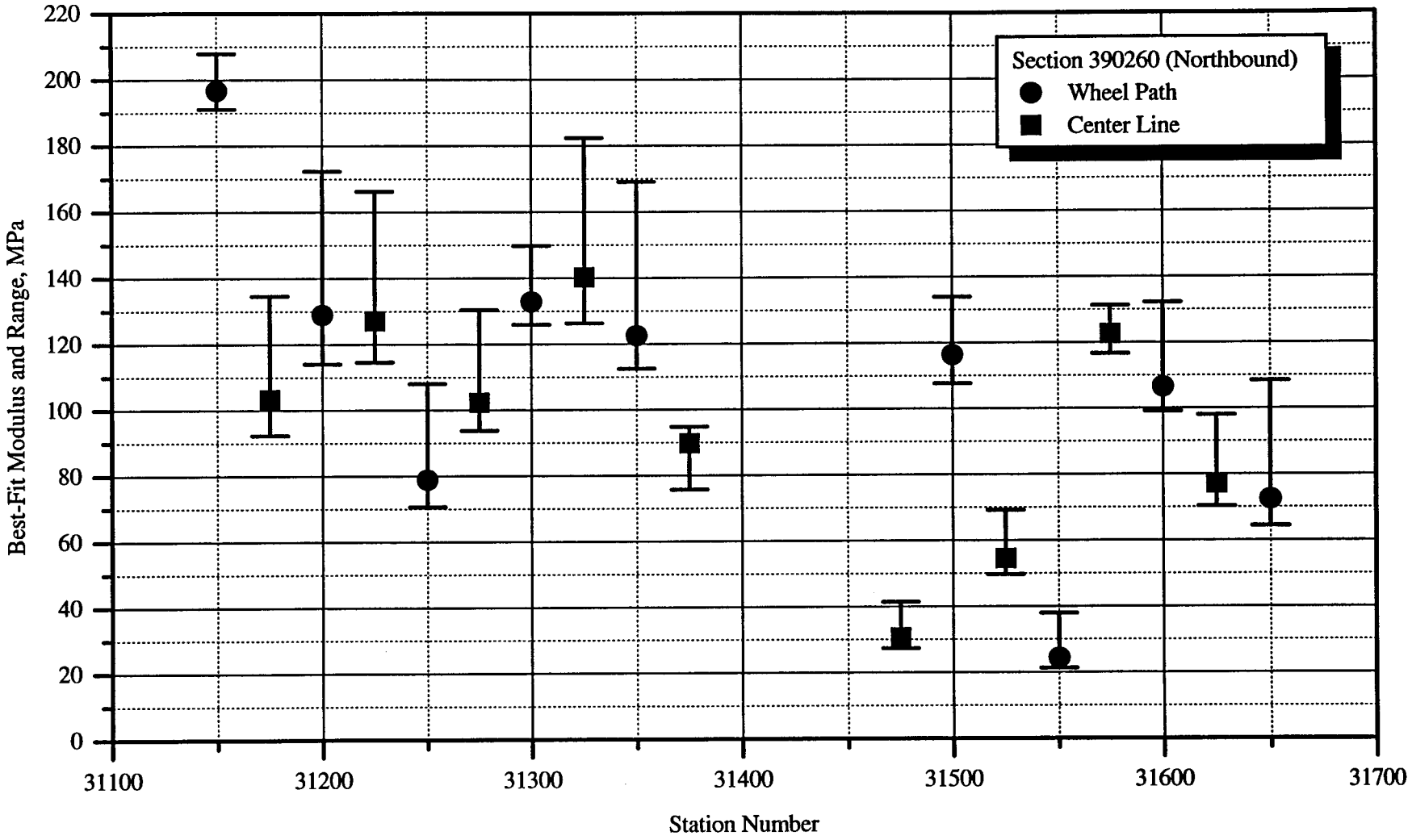

Figure A.28: Best-fit modulus and range at each falling-weight test location in section 390260.

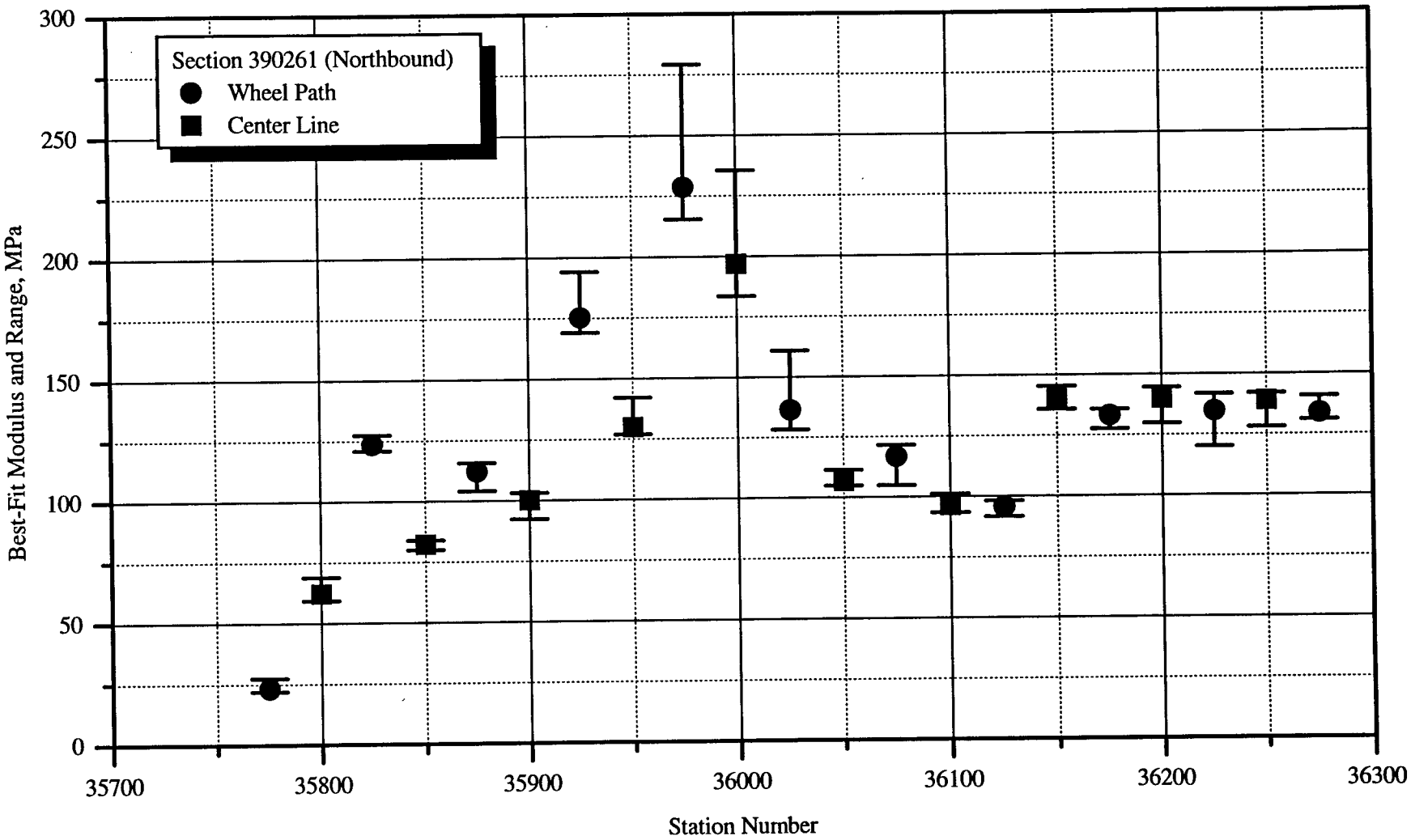

Figure A.29: Best-fit modulus and range at each falling-weight test location in section 390261.

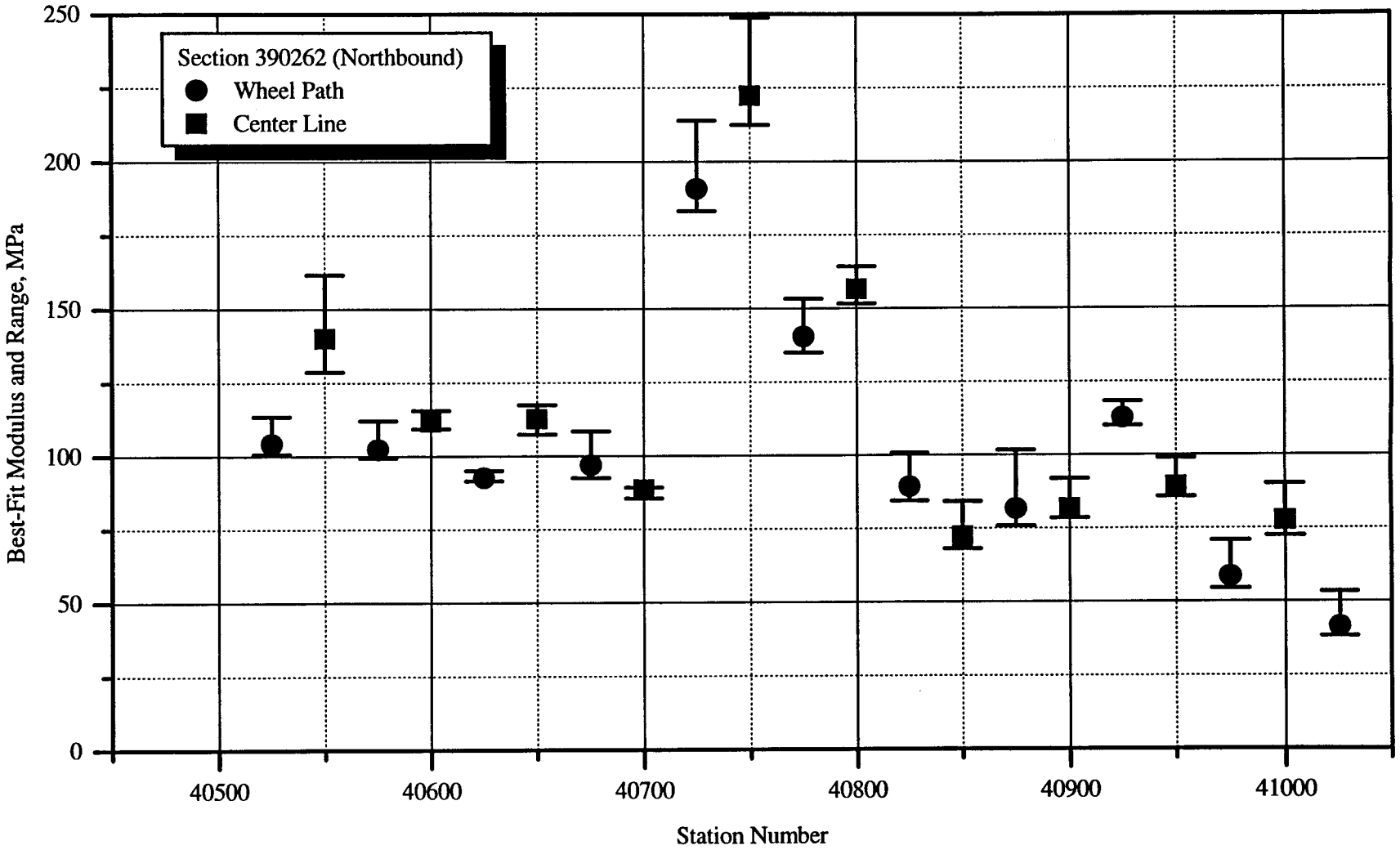

Figure A.30: Best-fit modulus and range at each falling-weight test location in section 390262.

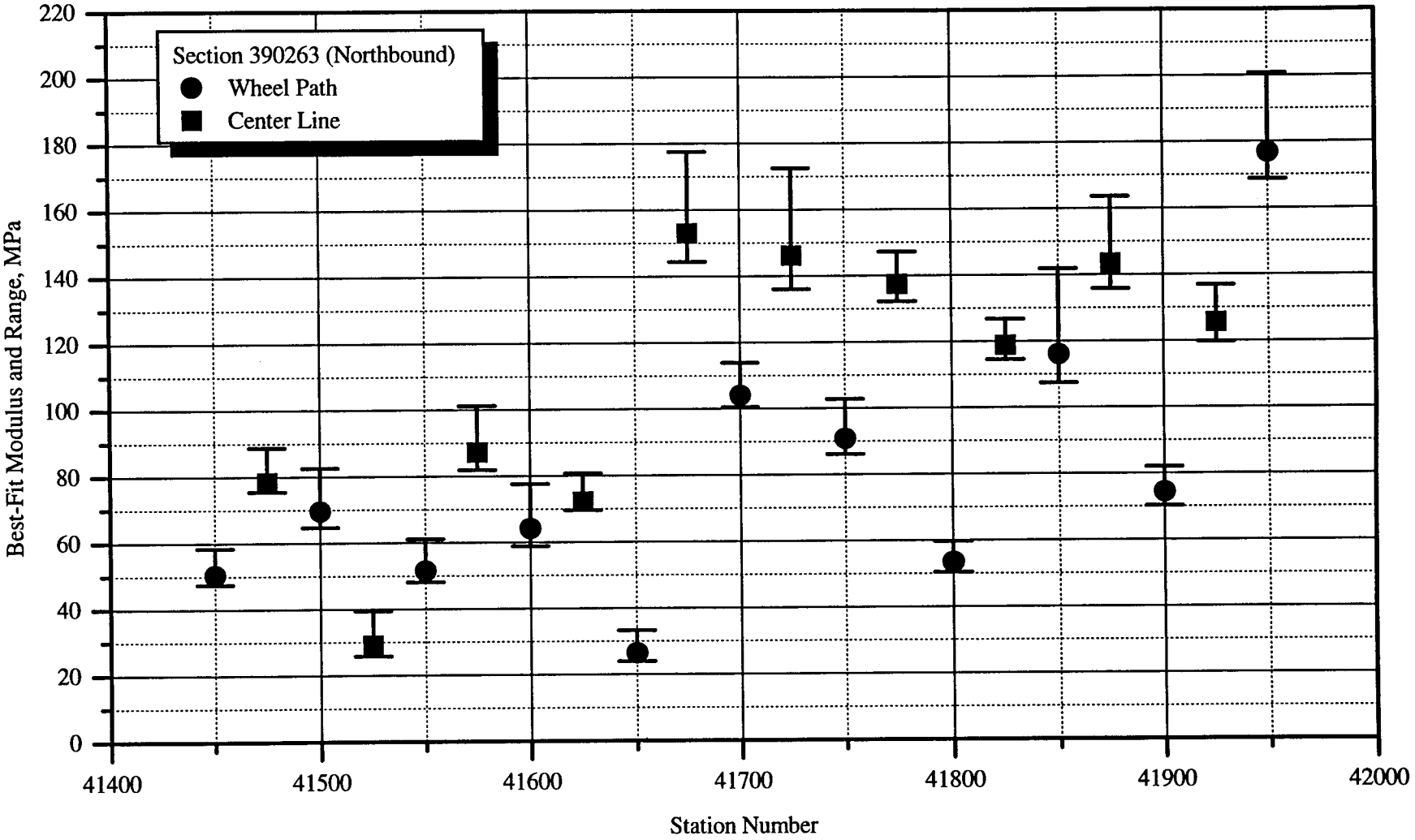

Figure A.31: Best-fit modulus and range at each falling-weight test location in section 390263.

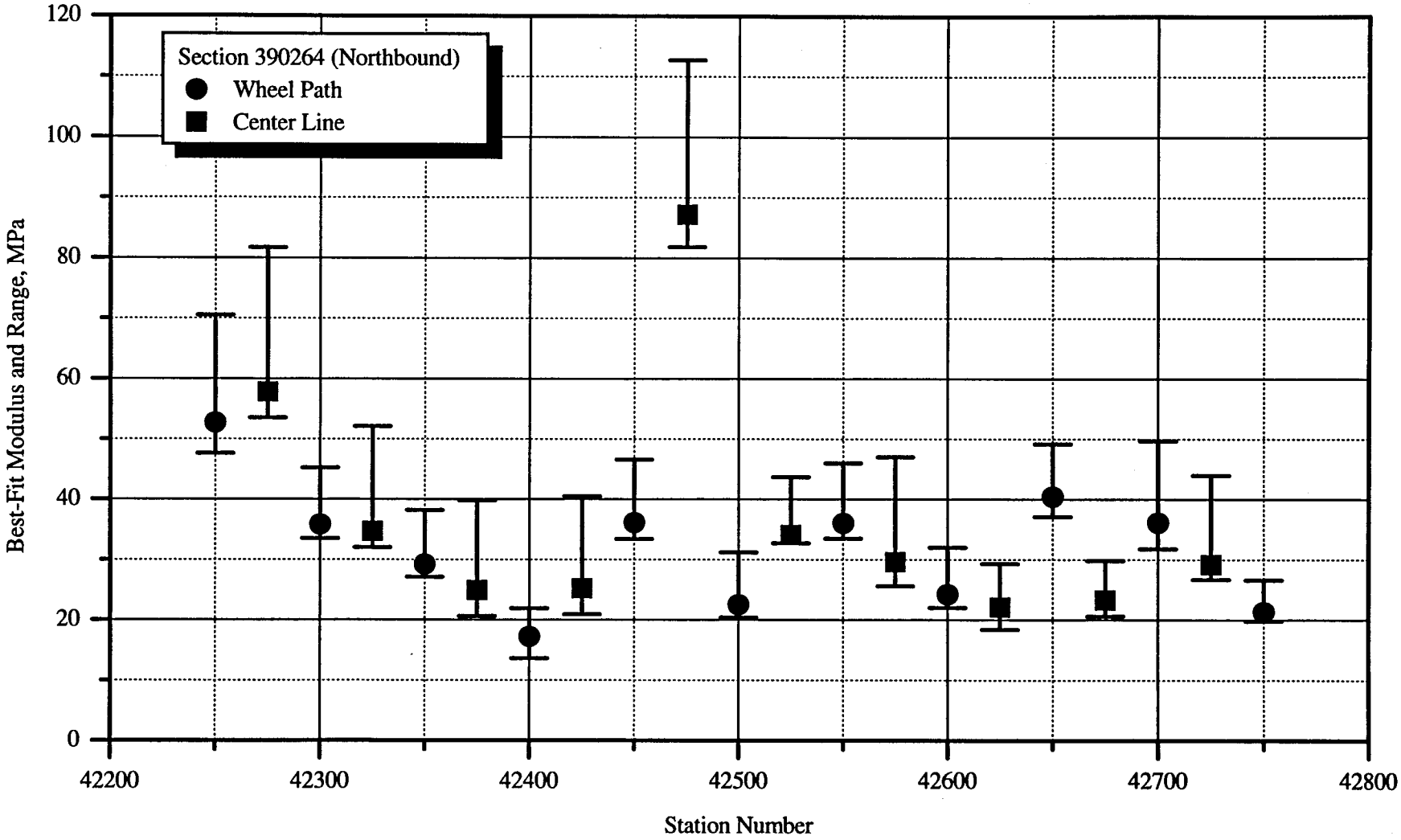

Figure A.32: Best-fit modulus and range at each falling-weight test location in section 390264.

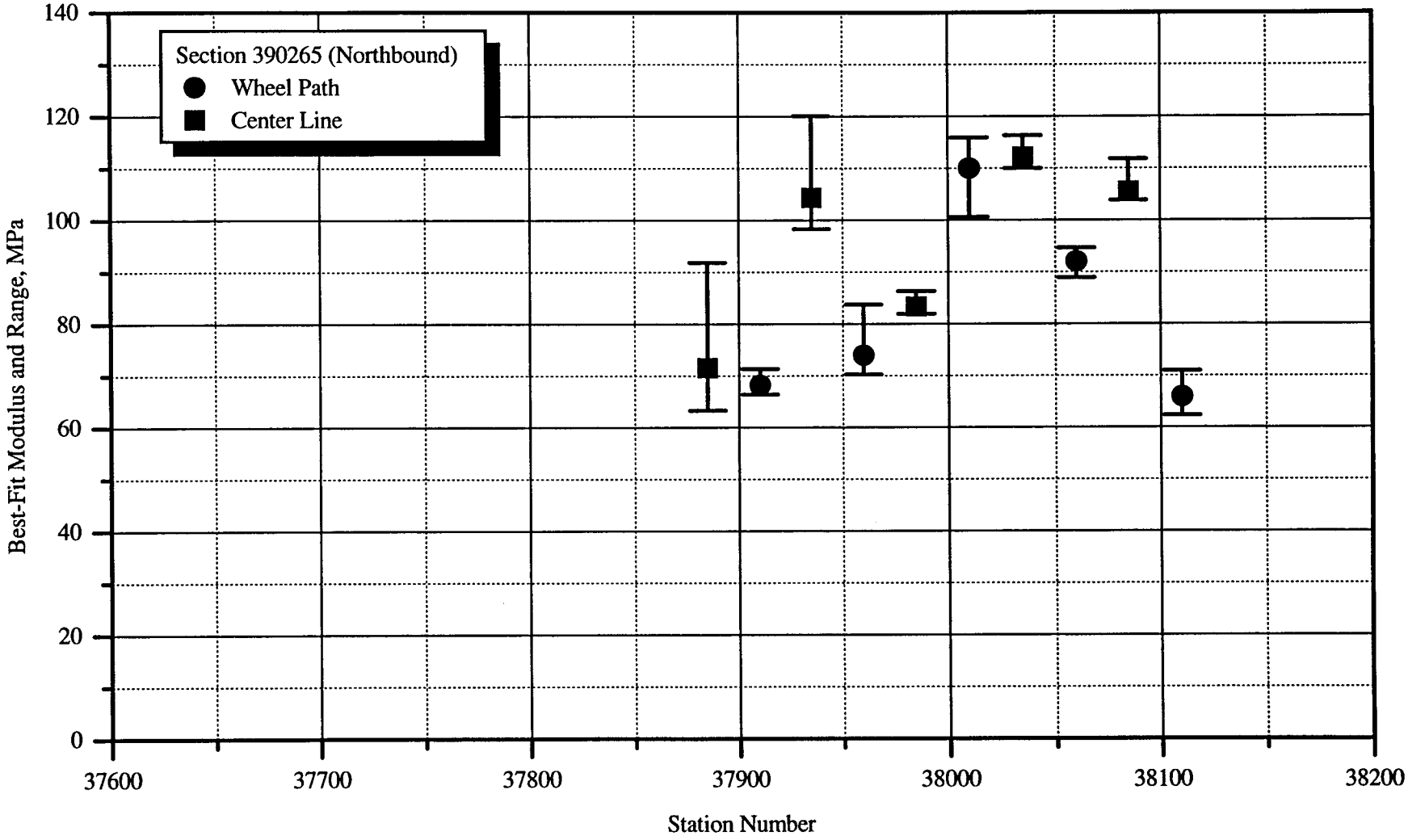

Figure A.33: Best-fit modulus and range at each falling-weight test location in section 390265.

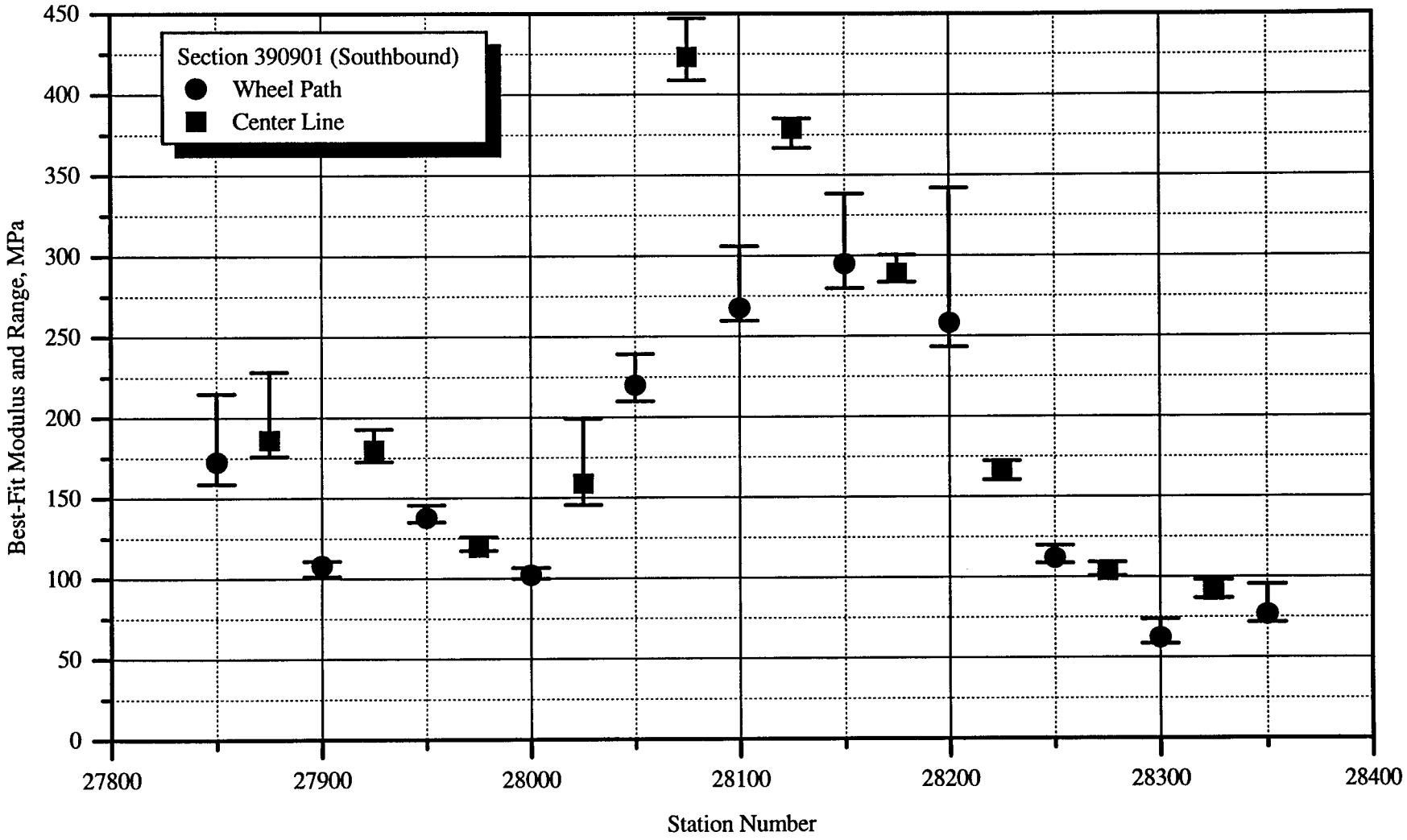

Figure A.34: Best-fit modulus and range at each falling-weight test location in section 390901.

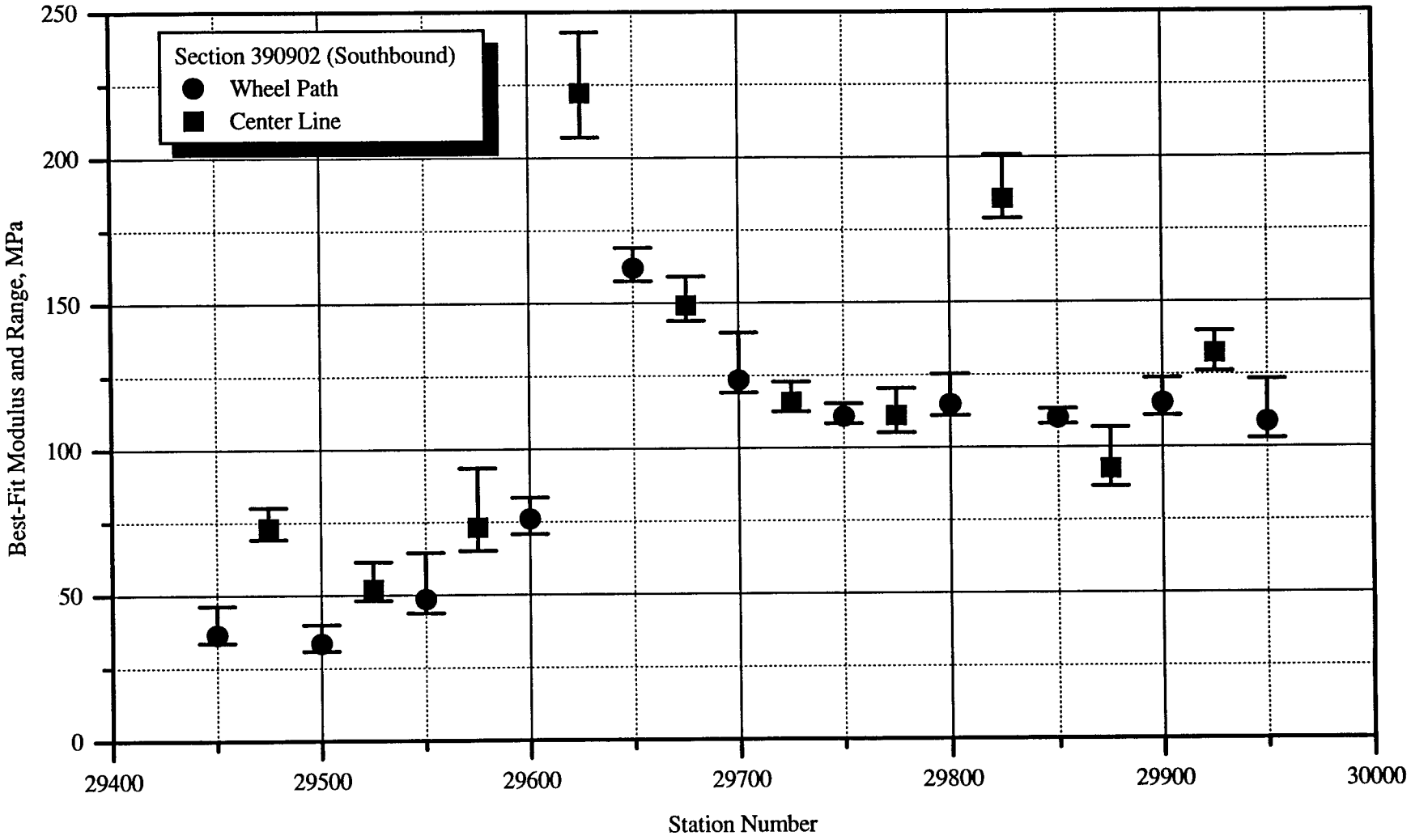

Figure A.35: Best-fit modulus and range at each falling-weight test location in section 390902.

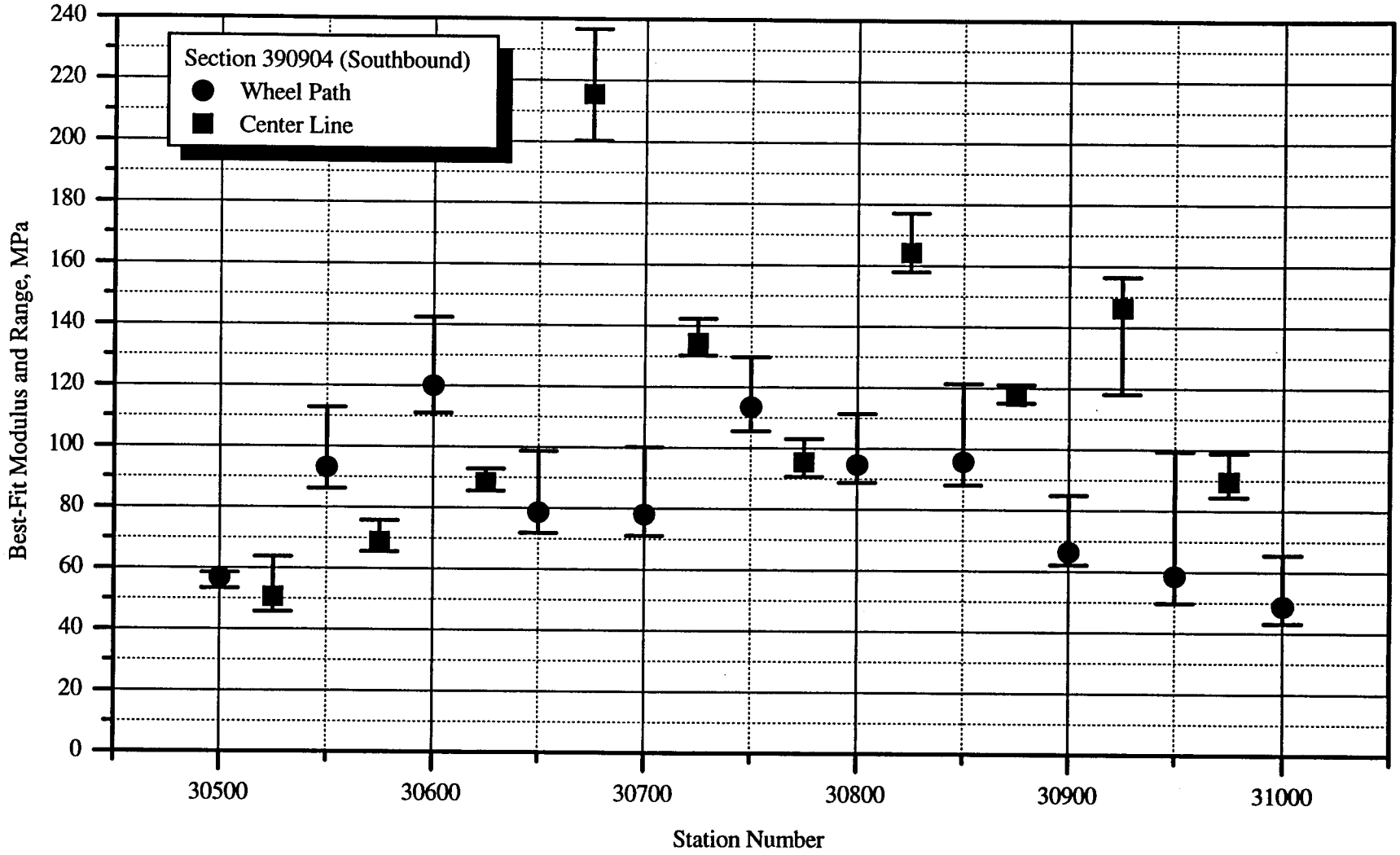

Figure A.36: Best-fit modulus and range at each falling-weight test location in section 390904.